Aus dem Institut für Anatomie I
der Heinrich-Heine-Universität Düsseldorf
Direktorin: Fr. Prof. Dr. Dr. Caspers

Upon the neuronal supply of the human interosseous membrane of the forearm

(Zur neuronalen Versorgung der humanen Membrana interossea antebrachii)

Dissertation

zur Erlangung des Grades eines Doktors der Medizin
der Medizinischen Fakultät der Heinrich-Heine-Universität Düsseldorf

vorgelegt von
Anne-Marie Kamp
2024

Als Inauguraldissertation gedruckt mit der Genehmigung der

Medizinischen Fakultät der Heinrich-Heine-Universität Düsseldorf

gez.:

Dekan: Prof. Dr. med. Nikolaj Klöcker

Erstgutachter: Prof. Dr. med. Timm J. Filler

Zweitgutacher: Prof. Dr. med. Philipp Albrecht

Für meine Familie und Freunde

„What is more important for us, at an elemental level, than the control, the owning and operation,
of our own physical selves?
And yet it is so automatic, so familiar, we never give it a thought."

Oliver Sacks
"The Disembodied Lady"
from
"The Man Who Mistook His Wife for a Hat and Other Clinical Tales"[1]

Auflistung der Publikationen

Teile dieser Arbeit wurden veröffentlicht als Posterpräsentation und Vortrag:

1. Kamp A-M, Albrecht P, Filler T. The antebrachial interosseous membrane exhibits a gender- and functionspecific distribution of mechanoreceptors *115th Annual Meeting Innsbruck (2021) - Men Or Mice - Both Are Nice, Innsbruck*: Anatomische Gesellschaft; 2021.

2. Kamp A-M. Untersuchung der Propiorezeptoren in der Membrana interossea antebrachii und der umgebenden Muskulatur *Neuraltherapie Tage in Kassel 2021, Kassel*: Internationale medizinische Gesellschaft für Neuraltherapie nach Huneke Regulationstherapie e.V.; 2021

3. Kamp A-M, Filler T. Upon the neuronal supply of the interosseous membrane of the forearm. *AAO Convocation 2024 - Maximizing Human Performance, Colorado Springs:* American Academy of Osteopathy; 2024.

Zusammenfassung

Die Membrana interossea antebrachii (MIA) verbindet den Radius und die Ulna und wurde in den letzten Jahrzehnten vor allem mit Fokus auf ihre biomechanische Funktion erforscht. Kürzlich wurden Mechanorezeptoren in der MIA entdeckt, die darauf hindeuten, dass ihre sensible Rolle bei der Propriozeption bisher weitgehend unterschätzt wurde. Der Unterarm ist für alltägliche Aufgaben von entscheidender Bedeutung, und Verletzungen des Unterarms können massiv einschränken. Manchmal bleiben Schmerzen nach Abheilung der Verletzungen bestehen, und es entwickeln sich Schmerzsyndrome wie das Komplexe Regionale Schmerzsyndrom Typ I. Bislang ist die Pathogenese dieses Schmerzsyndroms noch unbekannt, und die sensible Innervation der MIA und der umliegenden Gewebe könnte wichtige Informationen hierzu liefern. Ziel dieser Studie ist es, die MIA und die umgebenden Gewebe auf Mechanorezeptoren sowie auf sympathische Innervation zu untersuchen.

Wir entnahmen ein Querschnittstück der proximalen, medialen und distalen Teile von 14 MIAs von sieben Spendern, drei Männern und vier Frauen. Bei einer Spenderin wurden auch Längsschnitte der proximalen, medialen und distalen MIAs entnommen. Diese Abschnitte wurden histologisch präpariert und mit Azan-, Elastica-van-Gieson-, Goldner- und Pan-Neurofilament-Färbungen angefärbt. Einige Schnitte wurde auch mit Tyrosin-Hydroxylase-, S100-, MBP- und TRCP4-Färbungen angefärbt. Anschließend wurden diese Schnitte mit dem Motic EasyScanner, Infinity 100, gescannt und mit dem Computerprogramm MoticAssistant DS ausgewertet. Die Mechanorezeptoren wurden entsprechend ihrer ursprünglichen Beschreibung klassifiziert. Die Ergebnisse wurden in einer Excel-Tabelle festgehalten. Der Kruskal-Wallis-Test sowie der Mann-Whitney-U-Test wurden mithilfe des Programmes SPSS durchgeführt.

In 29 von 42 MIA-Abschnitten wurden Mechanorezeptoren identifiziert. In allen Schnitten wurden jedoch Mechanorezeptoren in den umgebenden Geweben identifiziert. In der MIA wurden Ruffini-Körperchen, Muskelspindeln, Golgi-Sehnen-Organe und Vater-Pacini-Körperchen gefunden. Darüber hinaus wurden einige sympathische Nerven in der MIA entdeckt. In den Geweben an der Grenze zur MIA und in den umgebenden Geweben wurden Ruffini-Körperchen, Muskelspindeln, Vater-Pacini-Körperchen und Golgi-Mazzoni-Körperchen entdeckt. Besonders interessant ist die Anzahl der entdeckten Golgi-Mazzoni-Körperchen. Dabei handelt es sich um eine Unterart der Vater-Pacini-Körperchen, die aus zwei oder mehr Axonen mit entsprechenden Kapseln bestehen.

Diese Ergebnisse bestätigen, dass die MIA eine wichtige Rolle bei der Propriozeption spielt. Entgegen der landläufigen Meinung, dass insbesondere das zentrale Band der MIA nur eine stabilisierende Funktion hat, sind das zentrale Band der MIA und seine Umgebung auch reichlich von Mechanorezeptoren innerviert. Ich empfehlen daher, die IOM und ihre Umgebung als wichtige propriozeptive Struktur zu betrachten.

Summary

The interosseous membrane of the forearm (IOM) connects the radius and the ulna and has been researched in the last decades, especially for its biomechanical function. Recently, mechanoreceptors have been discovered in the IOM, which indicates that its sensory role in proprioception has been largely underestimated. The forearm is crucial for everyday tasks, and injury to the forearm can be limiting. Sometimes, the pain of injuries persists, and pain syndromes develop, such as Complex Regional Pain Syndrome Type I. Until now, the pathogenesis of this pain syndrome is still unknown, and the sensory innervation of the IOM and the surrounding tissues might add important information. This study aims to explore the IOM and its surrounding tissues for mechanoreceptors as well as for sympathetic innervation.

We excised a cross-sectional piece of the proximal, medial, and distal parts of 14 IOMs of seven donors, three males, and four females. In one female donor, longitudinal sections of the proximal, medial, and distal IOMs were also excised. These portions were histologically prepared and stained with Azan, Elastica van Gieson, Goldner, and pan Neurofilament stains. A selected part of the sections was also stained with Tyrosine hydroxylase, S100, MBP, and TRCP4 stains. Then, these sections were scanned with Motic EasyScanner, Infinity 100, and analysed with the computer program MoticAssistant DS. Mechanoreceptors were classified according to their original descriptions. Results were noted in an Excel sheet. The Kruskal-Wallis test and the Mann-Whitney-U test were performed with the software SPSS.

In 29 out of 42 IOM sections, mechanoreceptors were identified. However, in all sections, mechanoreceptors were identified in the surrounding tissues. In the IOM, Ruffini bodies, muscle spindles, Golgi-Tendon organs, and Vater-Pacini corpuscles were found. In addition, some sympathetic nerves were discovered within the IOM. In the tissues at the border to the IOM and surrounding the IOM Ruffini bodies, muscle spindles, Vater-Pacini corpuscles, and Golgi-Mazzoni corpuscles were discovered. Particularly interesting is the number of Golgi-Mazzoni corpuscles discovered. These are a subvariety of Vater-Pacini corpuscles composed of two or more axons with corresponding capsules.

These findings prove that the IOM plays an important role in proprioception. Contrary to the current belief of having a solely stabilising function, the central band of the IOM and its surroundings are also richly innervated by mechanoreceptors. Therefore, I recommend considering the IOM and its surroundings as important proprioceptive structures.

List of Abbreviations

IOM	Interosseous membrane of the forearm
MIA	Membrana interossea antebrachii (latin)
cm	centimetre
mm	millimetre
µm	micrometre
°C	Celsius
g	Gramm
ml	Millilitre
ID	identification
PRUJ	Proximal radio-ulnar joint
DRUJ	Distal radio-ulnar joint
CRPS Type I	Complex Regional Pain Syndrome Type I
AV block	Atrioventricular block
MRSA	methicillin-resistant Staphylococcus aureus
COPD	chronic obstructive pulmonary disease
Vac	vacuum
Abs	absolute
LSAB	labelled Streptavidin-Biotin
MBP	Myelin Basic Protein
TRCP 4	Transient receptor potential canonical channel 4
MRI scan	Magnetic resonance imaging scan
CT scan	Computed tomography scan
RA	Rapidly adapting receptor
SA	Slowly adapting receptor
CT layer	Connective tissue layer
ML	Mean length
SD	Standard deviation
MW	Mean width
i.e.	id est, corresponding to this means
e.g.	exempli gratia, corresponding to example given
et al.	et alia, corresponding to and others

Table of Contents

1. Background

1.1 Introduction

Although the interosseous membrane of the forearm (IOM) only gets little attention in current anatomical textbooks, a multitude of studies on its anatomy and function show a high research interest in it. However, until very recently, the IOM has always only been investigated on its biomechanical aspect.

In 2020, mechanoreceptors and free nerve endings were discovered in the IOM. Nevertheless, nothing is known about mechanoreceptors at the transition of the IOM to adhering muscle as well as sympathetic supply to the IOM.

This study will fill this research gap by investigating the presence of mechanoreceptors in the IOM accordingly to muscle insertion and checking whether there is a sympathetic supply to the IOM.

1.2 Anatomy of the forearm

1.2.1 Bones and joints of the forearm

The forearm is divided into an anterior and posterior compartment by the IOM, the deep fascia and its two bones, the ulna, and the radius[2].

Ulna

The ulna is the long bone in the forearm and stabilises it. It gets narrower distally and does not participate in the radiocarpal joint. However, it participates in the elbow joint and proximal and distal radio-ulnar joint[2].

The ulna articulates with the humerus at the trochlear notch. This articulation is stabilised by the olecranon and the coronoid process. Thereby, a hinge type joint is formed, which allows primary flexion and extension of the elbow. Additionally, a small amount of abduction and adduction during pronation and supination of the forearm is possible through this joint[2]. The ulna articulates with the radius twice, once at the proximal radio-ulnar joint and the second time at the distal radio-ulnar joint. Both joints are pivot-type joints, allowing for supination and pronation. The proximal radio-ulnar joint lies between the radial notch by the ulna and the head of the radius. The distal radio-ulnar joint lies between the ulnar notch from the radius and the head of the ulna[2].

Radius

The radius lies laterally and is shorter than the ulna. It participates in the elbow joint, the proximal and distal radio-ulnar joint, and the wrist joint[2].

The radius articulates with the humerus via the radial head. Thereby, a hinge type joint is created, which allows for flexion and extension of the elbow. The two radio-ulnar joints allow the rotation of the radius around the ulna during pronation and supination. Next to the joints, the two bones are further connected by the IOM. Distally the radius articulates with the carpi of the hand at the wrist joint[2].

1.2.2 Muscles of the forearm

Although the forearm anatomically starts at the elbow joint, the distal humerus functionally forms part of the forearm as a region of muscle attachment.

17 muscles pass through the compartments of the forearm and either work on the different joints of the forearm, move the hand, or do both. As muscle bulk would interfere with the functionality of the hand, most muscles have their main body in the proximal part of the forearm and have long tendons which run distally. A further advantage of this is that the created win in lifting height offers an extensive range of contraction, allowing for the multitude of movements needed in the hands[2].

As the anterior and posterior compartments of the arm are occupied by the muscles acting at the shoulder joint, the muscles of the forearm are attached medially (flexors and pronators) and laterally (extensors and supinators).

<u>Anterior compartment</u>

The anterior compartment of the forearm is occupied by eight flexor and pronator muscles, which can be divided into superficial, intermediate, and deep muscles:

- Superficial
    - Pronator teres
    - Flexor carpi radialis
    - Palmaris longus
    - Flexor carpi ulnaris
- Intermediate
    - Flexor digitorum superficialis
- Deep
    - Flexor digitorum profundus
    - Flexor pollicis longus
    - Pronator quadratus

The four superficial and the intermediate muscles cross the elbow, whereas the deep muscles originate from areas within the forearm. The superficial muscles, as well as the flexor digitorum superficialis muscle are attached to the medial epicondyle of the humerus by the common flexor tendon. The two deep flexors are attached to the IOM as well as to the proximal part of the ulna (flexor digitorum profundus) and to the distal radius (flexor pollicis longus). The pronator quadratus muscle is attached to the ulna[2].

The pronator quadratus is the prime mover of pronation and is assisted by the pronator teres. It is the deepest muscle of the anterior compartment and inserts into the distal part of the radius. The distal attachments of the other muscles depend on their functions, six of these muscles insert at the hand and, therefore, also contribute to hand movements[2].

All anterior compartment muscles are innervated by the median nerve except for the flexor carpi ulnaris and the medial part of the flexor digitorum profundus, which are innervated by the ulnar nerve.

Posterior compartment

The posterior compartment of the forearm is occupied by eleven extensor and supinator muscles, which can be divided into superficial, deep, and muscles that outcrop the deep layer:

- Superficial
    - Brachioradialis
    - Extensor carpi radialis longus
    - Extensor carpi radialis brevis
    - Extensor digitorum
    - Extensor digiti minimi
    - Extensor carpi ulnaris
- Deep
    - Supinator
    - Extensor indicis
- Outcropping muscles of the deep layer
    - Abductor pollicis longus
    - Extensor pollicis longus
    - Extensor pollicis brevis

The brachioradialis muscle lies in the posterior compartment but is functionally a flexor of the forearm. It is attached to the supra-epicondylar ridge of the humerus.

The other muscles of the superficial layer originate from the lateral epicondyle of the humerus. Apart from the supinator, all deep muscles, also the muscles outcropping the deep layer, originate at least partly from the IOM. The extensor indicis, the abductor pollicis longus, and the extensor pollicis longus are proximally further attached to the posterior surface of the ulna. The extensor pollicis brevis originates further from the posterior surface of the radius[2].

The supinator is attached to the lateral epicondyle of the humerus and to the crest of the ulna. It is the prime mover for unopposed supination, particularly in extension. In flexion, the biceps brachii is the primary muscle contributing to supination. Similarly, to the flexors, the extensors insert distally at the anatomical structures where they produce movement. Nine of these muscles attach distally in the hand[2].

All muscles in the posterior compartment are innervated by the radial nerve[2].

1.2.3 Blood supply of the forearm

The two main arteries of the forearm are the ulnar and radial arteries. The common interosseous artery is a branch of the ulnar artery and originates in the cubital fossa. It runs laterally and deeply and ends with a separation into the anterior and posterior interosseous artery. The anterior interosseous artery runs distally on the anterior aspect of the IOM and pierces the membrane at the level of the proximal part of the pronator quadratus. Hereafter, it joins the dorsal carpal arch on the posterior side of the IOM[2].

The posterior interosseous artery runs on the posterior side of the IOM and gives rise to the recurrent interosseous artery. The recurrent artery runs superiorly and returns to the proximal radio-ulnar joint and capitulum. Here it anastomoses with the middle collateral artery. The posterior interosseous artery supplies the muscles in the posterior compartment of the forearm and ends before the anterior interosseous artery pierces the IOM[2].

1.3 The interosseous membrane of the forearm

1.3.1 Development of the IOM

Research about the development of the IOM is scarce. Three researchers in Argentina investigated the IOM in 32 embryos and foetuses aged between 7 to 22 weeks.[3] They noted that mesenchymal tissue builds up in between the radial and ulnar perichondrium and retracts around the 7th to 8th week, leaving the IOM. Further, they found out that the proximal anatomical structure of the IOM in the foetuses corresponds to the version in children and adults. The distal part, however, seems to develop later. The authors hypothesised that the proximal IOM is formed after "a preestablished pattern", whereas the distal part develops corresponding to stress and strain during wrist and forearm movement[3]. A German research team examined the fibre architecture of the IOM in twelve donor neonates aged 28 weeks and older[4]. At this point of development, they were able to distinguish between the central band, the accessory bundle, the anterior and posterior chorda oblique, and the distal ascending bundle[4]. This refutes the hypothesis of the Argentinian researchers that the distal part of the IOM develops in childhood through the movement of the forearm[3]. The fibre architecture and the insertion angles of the individual parts of the IOM and the radius and ulna resembled those in adults[4]. Kreutzer et al. hypothesised that the IOM serves as muscle origin for the deep arm muscles. Further, they assume that the deep muscles and the IOM form a functional unit to prevent the radius from proximal and distal migration[4].

1.3.2 Anatomy and Function of the IOM

In current anatomical textbooks, the IOM receives only little attention and is described as "sheet of fibrous tissue that joins the radius and ulna in a syndesmosis"[5] or similar. Multiple studies, however, show that the anatomy of the IOM is far more complex. In addition to the morphology, numerous researchers investigated the function of the IOM in the forearm. In 1989, Hotchkiss et al.[6] examined the IOMs in twelve donors and measured their thickness and mechanical stiffness. The researchers found out that there is a consistent structure present in all donors, they named it "central band". This central band is attached approximately 3,2 cm distally from the ulnar styloid and is proximally attached to the radius. Its width measures around 3.5cm from ulna to radius and approximately 2.6 cm when measured according to the fibre direction. Although only maximally 0.94 ± 0.2mm thick, the central band was still 3-4 times thicker than the other parts of the IOM.[6] The researchers showed that the stiffness of the IOM varies depending on the position of the forearm. In their experiments, the IOM was the stiffest in supination, then in neutral position and less stiff in pronation. Hotchkiss et al.[6] investigated the IOM not only to explore its anatomy but also to explore its role in the prevention of proximal migration of the radius. They found that without radio-capitellar contact,

for example, after radial head trauma and excision, the central band is the essential stabilizer and prevents the radial head from migration. They concluded that injury to the central band might reduce longitudinal stability and lead to proximal migration of the radius. Based on their findings that the IOM is stiffest in supination and less stiff in pronation[6] and on findings of Morrey et al.[7] that in supination of the forearm, there is decreased contact at the radio-capitellar joint, Hotchkiss et al.[6] hypothesised the following: there might be an increased demand in supination of the forearm on the central band to guarantee effective load sharing through the radio-capitellar joint. To accommodate this increased demand, the central band gets stiffer[6].

In 1987, Werner et al.[8] investigated the functional relationship between the deep extensor and flexor muscles and the fibres of the IOM. They examined the IOM and its muscle attachments in 33 donors and discovered that the connective tissue bundles in the central portion of the IOM run in the direction of forces applied onto the IOM by the tension of the two muscle groups. In the proximal and distal parts of the IOM, no functional relationship was seen regarding the attachment of muscles and the direction of connective tissue bundles. Werner et al.[8], therefore, state that the central portion of the IOM is functioning as tendon of origin.

In 1997, Skahen et al.[9] pursued the aim to define the IOMs anatomy as well as to investigate the role of the IOM in longitudinal stability of the forearm. Therefore, they examined 20 forearms and found three consistent structures: a central band, accessory bands as well as a ligament they called proximal interosseous band. Secondly, in six forearms, they investigated the dynamic strain response of the central band towards loading and rotation of the forearm with and without radial head. They established that under physiological conditions, strain on the central band is most significant in neutral position and is slightly reduced in pro- and supination. Without radial head, the strain on the central band is generally higher and increases from supination over the neutral position towards pronation. Skahen et al.[9] support Hotchkiss`s hypothesis that the central band works together with the triangular fibrocartilage complex as secondary stabilizer of the forearm and, without the radial head, becomes the primary stabilizer. They suggest that in some individuals, after radial head removal, the central band might get insufficient over time as primary stabilizer, and these patients may suffer from late instability symptoms of the distal radio-ulnar joint. Skahen et al.[9] recommend reconstructing the central band in neutral position as, under physiological conditions, strain is highest in this position, probably as a compromise to guarantee optimal longitudinal and transversal stability during forearm rotation.

In 2009, Noda et al.[10] decided to define and standardize all IOM ligaments consistently and measure their attachments. The researchers examined 30 forearms of 15 donors and assigned the found structures into proximal membranous, middle ligamentous, and distal membranous portions[11]. In total, they found five regularly present structures: the proximal oblique cord, the dorsal oblique accessory cord, the central band, the accessory band, and the distal oblique

bundle. The proximal membranous complex lays under the flexor digitorum profundus anteriorly and supinator muscle posteriorly. The proximal oblique cord was found in all donors in this portion and originated from the ulnar tuberosity and inserted more distally into the radial tuberosity. The mean width of the proximal oblique cord measured 3.7 ± 1.6mm, and its mean thickness was 1.1 ± 0,5mm. The dorsal oblique accessory cord was also found in the proximal membranous complex but was only present in 16 out of the 30 arms. It started distally from the ulnar shaft and inserted into the interosseous crest of the radius. The mean width lays at 3.2 ± 1mm, and the mean thickness at 0.9 ± 0.2mm. This ligament corresponds presumably to Skahens[9] proximal interosseous band. In the middle ligamentous complex, Noda et al.[10] confirmed the presence of the central band in all specimens. They noted its origin at the interosseous crest of the radius and its insertion at the interosseous border of the ulna. The researchers measured a mean width of 9.7 ± 3mm and a mean thickness of 1.3 ± 0.2mm. These values differ slightly from Hotchkiss et al.[6] measurements, which can probably be led back to the interindividual variances seen in the wide range of central bandwidth from 4.4-16mm in Nodas study[10]. Further, Noda et al.[10] found accessory ligament structures next to the central band in the middle ligamentous complex: the so-called accessory band. The fibres run mostly in the same direction as the central band, and most ligaments were seen distally to the central band. Only in three specimens no ligaments corresponding to accessory bands were seen distally to the central band. Inversely, proximally to the central band accessory band structures were only seen in 13 specimens. One structure was found in the distal membranous portion: the distal oblique bundle. It was clearly present in twelve specimens. The origin of the distal oblique bundle lays at the distal ulnar shaft next to the origin of the pronator quadratus, and its fibres blend into the capsular tissue of the distal radio-ulnar joint and insert into the sigmoid notch of the radius.

Noda and his colleagues[10] hypothesised that the distal oblique bundle functions as a stabilizer at the distal radio-ulnar joint together with the triangular fibrocartilage complex. They assume that the accessory band has only a complementary role to the central band because of its wide anatomical variations. In addition, based on previous literature and their findings, they hypothesize that the proximal oblique cord has no vital function in humans[10].

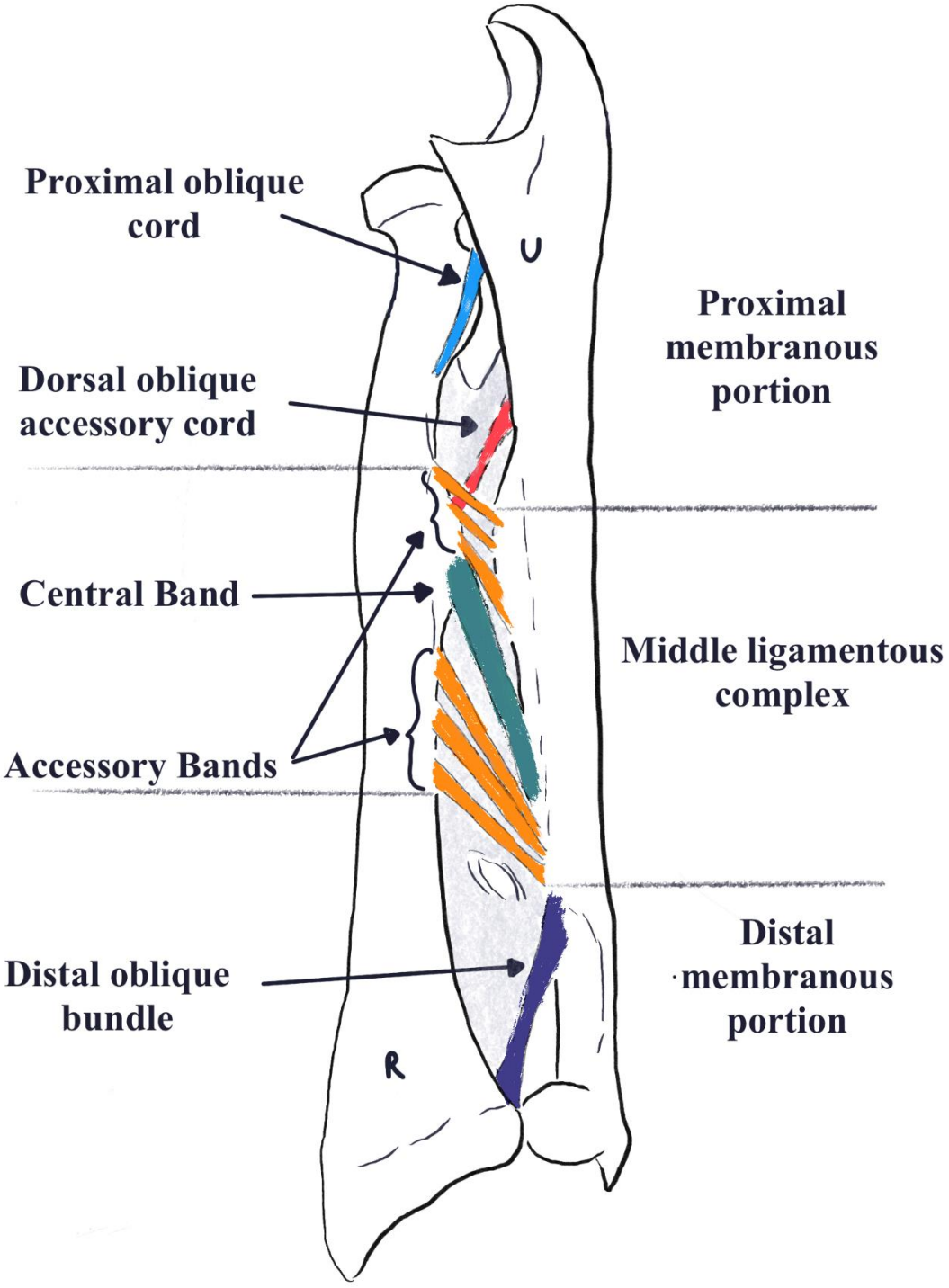

Figure 1: **Left forearm with the individual bands of the IOM modified after Noda et al.[10]**
R = Radius, U= Ulna
The IOM is divided into three portions: the proximal membranous portion, the middle ligamentous portion, and the distal membranous portion. These portions of the IOM consist of a membranous connective tissue sheath, and thicker areas, which are band-like or ligamentous. Proximally lies the proximal oblique cord (light blue) and the dorsal oblique accessory cord (red). Centrally lies the central band (turquoise) surrounded by accessory bands (orange). The distal oblique bundle is located distally (purple).

Moritomo et al.[11] investigated the changes in length of the five different IOM ligaments in vivo during supination, pronation, and in a neutral position. In addition, they examined the axis of forearm rotation and its relationship with every ligament. They found only little length changes in the central bands (mean difference 0,7mm), accessory bands (mean difference 2,1mm), and distal oblique bundles (mean difference 0,6mm). The proximal oblique cords were significantly longer in pronation than in the neutral position or in supination. The average mean difference between pronation and the neutral position was 4.2mm. The dorsal oblique accessory cord changed as well significantly in length during forearm rotation – in average 4.7mm between pronation and supination. The axis of rotation of the forearm was similar in all donors and ran along the ulnar attachments of the central band, the accessory band, and the distal oblique bundle. The proximal oblique cord and the dorsal oblique accessory cord have no attachment along the axis of rotation. The researchers offered the hypothesis that the distal three ligaments are isometric and stabilize the forearm. The slight reduction in length, which was measured here, could be brought upon by the muscle strain of the pronator quadratus muscle during pronation. Further, the authors hypothesise that the distal oblique cord might work as a secondary stabilizer of the distal radio-ulnar joint. As it was only present in 40% of cadavers in Nodas study[10], it might explain why there are great differences between patients suffering from triangular fibrocartilage complex injuries. Patients with a triangular fibrocartilage complex injury and distal oblique cord might suffer less instability of the distal radio-ulnar joint than those without a distal oblique cord acting as a secondary stabilizer. Finally, they concluded that the proximal oblique cord, as well as the dorsal oblique accessory cord, might act as restraints from excessive pronation and not as isometric stabilizer[11].

Hohenberger et al.[12] were interested in the true prevalence of the distal oblique bundle and investigated 185 Caucasian forearms for its presence. They defined it as structure thicker than 0,5mm based on Nodas previous results[10] and identified it in 53 forearms corresponding to 29%. Poitevin et al.[13] found a distal oblique bundle in all of their 20 forearms but stated that in 14 (70%) forearms, this structure was rather membranous, whereas in 6 (30%), it was cord-like. Both results differ greatly from each other and from Noda et al.[10], who found it in 40% of their cadavers. A possible reason might be different definitions regarding this structure, i.e., Hohenberger et al.[12] might have excluded all membranous structures as they did not reach the 0,5mm minimum thickness as previously defined by Noda et al.[10].

In 2020, Carrillo et al.[14] created three-dimensional models of five different IOMs via micro-CT scans and explored the tensile properties of the dorsal oblique accessory cord, the central band, the distal accessory band, and the distal oblique bundle. The proximal oblique cord was not found in any of the five forearms. They found more proximal attachment sites for the accessory

band as well as for the distal oblique bundle than Noda et al.[10]. To investigate the tensile properties of the different ligaments, Carrillo et al.[14] measured amongst other their cross-sectional area and their ultimate failure strain. With ultimate strain, all fibres of the accessory band ruptured in the middle, the central band ruptured at its proximal ulnar and distal radial attachment sites. Both distal oblique bundle and dorsal oblique accessory cord tore at their ulnar attachment. The ultimate strain to rupture the central band was 2% higher than in any other ligament. The sites of rupture correspond to the thinnest cross-sectional areas. The central band had the widest, which may be, following the authors, a reason for its higher strain resistance. Another important aspect was the high stiffness of the dorsal oblique accessory cord, 77% higher than the stiffness of the central band. The authors suggest, therefore, that the dorsal oblique accessory cord has an important role in stabilizing the proximal forearm.

In 2020, two research teams explored the biomechanical properties of the IOM. Each investigated the IOM divided into its proximal, middle, and distal portions. Bin Abd Raza et al.[15] observed the greatest strain on the IOM during pronation, although the absolute displacement of the IOM between pro- and supination was minimal. They concluded that the IOM provides rather static stabilization than rotational. Kholinne et al.[16] observed the central band to have the greatest tensile strength and the greatest ability to withstand plastic deformation under loading. Further, they found the proximal and the distal portions to be stiffer than the central band. They derive that the proximal and distal portions maintain proximal stability during wrist and elbow movement.

Rein et al.[17] explored the histology of the IOM in 2020. They dissected eleven forearms for six ligaments, the proximal oblique cord, dorsal oblique accessory cord, proximal accessory cord, central band, distal accessory cord, distal oblique bundle, and prepared the specimens histologically. They found predominantly densely packed parallel collagen fibre as well as some mixed tight and loose parallel collagen fibres. They discovered a significantly higher number of elastic fibres within the distal oblique bundle and the proximal oblique cord. Elastic fibres were absent in some structures, predominantly in five central bands and seven dorsal oblique accessory cords. Elastic fibres within the ligaments were equally distributed, leading the authors to the hypothesis that the equal elasticity is crucial in forearm rotation. The authors hypothesised that the parallel and densely packed collagen fibres in most structures are a sign of unidirectional tensile strength along the direction of the ligament. On the one hand, the absence or small number of elastic fibres in the central band may underline its resistant nature toward tensile forces, whereas, on the other hand, the distal oblique bundle and proximal oblique cord with their proximity to the distal radio-ulnar joint and proximal radio-ulnar joint have a higher number of elastic fibres reinforcing their supportive role in forearm rotation.

Kholinne et al.[18] were also interested in the histology of the IOM but concentrated on its insertion into the radius and ulna. Other than most of the previous researchers, Kholinne et al. investigated the IOM divided into three components, the proximal, middle, and distal portion. At the interface of bone to IOM, they identified four layers: a lamellar bone layer, a thin mineralized fibrocartilage layer, an oblique collagen layer, and an interwoven collagen layer. These layers were not distinct but rather a gradual shift of tissues. They considered the thin mineralized fibrocartilage layer as an anchoring layer for the collagen fibres and called it tidemark. They found out that the tidemark of the middle portion is thicker than that of the other two components and hypothesise that a higher number of mechanical signals received by the central band ultimately lead to cell remodelling. Kholinne et al. classify the IOM as a ligament[18].

Anderson et al.[19] were interested in the role of the IOM regarding transversal stability of the forearm and discovered that the central band played a major role in preventing the radial head from dislocation. Werner et al.[20] had a similar interest but focused on the transversal stability of the distal radio-ulnar joint after injury to the IOM. They found out that the IOM is crucial in stabilizing the distal radio-ulnar joint during forearm rotation, especially in supination. They propose to reconstruct the central band in persistent distal radio-ulnar joint instability and after reconstruction of the dorsal radioulnar ligament and palmar radioulnar ligament.

Kholinne et al.[21] also examined the mechanical properties of the IOM in a dynamic setting and focussed on the central band, a proximal band, and a distal band. They discovered that the central band is under constant strain during forearm rotation, whereas the strain on the proximal and distal bands was higher and fluctuating. They concluded that the proximal and distal bands have a different role than the central band because of this strain variation.

Birkbeck et al.[22] showed that the IOM plays a crucial role in load transfer from the radius at the wrist to the ulna at the elbow. After the incision of the IOM, there was no load transfer between the radius and ulna anymore.

LaStayo et al.[23] and Soubeyrand et al.[24] even went so far as to categorize the IOM as a joint because it connects the radius and ulna, provides stability, and allows for movement. They called it the middle radioulnar joint, and Soubeyrand et al.[24] argued well how the fibre structure of the central band reflects its supportive role in transverse and longitudinal stability: The oblique running of fibres sums up two vectors: a transverse vector where the fibres limit the interosseous space expansion and a longitudinal vector where the fibres compromise proximal migration of the radius[24].

In summary, it is widely accepted that the IOM consists of up to five distinct ligaments classified by Noda et al.[10], six if proximal and distal accessory bands are present[17]. These

ligaments run in different directions and are partly overlapping[10]. However, because of the great anatomical variation of these ligaments, in recent studies, researchers focussed often on the proximal, central, and distal portions of the IOM[15,16,18,21]. Further, it was found that the single ligaments consist of different layers of connective tissue[18]. Therefore, displacement regularly occurs between the single ligaments and between the fibres of a ligament.

Regarding the function of the IOM, it is widely accepted that it acts as muscle attachment[2,22,24] and load transmitter[22,24]. Most researchers agree that especially the central band functions as secondary stabilizer of the forearm, providing longitudinal as well as transversal stability. Nonetheless, regarding the other ligaments, no consensus about their function is yet reached. It is striking that the IOM is highly researched regarding its biomechanical role, but only very few researchers question its role in sensory feedback[14,25].

1.3.3 Clinical interest in the IOM

The scientific interest in the function and morphology of the IOM is unbroken. Many researchers and surgeons hope that new knowledge about its properties may improve patient outcomes after forearm traumata.

Diagnosis of Injury to the IOM

Studies have been conducted to establish the reliability of ultrasound in diagnosing the presence of the distal oblique band[26] or in diagnosing an injury to the central band[27]. In both studies, ultrasound proved to be a useful diagnostic tool, in the latter study[27], MRI scans were tested as well and were proven similarly useful.

Essex-Lopresti Injury

In 1951, Essex-Lopresti[28] described two cases of men with comminute radial head fractures, instability of the distal radio-ulnar joint and injury to the IOM. Both men suffered from a longitudinal compression force upon their forearms as trauma mechanism. This triad of symptoms: radial head fracture, distal radio-ulnar joint disruption, and IOM rupture is since known as Essex-Lopresti injury[29]. Before him, there was only one case-report by Curr and Coll[30], which is widely accepted as first description of this kind of injury[28,29,31].

Essex-Lopresti injuries are rare and are often missed at primary diagnosis of radial head fracture[31]. They constitute a problem to the longitudinal stability of the forearm[24].

Many studies focus on the reconstruction of the IOM to enhance forearm stabilization after Essex-Lopresti injury[32,33]. Masouros et al.[34] compared three different regional grafts after removal of the radial head and incision of the IOM in donors. After IOM incision, the forearm was fully destabilized. The researchers used the pronator teres, the brachioradialis, or the flexor carpi radialis tendons to reconstruct the IOM and investigated the stability of the grafts. All

grafts yielded good results in re-establishing stability of the forearm, especially the pronator teres graft, however, no graft was as good in preventing radio-ulnar displacement as the intact IOM.

Monteggia and Galeazzi Fractures

In 1814, Monteggia[35] described an injury pattern consisting of a fracture of the ulna shaft and an anterior dislocation of the radial head. Since then, this injury pattern has been known as Monteggia fracture.

Galeazzi[36] presented 18 cases of radius shaft fracture and dislocation of the distal radio-ulnar joint in 1934 since this injury pattern is named after him. Both fracture types impair the transversal stability of the forearm.[24]

Brachial Plexus Birth Palsy

In children with brachial plexus birth palsy, the supination deformity exacerbates with time because of IOM contracture[37]. Therefore, release of the IOM is one key strategy in improving those patients' outcomes[37].

Complex Regional Pain Syndrome

Complex Regional Pain Syndrome Type I (CRPS Type I) is a chronic pain condition in the extremities characterised by persisting pain which is disproportionate to any triggering event (e.g., trauma or operation to the limb)[38,39]. Further, patients present with changes in sensory, vasomotor, sudomotor and/or motor modalities and no other diagnoses explain their symptoms better[38,39], i.e. CRPS Type I is a diagnosis of exclusion.

The pathophysiology of CRPS Type I is still largely unknown, although multifactorial pathogenesis seems to underly. Three widely discussed hypotheses suggest exaggerated neurogenic inflammation, sympathetic-afferent coupling, or re-organisation of the central nervous system as pathophysiological mechanisms[40].

The incidence rate lies between 5.46 to 26.2 per 100 000 person years[41-43]. Some accepted risk factors for the development of this condition are intra-articular fractures and fractures of the distal radius[44,45]. CRPS Type I is more common in the upper extremity (59.2% vs. 39.1%)[43]. Postmenopausal women seem to have a higher risk of developing CRPS than men[41,44,46].

The sensory role of the IOM within CRPS Type I, e.g., in the form of sympathetically maintained pain, has not yet been investigated.

1.4 Mechanoreceptors

1.4.1 General

Proprioception is commonly known as the sixth sense, providing us with information about the position of our body in the room, perception of movement of our body, and detection of forces applied to our body[47,48]. It is crucial for any interaction with the environment, and a loss of it is as rare as devastating[47]. The term proprioception was coined by Sherrington in 1907[49]. He chose it as a combination of the terms "proprio" (oneself) and "reception". Derived from this term, he called the receptors proprioceptors. For Sherrington, proprioception was a sensation coming from within the body, from within the "deep field", and therefore, proprioceptors were also receptors within the deep field. However, he also acknowledged that proprioception depends not only on the information from the "deep field" but also on information from the outside world, the "extero-ceptive field"[49].

1.4.2 Distribution of mechanoreceptors

For a long time, researchers were differentiating between mechanoreceptors, superficial receptors within the skin and subcutaneous tissues, and proprioceptors, muscle and joint receptors, especially muscle spindles and Golgi-Tendon organs[48]. However, Mueller et al., pointed out that this definition might create the impression that only the latter two sensory nerve endings are responsible for proprioception, which is not the case.[48] Proprioception is created by a finely tuned and matched cooperation of a multitude of receptors within all tissue layers. To avoid confusion by mixing different terms, the term mechanoreceptors will be used in the following to describe all sensory nerve endings which are sensitive to mechanical stimuli and thus provide information for proprioception.

It is known that some mechanoreceptors are only present in certain tissues: Meissner and Merkel cells are only present in cutaneous tissues[50], whereas Golgi-tendon organs are limited to transition zones of muscle to tendon and rarely tendons, ligaments, and joint capsules[48], as well as muscle spindles which are limited to muscle tissue[48]. Other mechanoreceptors have been found in several tissues: Ruffini bodies within the skin, joint capsules, fascia, iris, dura mater, amongst others[48], and Vater-Pacini corpuscles in the dermis and subcutis as well as in fascia, ligaments, periost, peritoneum, pancreas, genital region, and more[48].

Until now, there is no study investigating the total number of mechanoreceptors within the human body, but a recent estimation offers various hundreds within one cubic centimetre of human tissue[48].

1.4.3 Types of mechanoreceptors

In his comprehensive review of nerval expansions in the human skin in 1905, Ruffini summarised the then current state of knowledge about dermal proprioceptors. As many original descriptions by the first describers were written in different languages and independent of each other, Ruffini managed to gather the knowledge together and to add his own findings. His manuscript is often seen as the first gold standard description of proprioceptors.[51]

In his manuscript, Angelo Ruffini explains how to differentiate between a new nerval expansion form and only a new variety. He compares the terms form to the biological classification term "genus" and variety to the term "species". Genus is a generic term describing a class of plants, animals, etc., e.g., monkeys. Species is a more specific term for classifying subgroups, e.g., chimpanzees. Ruffini points out that generic factors defining a form of nerval expansions include their external configuration, including its size, the presence or absence of structures such as the capsule or the inner supporting structures, the central nerve structure, and the blood supply. A variety of nerval expansion results in a variation or absence of generic factors. Therefore, generic factors are differently valued: some factors have no or only secondary value and do not really define a variety, e.g., the corpuscle size or the form of the supporting tissue. Other factors, e.g., the central nerve structure or the presence or absence of a capsule, is of "capital value". Therefore, he argues that Golgi-Mazzoni corpuscles are a real variety of the Vater-Pacini corpuscle form.

Vater-Pacini corpuscles

Vater-Pacini corpuscles are named after their first describer in 1719, Abraham Vater, and Filippo Pacini, who detailly portrayed these structures in 1831.[51]

Ruffini studied them extensively and summarised his findings in his manuscript in 1905.[51] He describes Vater-Pacini corpuscles as pearly white structures measuring between 1 to 4cm in length and at least 1cm in width and, therefore, macroscopically visible. They are ovoid shaped and have two poles. Through one pole the myelinated nerve fibre enters the corpuscles. He differentiates them into five different parts:

1. The capsule
2. The internal bulb
3. The central nerve fibre
4. The nerval apparatus of Timofeew
5. The blood vessels

The capsule is formed by around 20 to 60 lamellas, which are concentrically arranged, similar to an "onion bulb". The internal lamellas are more closely ordered than the external. They are

separated from each other by lymph fluid. However, some connections via trabecular structures are present. Each lamella is covered by endothelial cells. Ruffini describes the capsule as a continuation of the perineural sheath of the central nerve fibre belonging to the Vater-Pacini corpuscle.[51]

The internal bulb is the cylindrical body surrounded by the lamellas. In the middle of the internal bulb is a path for the central nerve fibre. The rest of the bulb is filled with a "granulated protoplasmic mass". The internal bulb is formed by fibrillar connective tissue, resulting from the subsidiary sheath of the central nerve fibre.[51]

The central nerve fibre is covered by four different sheets: the myelin sheath, the Schwann sheath, the subsidiary sheath, and the perineural sheath. As previously described, the subsidiary sheath gives rise to the internal bulb, and the lamellas of the corpuscles are formed by the perineural sheath. The myelin and Schwann sheets disappear at the "étranglement preterminal", a bottleneck within the corpuscle. After this bottleneck, the nerve fibre runs without covering within the path in the internal bulb and ends at the other pole in a bulge. Ciaggio[52] stated that this final bulge corresponds to the nerval end.

The nerval apparatus of Timofeew consists of a thin, myelinated nerve fibre that enters the corpuscle by the same pole as the bigger central nerve fibre. After the bottleneck, the small nerve fibre divides into a number of smaller filaments, interlacing with each other around the central nerve fibre. Ruffini named this structure apparatus of Timofeew in 1895 after his first observer.

There are multiple blood vessels supplying the Vater-Pacini corpuscles. The arterioles enter the corpuscles most often by one of the poles and give rise to many smaller arterioles and capillaries supplying the lamellas. The arterioles and capillaries generally run tortuously and end in venules, which leave the corpuscle from multiple exits.

Ruffini points out that there is a variability of Vater-Pacini corpuscles, especially regarding the sizes. The description above applies especially to the common, bigger corpuscles. The smallest Vater-Pacini corpuscles have a very typical morphology and are called Golgi-Mazzoni corpuscles.

Vater-Pacini corpuscles are rapidly adapting receptors (RA-II) and detect vibration between 10-1000 Hertz and acceleration of movements[48]. It is assumed that they also react to pressure[50]. They react to the onset and offset of a stimulus[53], and their receptive fields are broad, which means that localization of stimuli is rather poor[54]. Through bones, joints, and teeth, vibration is transmitted, therefore, one stimulus often activates multiple Vater-Pacini corpuscles in the body[48].

Golgi-Mazzoni corpuscles

Golgi-Mazzoni corpuscles were first discovered by Camillo Golgi in 1878 in human connective tissue and perimysium[55] and detailly described by Vittorio Mazzoni in 1890[56]. Ruffini named them Golgi-Mazzoni in 1894 after finding them in the subcutaneous connective tissue of the finger pad in humans[57]. Golgi-Mazzoni corpuscles can have multiple shapes and varying sizes. Similar to the bigger Vater-Pacini corpuscles, their structure can be divided into:

1. The capsule
2. The internal bulb
3. The central nerve fibre
4. The nerval apparatus of Timofeew
5. The blood vessels

The capsule is formed by a varying number of lamellas, rarely only one. If there are multiple lamellas, their structure is similar to those in the Vater-Pacini corpuscles.

The internal bulb is massive in comparison to the size of the corpuscle and mirrors the form of the capsule. It is formed by the subsidiary nerve sheath.

In Golgi-Mazzoni corpuscles, one single or more central nerve fibres, all subdivisions of one central nerve fibre, can enter the corpuscles via one pole. The central nerve fibre(s) then behave in two distinguished ways: more often, the fibre divides into multiple little strings which tortiously run towards the extremity of the internal bulb, in certain corpuscles even completely filling the internal bulb. In other corpuscles, the fibre also divides in multiple little strings which run tortuously towards the extremity of the bulb but without forming a dense web like in the previous type of Golgi-Mazzoni corpuscles.

The nerval apparatus of Timofeew is formed by one or more small nerve fibres which can enter the corpuscle everywhere. At the beginning of the internal bulb, they divide and form a plexus. Sometimes, the fibres enter the internal bulb and mix with the central nerve fibre, sometimes, the fibres form a net around the bulb.

The blood supply in Golgi-Mazzoni corpuscles depends upon their sizes: the smallest corpuscles are not supplied by blood vessels but lay next to capillaries. Bigger corpuscles are tightly surrounded by capillaries, of which one or two enter the corpuscles.

In comparison to Vater-Pacini corpuscles, Golgi-Mazzoni corpuscles consist of two or more axons with corresponding capsules or inner bulbs[48,51] (see Figure 2). Thereby, they can detect stimuli from different directions. As Golgi-Mazzoni corpuscles are a variety of Vater-Pacini

corpuscles, it is assumed that they detect the same stimuli, which means vibration, pressure, and acceleration of movements[48,50].

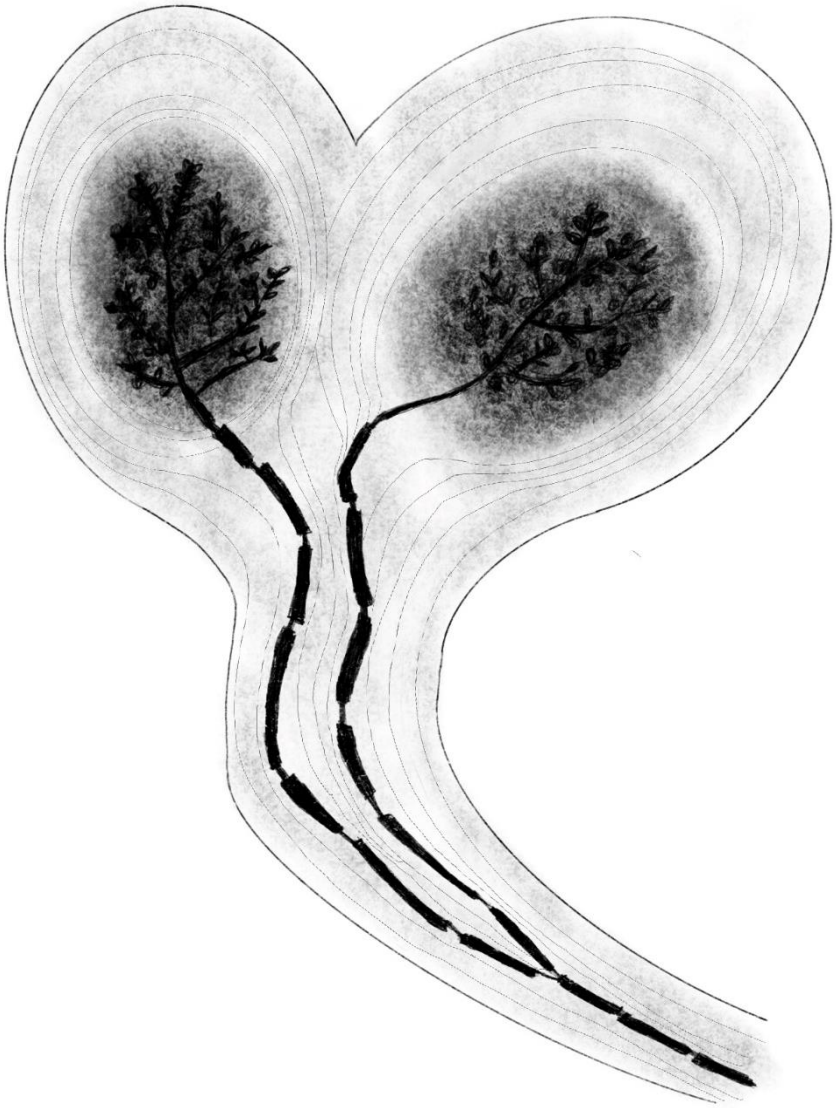

Figure 2: **One Golgi-Mazzoni corpuscle consisting of two capsules adapted and modified from Ruffini[57]**

Ruffini bodies

Angelo Ruffini was the first observer and describer of the after-him named Ruffini bodies in 1891. Ruffini bodies vary greatly in size, and in his manuscript from 1905, Ruffini describes the biggest bodies, which are defined as typical ones. Their form is fusiform or cylindrical. Their length varies between 0,24 to 2mm and 0,05 to 0,2mm or bigger in width. Ruffini divides the structure of Ruffini bodies into

1. The capsule
2. The supporting tissue

3. The central nerval expansion
4. The unmyelinated fibre plexus
5. The blood vessels

The capsule is composed of four to five lamellas, formed by the sheath of Henle of the entering nerve fibre. At the beginning of the corpuscle, the sheath of Henle separates from the nerve fibre and forms funnel like, thin, and tightly adhering lamellas. These lamellas cover the underlying supporting tissue. The lamellas end at both extremities of the Ruffini body, fading one by one away.

The supporting tissue lies underneath the capsule and is generally shaped fusiform. Therefore, Ruffini also called it "fuseau de soutien", translatable to supporting spindle. The size of the supporting tissue is variable and not necessarily related to the size of the central nerve expansion. The supporting tissue ends before the extremities.

The central nerval expansion is most often formed by one big central nerve fibre, dividing into smaller, secondary fibres, all entering one Ruffini body. The fibres can enter the Ruffini body from everywhere, rarely even by the extremity. After the sheath of Henle separates at the beginning of the body, the myelin sheath and the Schwann sheath stop at a preterminal narrowing. The pale fibre continues and ends in numerous branching of small and short nerve fibres, which are all connected to each other and thereby form a continuing expansion.

Next to the central nerval expansion, there exists another reticulum of small and delicate nerve fibres within the Ruffini body. These fibres have little expansions, Ruffini describes them as looking like "gracious little garlands". Although he could not say where these nerve fibres are coming from, he noticed that sometimes they mix with the central nerve expansions, and sometimes they just surround it.

Ruffini bodies have their own blood supply. Capillaries run next to the central nerve fibre and divide before joining the capsule into secondary branches, which closely encircle the corpuscle. The capillaries do not enter the spindle of supply.

Ruffini bodies are slowly adapting receptors (SA-II) with wide receptive fields and, therefore, poor localization of stimuli[48]. They react to stretching stimuli and are important for proprioception as they add information about movements[48].

Golgi Tendon organs

Camillo Golgi[58] wrote an extensive review in 1878 about musculo-tendinous end organs and their function. These were soon named after him: Golgi-Tendon organs. He described them as follows: They are only present at the tendon origin or at the transition zone of muscle tissue to tendons. They are fusiform, and one of the ends is always in contact with the fascia of the

muscle. The other end often separates into a bifid end and fades into the tendon. Golgi describes their size as varying between 70-120µm in width and 300-800µm in length.[59] Most often, one nerve fibre, but sometimes up to four, tends to enter the organ by the extremity on the side of the tendon. Within the organ, the nerve runs toward the middle and then divides into further smaller fibres which run toward the periphery.[59] The organ is composed of collagen fibres running parallel with the muscle fibres, it is attached to[60]. Golgi Tendon organs have a low threshold and are fast conducting mechanoreceptors[60]. Their stimulus is muscle contraction, and they give feedback about muscle tension[60].

Muscle spindles

Muscle spindles are stretch-sensitive mechanoreceptors that are found abundantly in mammalian muscles[61]. Thoroughly described by Barker in the cat in 1948[58], in humans, they were first described in intercostal muscles by Davis in 1973[62]. Muscle spindles consist of spindle-formed connective tissue capsules surrounding specialised, striated muscle fibres which are positioned on the same axis as the surrounding muscle fascicles.[61]

They are innervated by afferent nerve fibres in the centre and at the poles of each capsule.[61] Muscle spindles react on changes in muscle length.[61] The afferent nerve fibres can functionally be separated in group Ia (primary) and group II (secondary) nerve fibres. The primary nerve fibres have a larger diameter and therefore are faster conducting. Each muscle spindle is supplied by a single group of Ia nerve fibres which spiral around each intrafusal fibre in the centre. Zero to five group II nerve fibres supply one muscle spindle, spiraling each around one nerve fibre. Both afferents differ in their reactions: primary afferents fire on dynamic stretch, whereas secondary afferents rather fire regularly on tonic movement.[61] In contrast to any other proprioceptor, muscle fibres possess not only an afferent but also an efferent nerve innervation via gamma motorneurons.[61] It is assumed that the gamma motorneurons help restore the sensitivity of muscle spindles by contracting the intrafusal muscle fibres and restoring tension after desensitization through extrafusal muscle contraction.[61]

1.4.4 Other classifications of mechanoreceptors

Since their original descriptions, these mechanoreceptors have been further investigated by a multitude of researchers. Although some researchers were working closely with the drawings and descriptions of the original publications, bias through different histological preparation techniques as well as anatomical variations of structures in different tissues, different donor animals, and introductions of synonyms led to confusion and inconsistent reports of morphology. Therefore, descriptions of mechanoreceptors vary vastly. Freeman and Wyke tried to solve this problem by introducing a new classification system for mechanoreceptors in joints.[63,64]

Freeman and Wyke examined different joints in the cat and categorised the articular nerve endings they found in "an arbitrary numerical classification"[63]. They state their aim is to avoid confusion caused by multiple different names for the same nerve endings and differences between non-articular and articular nerve endings. Freeman and Wyke divide the articular nerve endings they found into four types according to their morphology: Type I to III are mechanoreceptors and Type IV encompasses unorganized nerve terminals, i.e., vasomotor endings or pain receptors.

Type I endings are "globular or ovoid" corpuscles with a thin capsule consisting of one to two cell layers. The corpuscle sizes vary between 40µm to 100µm. Through a hilar indentation on one side, a small, myelinated axon supplies the corpuscle, losing its myelin at the hilum. Within the corpuscle, the axon divides into smaller filaments, forming an arborisation. A small blood vessel enters the corpuscles together with the axon and divides within the corpuscles into multiple smaller blood vessels forming arcades. Next to the myelinated axon and the blood vessel, a very small, unmyelinated nerve axon enters the corpuscle as well and breaks up into a multitude of thin filaments spreading around the capillary arcades. These endings are predominantly found in clusters of 3-6 corpuscles in fibrous capsules of joints, on joint ligaments as well as in tendons and aponeuroses. The clusters are arranged in three dimensions, and all corpuscles within them are innervated by one parent axon. Freeman and Wyke identify the cluster of corpuscles as mechanoreceptor not every single corpuscle[63]. They classify these clusters as low threshold and slowly adapting sensory nerve endings and list Ruffini endings. Previous used eponymous for Type I endings are Ruffini endings, Golgi-Mazzoni endings, Meissner corpuscles, Spray-type endings, Basket endings, Ball-of-thread endings, and Bush-like endings.

Type II endings are "elongated, conical corpuscles" within a multiple layer thick connective tissue capsule, which is larger at its base. The corpuscles measure around 280µm in length and 120µm in width. A single myelinated nerve fibre joins the capsule and loses its myelin sheath at the base of the corpuscle. Unmyelinated but surrounded by a sheath of columnar cells from the capsule, the nerve fibre runs centrally until the tip of the corpuscle, where it ends. A small blood vessel approaches the corpuscle with the nerve fibre but loops around the capsule arcade-like and little branches pass through the capsule layer and enter the corpuscle. Type II endings are also present in the fibrous capsule of joints next to Type I endings, but they are also found in clusters of two to four in the internal layers of the fibrous capsules next to branching blood vessels as well as in fat pads. All members of a cluster are innervated by a nerve fibre from one parent axon, as these nerve fibres are bigger in comparison to Type I ending fibres, these mechanoreceptors are classified as low threshold and rapidly adapting. Type II endings vary greatly in their morphology, bifid and trifid forms, where the corpuscle divides at the base into

two or three cones, are especially common near branching blood vessels. Previously used eponyms are Krause's Endkörperchen, Vater'sche Körper, Pacinian corpuscle, Vater-Pacinian corpuscle, simple Pacinian corpuscle, Paciniform corpuscle, Golgi-Mazzoni body, Meissner corpuscle, Gelenknervenkörperchen, Corpuscle of Krause, clublike ending, bulbous corpuscle, corpuscula nervosa articularia.

Type III endings are "large fusiform bodies" with a thin capsule. They measure around 600µm in length and 100µm in width. They are innervated by one large myelinated nerve fibre, which loses its myelin sheath on entering the capsule. Within the capsule, the nerve fibre branches into a fine network of filaments. Type III endings are only present in joint ligaments and are therefore classified as "characteristic ligament receptor". The capsule of the ending fades with the fibres of the underlying ligament. Mechanoreceptor and ligament lie on the same axis. Sometimes Type III endings are present in groups of few corpuscles, then each corpuscle is smaller and all corpuscles within a cluster are innervated by branches of the same parent axon. Freeman and Wyke state that there is no sign of an extra nerval innervation or individual blood supply. They classify these mechanoreceptors as high threshold and very slow adapting. They state that "the Type III endings probably represent the articular equivalent (both structurally and functionally) of the tendon organs".[63] Previous eponyms are Golgi endings and Golgi-Mazzoni corpuscles.

Type IV endings are free nerve endings which are further classified into IVa: plexus or free nerve endings and IVb: unmyelinated efferent terminals. Freeman and Wyke hypothesise that Type IVa endings act as nociceptive fibres, whereas Type IVb endings have a vasomotor function.

Freeman and Wyke[63] point out that they would classify Type I endings most likely as Ruffini endings, Type III endings as Golgi-Tendon organs. Although Type II endings might resemble Vater-Pacini corpuscles, the two authors refuse to classify them this way as Vater-Pacini bodies would only exist outside of joints.

In some recent studies, this classification was preferably used[25,65,66]. However, the copious eponyms the authors offered show that their classification may not account for anatomical variations of structures. Further, as they created their classification system based on mechanoreceptors in the cat, it is not clear in how far it can be conferred to the human mechanoreceptors. In addition, they limit their classification system strictly to mechanoreceptors within ligaments and joints[63], which limits its use for studies investigating different tissues.

1.5 Mechanoreceptors in the IOM

While the anatomy and function of the IOM have been investigated and discussed in several studies, its sensory role is still largely unknown.

To our knowledge, only one research team[25] explored the IOM in humans for sensory nerve endings until now. Rein et al.[25] dissected eleven donor arms of six females and one male and tried to extract six ligaments of the IOM (distal oblique bundle, distal accessory band, central band, proximal accessory band, dorsal oblique accessory cord, and proximal oblique cord after Noda et al.[10]). One distal oblique bundle, one dorsal oblique accessory bundle as well as two proximal oblique cords were absent so that 62 specimens were examined. The researchers stained the specimens with histological and immunofluorescent stains. They used the Freeman and Wyke classification[64], modified by Hagert[67] to name the sensory nerve endings found. They found the following mechanoreceptors in descending order regarding their predominance: free nerve endings, unclassifiable corpuscles, Vater-Pacini corpuscles, Ruffini bodies, and Golgi-like endings. In 48 structures free nerve endings were observed, in 24 specimens, unclassifiable corpuscles were seen, 10 specimens contained Vater-Pacini corpuscles, in nine structures Ruffini endings were found and in four specimens Golgi-like-endings were identified. In 13 structures consisting of one distal accessory band, two central bands, two proximal accessory bands, six dorsal oblique accessory cords and two proximal oblique cords, no mechanoreceptors were found.

Free nerve endings were most abundantly found in the distal oblique bundle and in the proximal oblique cord but were present in all ligaments. Vater-Pacini corpuscles were most abundant in the distal oblique bundle. Ruffini endings were seen in the distal oblique bundle, distal accessory band, proximal accessory band, and proximal oblique cord. Statistically, Ruffini endings, Golgi-like endings, and the unclassifiable corpuscles were equally distributed between all structures.

Positive correlation was seen between free nerve endings, Ruffini endings, Vater-Pacini corpuscles and unclassifiable corpuscles. Furthermore, a higher number of unclassifiable corpuscles was seen with a higher number of Golgi-Tendon organs.

In accordance with the literature, Rein et al.[25] found free nerve endings more often than any other sensory nerve ending. They hypothesised that this could indicate that nociception plays a great role in forearm movement and weight loading. They expected to find a statistically clear "polarization" of sensory nerve endings within the ligaments – this was not the case. They theorised that the shifting strain in different movements on the IOM as well as the longitudinal but also transversal stability the IOM provides require a similar distribution of receptors within the ligaments to create an optimal feedback loop. Between the ligaments, a statistically relevant,

greater innervation of free nerve endings and Vater-Pacini corpuscles were seen in the distal oblique bundle as well as the proximal oblique cord, whereas the central band and the dorsal oblique cord were only little innervated. Rein et al.[25] contemplate the proximity to the proximal and distal radio-ulnar joints as the underlying reason so that joint movements can be closely monitored. The positive correlation regarding the presence of different mechanoreceptors was explained with their complementary functions, especially regarding the demanding and complex movements of the forearm.

Limitations of their study were the small number of donors, donor age, post-mortem conditions, and interval, as well as the fact that unclassifiable corpuscles were the second most common sensory nerve endings found and that only two-dimensional analysis of receptors was possible.

Rein and her colleagues derived recommendations for other surgeons reconstructing the IOM. They stated that the central band could be replaced with non-sensory tissue as it seems only sparsely innervated, whereas the distal oblique bundle should be replaced with highly sensorily innervated tissue.

They conclude:

> "Consequently, the IOM plays a crucial role in dynamic forearm stabilization, in which nociception is key. The DOB [distal oblique bundle] and POC [proximal oblique cord] have pronounced proprioceptive functions; therefore, dynamic stabilization of the forearm mainly takes place in the vicinity of the DRUJ [distal radio-ulnar joint] and PRUJ [proximal radio-ulnar joint], whereas the CB [central band] and DOAC [dorsal oblique accessory cord] have primary static functions"[25]

1.6 Sympathetic supply to the IOM

Some researchers examined the sympathetic innervation of the upper extremity, especially regarding the pain syndrome CRPS Type I[68]. Marx et al.[68] were interested in the distribution of sympathetic fibre within the radial nerve just before the cubital fossa and two derivatives: the superficial nerve in the cubital nerve and the superficial nerve at the wrist. The radial nerve has, in absolute terms, the greatest area of sympathetic nerve fibres, but the superficial nerve in the cubital fossa had in comparison to its other fibres, the highest percentage of sympathetic nerve fibres. Balog et al.[69] investigated the sympathetic fibres in the median and ulnar nerves at the wrist level and found more fascicles with corresponding sympathetic fibres in the median nerve. Comparing the number of fascicles in both nerves, the researchers conclude that there is no significant difference between sympathetic fibres within both nerves.

To our knowledge, no study investigating the sympathetic innervation of the IOM exists.

1.7 Aims of the study

This study pursues three aims:

1. To confirm the presence of mechanoreceptors in the interosseous membrane of the forearm
2. To identify the mechanoreceptors, present in the interosseous membrane and in the adjacent tissues
3. To derive implications for clinicians and future research

2. Methods

2.1 Ethics approval and Study Set-Up

This anatomical study numbered 2019-692 was approved by the Ethics committee of the Heinrich-Heine-University Düsseldorf in April 2021.

The data collection consisted of two parts. The first part was performed with the samples of six donors. However, we noticed after staining with the immunohistochemical stains Tyrosine hydroxylase as well as Pan Neurofilament stain that structures were not well demarcated. Similar results were reported by other researchers from our laboratory at that time, different to successful staining results in the previous months and years. Therefore, a trial was started to determine the source of error and to improve the staining protocols. Staining results improved with higher quantities of antibodies and in donors who were only shortly in contact with formaldehyde i.e. shorter time period between entry of death and sample collection. Later, it was detected that the supplier of formaldehyde had started to add more Methanol without notice, a substance with a lot of interference with antibody staining. We circumvent this shortcoming with the new protocol at that time without knowing the reason.

Therefore, we decided to perform a second sample collection. We prepared further sections from donor 4 (entry of death was most recent from the six donors) and stained those according to the new staining protocols. Further, we collected both interosseous membranes of a fresh and unfixed female donor.

To improve the comprehension of the method chapter, we decided to combine both data collection steps in the following. When specimens were treated differently between both steps, it is mentioned separately.

2.2 Utilised Chemicals, Materials and Equipment

The following table (Table 1) lists all chemicals, materials and equipment which were used during the sample collection and preparation of samples:

Utilised chemicals, materials, and equipment for sample preparation	
Chemicals	Formaldehyde solution 37%, acid-free, diluted to 4%, *(Merck, Darmstadt)*
	2-Propanol >99.5% *(Carl Roth GmBH + CoKG, Karlsruhe)*
	Roticlear® *(Carl Roth GmBH + CoKG, Karlsruhe)*
	Paraffin*:* ParaplastPlus®, McCormick Scientific *(Leica Biosystems Richmond Inc.)*
	Roti®Mount ready-to-use *(Carl Roth GmBH + CoKG, Karlsruhe)*
Materials	Airtight containers*,* PP *(Sarststedt, Nürnbrecht)*
	Disposable scalpels (commercial)

	Tissue Marking Dye 2 oz. TMD-2-green *(SMP Chicago, IL)*
	Cassettes, Q Path® MacroStar II *(VWR International GmbH, Darmstadt)*
	Frosted microscope slides, Superior, 76x26x1mm, *(Paul Marienfeld GmbH & Co. KG, Lauda-Königshofen)*
	Securline © Marker II, Superfrost *(Aspen Surgical, Calendonia)*
	FEATHER® disposable microtome blade, *(VWR International GmbH, Darmstadt)* for the microctome Leica RM 2255 and microtome MICROM, HM360
Equipment	Tissue processor, Leica TP1020 *(Leica Biosystems Nussloch GmbH)*
	Paraffin Embedding Center, TES Valida *(MEDITE Medical GmbH, Burgdorf)*
	Metal moulds
	Anatomical Forceps
	Microtome, Leica RM 2255 *(Leica Biosystems Nussloch GmbH)*
	Rotatory Microtome, MICROM, HM360 *(MICROM)*
	Tissue Float Bath, GFL 1052 *(Gesellschaft für Labortechnik mbH, Burgwedel)*
	Drying oven *(Memmert GmbH + Co. KG, Schwabach)*
	Motic Microscope BA410E *(Motic Richmond)*
	Motic EasyScanner Infinity 100 *(Motic Richmond)*
	Extreme Portable SSD 1 TB *(SanDisk)*

Table 1: **Utilised chemicals, material, and equipment for sample preparation**
Listing of chemicals, material and equipment used to collect the samples, fixate the tissues, trim and transfer the specimens to cassettes, and process and section them.

A detailed list with all chemicals, material and equipment used during staining can be found in Table 2 in the appendix. Table 3 summarises chemicals, material and equipment which were used in most histological and immunohistochemical stains.

Summary of utilised Chemicals, Material and Equipment used in most histological and immunohistochemical stains	
General chemicals	Ethanol *(VWR International GmbH, Darmstadt)*
	Xylene (isomers), >98 % pure *(Carl Roth GmBH + CoKG, Karlsruhe)*
	Roti®Mount ready-to-use *(Carl Roth GmBH + CoKG, Karlsruhe)* [except for most immunohistochemical stains]
Material	Human stomach mucosa or human tongue (positive control)
	Super Pap Pen Liquid Blocker *(COSMO BIO co., LTD., Tokyo)*
	Syringe (commercial)
	Filter (commercial)
	Menzel™ Microscope Coverslips *(Thermo Scientific Menzel)*

Equipment	Drying oven *(Memmert GmbH + Co. KG, Schwabach)*
	Pressure cooker (commercial)
	Laboratory pipette (commercial)
	Fridge (commercial, at 4°C)

Table 3: **Summary of utilised Chemicals, Material and Equipment used in most histological and immunohistochemical stains**
Listing of chemicals divided accordingly to the different stains, material and equipment which were used to stain the sections. °C = degree Celsius

2.3 Sample Collection

2.3.1 Inclusion and Exclusion Criteria

To investigate the presence of mechanoreceptors and sympathetic nerves in the IOM, 48 specimens from seven donors were collected. Six of these donors were part of the Heinrich-Heine University Düsseldorf Faculty of Medicine anatomy course. Therefore, the superior muscle structures of the forearms had already been dissected. Important for including the donors were two forearms with intact anterior deep muscle compartments and untouched interosseous membranes (as detailed in table 4). The seventh donor was not part of the anatomy course; therefore, her arms were completely intact.

Inclusion criteria	**Exclusion criteria**
Both arms present	Less than two arms through amputations or for dissection purposes
Intact anterior deep muscle compartment	Manipulation through previous operations or dissections of anterior deep muscles on one or both (left and right) sides
Intact left and right interosseous membranes	Manipulation through previous operations or dissections of one or both (left and right) membranes

Table 4: **List with in- and exclusion criteria for donors**
Listing of in- and exclusion criteria for the choice of the donors to obtain optimal specimens

2.3.2 Donors

The left and right forearms of four female and three male cadavers were chosen. They were aged between 67 and 91 years. The age, sex, and details given in the death certificates are provided in Table 5. All donor details are saved pseudonymously and are encoded by a 4 numbered individual ID. Due to the limited amount of information, which is saved about the donors, no information about previous injuries could be obtained. Recent injuries to the arms were excluded macroscopically before extraction of the specimens.

Donor	Sex	Age	Death certificate details according to computer system
1	♀	91	Respiratory insufficiency right, Chronic heart failure
2	♀	78	Asystole, AV-block 3rd degree, Post gingival recession operation, Atrial fibrillation, Arterial hypertension
3	♂	67	Cardiopulmonary insufficiency after septic shock, Staphylococcus due to infection, Post-stenotic pneumonia in right upper lobe due to central bronchial carcinoma, Coronary heart disease
4	♀	89	Cardiac decompensation with congestive pneumonia, High-grade left ventricular failure, Atrial fibrillation, Post-aortic valve replacement, Dementia, MRSA
5	♂	71	Global respiratory insufficiency after COPD, Coronary heart disease, Heart failure, Diabetes mellitus
6	♂	85	Multi organ failure, Sepsis, Urinary Tract Infection, Contusion right temporal region, Heavy subdural bleeding
7	♀	80	Acute shortness of breath with unsuccessful reanimation Dementia

Table 5: **List of Donors**
List of donors, specifying sex, age, and death certificate details according to the computer system of the Heinrich-Heine-University (saved anonymously). AV block = atrio-ventricular block, MRSA = methicillin-resistant Staphylococcus aureus, COPD = chronic obstructive pulmonary disease.

2.3.3 Anatomical Approach

The forearms were approached anteriorly in the neutral position, i.e. supinated and extended. The superficial and deep layers of the anterior compartment were dissected from the antecubital

fossa until the wrist. The interosseous membrane was located. Excessive muscle fibres were cleared until only directly to the IOM attaching muscle fibres were left. Then, the IOM with the remaining muscle fibres was separated from the radius and ulna. We cut 1cm x 1cm x 1cm blocks from the highest (at the level of the tuberculum radii) and lowest parts of the membrane. Additionally, we dissected a 1cm x 1cm x 1cm cube from the middle, tendon-like part of the membrane. Thereby, samples from the proximal membranous portion, middle ligamentous complex, and distal membranous portion of the IOM were obtained. These correspond most likely to parts of the proximal oblique cord, central band, and distal oblique band respectively[10].

Specimens were stored and labelled according to their anatomical origin as listed in Table 6. A total of 36 samples, three samples from each forearm of the 6 donors, were collected. In the second step, 12 samples were collected from donor 7. Therefore, a longitudinal and a transverse sample of the abovementioned parts of the membrane were gained.

Label	Specimen
L tr	Left arm, proximal part of interosseous membrane at the level of the tuberculum radii
L m	Left arm, middle part of interosseous membrane
L d	Left arm, distal part of interosseous membrane at the distal forearm shaft
R tr	Right arm, proximal part of interosseous membrane at the level of the tuberculum radii
R m	Right arm, middle part of interosseous membrane
R d	Right arm, distal part of interosseous membrane at the distal forearm shaft

Table 6: **List with Specimen Label (excluding donor IDs)**
Listing of specimen labels excluding the study code and the individual donors ID

2.3.4 Collection and Tissue fixation

The dissections were performed, and the specimens were obtained with disposable scalpels.

The samples where then stored in water-filled, labelled airtight containers (100 ml, Sarstedt, Nürnbrecht). The labelling includes the donors ID, the anatomical location, and the side of the patient (see Table 6).

After all samples were collected, the water in the airtight containers was exchanged for 4% formaldehyde (37% formaldehyde solution, acid-free, diluted to 4%, Merck Darmstadt). The aim of this step is to prevent tissue autolysis. The tissues need to be fully penetrated with the fixative formaldehyde to be protected in the following processing steps.

2.3.5 Pre-Study

A pre-study on the three samples of one left forearm was conducted to ensure that mechanoreceptors are present. The tissues were fixed, trimmed, transferred to cassettes, and then dehydrated and cleared in a 3-days programme in the tissue processor, Leica TP1020 (Leica Biosystems Nussloch GmbH). The specimens were then embedded and sectioned with the microtome, Leica RM 2255 (Leica Biosystems Nussloch GmbH). Three histological stains (Azan dye, Goldner dye and Elastica van Gieson dye) and one immunohistochemical stain (pan Neurofilament dye) were utilized.

After positive findings, the main study was conducted. For completeness, the specimens were transferred and included into the main study.

2.4 Preparation of Samples

2.4.1 Purpose

The purpose of the following steps was to process the extracted samples to gain tissue slices that could be stained and observed under the microscope. The following steps were all performed according to B. Romeis "Mikroskopische Technik"[70].

2.4.2 Trimming and Specimen transfer to cassettes

For the samples to be further processed, their sizes needed to be adapted to fit into cassettes, Q Path® MacroStar (VWR International GmbH, Darmstadt). Therefore, the cubes were cut transversely by both sides. In donor 7, half of the obtained specimens were cut longitudinally so that a maximum of IOM was exposed. The cassettes were chosen according to the sample sizes. Most samples fitted into Q Path® MacroStar II cassettes. They were labelled with the study code, the donor code, the extremity, and the site (see Table 6 for more information). Most of the samples were placed transversely into the according cassette, so that macroscopically muscle – IOM – muscle was seen. The longitudinally cut specimens of donor 7 were placed with the exposed IOM facing upward into the cassettes. The cassettes were firmly closed and then stored in a formalin filled container.

2.4.3 Tissue processing

The overall objective of the following steps was to create the chemical basis for fetching tissues in paraffin. Paraffin is a hydrophobic agent, and our tissue samples were impregnated with water and formaldehyde, which first needed removal. The dehydration, clearing, and wax infiltration processes were all performed with the tissue processor, Leica TP1020 (Leica Biosystems Nussloch GmbH) in a 5-day-programme. This tissue processor can create a vacuum which improves the infiltration of the specimens.

Dehydration

To remove the water and formaldehyde out of the tissues, the specimen-filled cassettes got immersed in increasing concentrations of ethanol solutions. The water and alcohol mixed, and the increasing alcohol concentrations slowly replaced the remaining formaldehyde and alcohol. The gradual increase serves the purpose to avoid tissue distortion. The samples in this study were dehydrated over 70 hours in the following sequence (Figure 3):

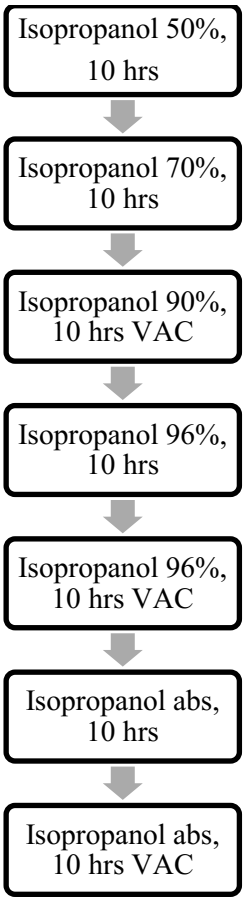

Figure 3: **Ascending alcohol concentrations for specimen's immersion**
Graphical representation of ascending isopropanol concentrations and time specimens were immersed. VAC = Vacuum, abs = absolut

Clearing

The tissues were now free from water and formalin and instead penetrated by alcohol. To be able to embed the samples in paraffin, the alcohol had to be removed. Alcohol and paraffin wax are not miscible and therefore the alcohol is replaced by a clearing agent. It has the properties to mix with alcohol as well as with paraffin. Here, Roticlear® *(Carl Roth GmBH + CoKG, Karlsruhe)* was used as clearing agent. The specimens were infiltrated with increasing concentrations of Roticlear until the samples were cleared from alcohol. In this study, the following concentrations and durations were chosen (Figure 4):

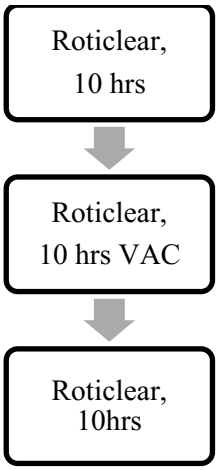

Figure 4: **Time the specimens spent in Roticlear**
Specimens were infiltrated in Roticlear for 30hrs to remove the isopropanol. VAC = Vacuum

Wax Infiltration

As last step in the tissue processor, the cassettes were now placed in containers with wax. There, the Roticlear was replaced by paraffin wax in 2 rotations over the length of 20 hours (see Figure 5).

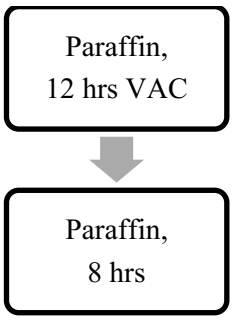

Figure 5: **Time spent in Paraffin**
Specimens were infiltrated with Paraffin over 20hrs to remove the Roticlear. VAC = Vacuum

After the dehydration with ethanol, the clearing with Roticlear and the infiltration with paraffin, the specimens were now set to be embedded with paraffin wax to form sliceable blocks.

Embedding

The purpose of the embedding step is to fixate the specimen in a block of paraffin wax so it can be sectioned with a microtome.

This step was performed with the paraffin embedding center, TES Valida (MEDITE Medical GmbH, Burgdorf) which consists of a thermal, a dispenser and a cooling unit. Further, Paraffin, ParaplastPlus®, McCormick Scientific (Leica Biosystems Richmond Inc.), metal moulds, anatomical forceps and the prepared cassettes were used.

The paraffin wax is melted at 60°C by the thermal unit of the paraffin embedding centre. The base of a metal mould is filled with the melted paraffin, a cassette is opened, the specimen is removed with the forceps and placed in the mould. The sample is placed carefully so that the

IOM is seen (either transversely or longitudinally in half of the samples of donor 7). The mould is then placed on the -1°C cold cooling unit until the paraffin is hardened, and the sample is fixed. The labelled cassette is divided into its top and bottom. Then, the mould is filled with melted paraffin and the labelled cassette bottom is placed on top of the filled mould and slightly pushed into the paraffin. The mould-cassette construction is placed onto the cooling plate until the block is solidified. These blocks are stored at room temperature in a box until the next step. The specimen is now embedded in a block of paraffin and can be sectioned.

2.4.4 Sectioning

The aim of sectioning is to receive 5µm thin specimens' slices that can be mounted on microscope slides and be stained and analysed. For this study, 5 different stains were originally planned, 4 of them applied to all specimens and one only to the samples of one donor. Three histological and one immunohistochemical stain were drafted for all specimens. For immunohistochemical stains, one isotype control is needed per section. This works as a negative control and shows the unspecific binding capacity of the antibody. Therefore, 2 sections per specimen are needed for an immunohistochemical stain, thus, 5 sections per specimen were envisioned. In addition, another immunohistochemical stain (Tyrosine hydroxylase) was planned for the specimens of one donor, thus 2 further sections were taken from these (see Table 7 for more detailed information). In a second step, donor 7 was added, and new sections were produced from donor 4. Further, it was decided to expand the immunohistochemical stains by 3 for donor 7. Therefore, a total of 360 sections were produced.

Frosted microscope slides, Superior, 76x26x1mm, (Paul Marienfeld GmbH & Co. KG, Lauda-Königshofen) were labelled using the pen Securline © Marker II, Superfrost (Aspen Surgical, Calendonia) with the study number, the donor ID, the side and site of the specimen, and the stain this specimen would receive (see Table 6 and 7 for more information).

As a final step before cutting the microscopic thin slices, superfluous paraffin must be removed on top of the specimen to uncover the tissue surface in the paraffin block. Therefore, the paraffin blocks were placed into a microtome (Leica Reichert Jung 2030), adjusted so that the FEATHER® disposable microtome blade (VWR International GmbH, Darmstadt) meets the top of the block, and the slice thickness is set at 20µm. The block was now sectioned until the specimen surface was exposed.

After exposing the specimen's surfaces, the paraffin blocks were laid on a plate with ice cubes for approximately one hour to harden the paraffin. This shall align the densities of the different structures in the block, here paraffin, muscle fibres, membrane, so that cohesive structures can be gained. Parallelly, a water bath was heated to 30°C Tissue Float Bath, GFL 1052 (Gesellschaft für Labortechnik mbH, Burgwedel).

A new blade was inserted to the rotatory microtome, MICROM, HM360 and the cold paraffin block was inserted and adjusted for an optimal blade clearance angle. The slides thickness level was set to 6µm. The specimen-block was now sectioned, and the resulting tissue sections ribbon was transferred with two anatomical forceps to the water bath. The sections were set with their shiny surface down (this surface will also face the slide's side). The warm water straightened folds in the specimen that possibly resulted from sectioning. After the sample was flattened, the ribbon was separated at the specimen's borders with forceps. Now, the microscopic slide was put vertically in the water and the specimen was carefully mounted on the slide. Two specimen slices were mounted on the slides for the immunohistochemical stain or if two slices were too big for one microscopic slide, two slides were used. The slide was removed from the water bath and drained from excess water vertically. The slides were shortly left to dry and then transferred according to their stain labelling to racks. For the next 24hrs, they were dried in the drying oven (Memmert GmbH + Co. KG, Schwabach) at a constant temperature of 37°C.

6 specimens (noticeable always specimens from the middle section) were difficult to cut because they had several different densities and were therefore stored longer on ice cubes, partly even during the sectioning process.

For a summary of the methodological process, see Figure 7.

2.5 Staining

Stains	Type of stain	Applied to n° of specimens	N° of sections required per specimen
Azan stain	Histological	48	1
Elastica van Gieson stain	Histological	48	1
Goldner stain	Histological	48	1
Pan Neurofilament stain	Immunohistochemical	48*	2
Tyrosine hydroxylase stain	Immunohistochemical	18	2
S100 stain	Immunohistochemical	12	2
MBP stain	Immunohistochemical	12	2
TRPC4 stain	Immunohistochemical	12	2

Table 7: **Type of stains and number of specimens applied to**
*List with stains, type of stains and number of specimens applied to plus number of sections required per specimen for each stain. N° = number, *Pan Neurofilament was applied twice to sections of donor 4, the second time with a higher antibody quantity.*

In preparation for the staining, the slides were deparaffinated and partially hydrated (depending on the stain). The process is shown in Figure 6.

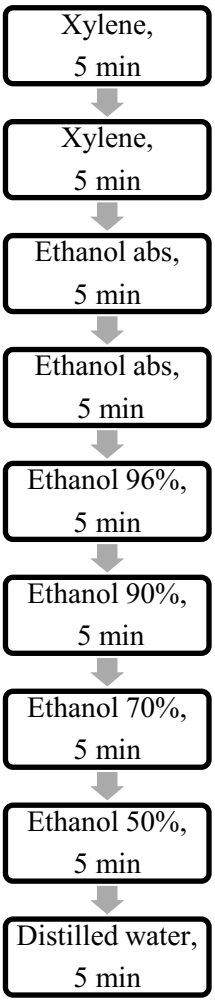

Figure 6: **Descending alcohol concentrations for specimen's deparaffination**
Graphical representation of descending Roticlear, isopropanol concentrations and distilled water and time specimens were immersed.

The staining protocols followed for the Azan according to Heidenhain and Elastica Haematoxylin van Gieson dye were taken from B. Romeis "Mikroskopische Technik"[70]. The Masson-Goldner dye protocol originated from H.-C. Burck "Histologische Technik"[71]. The immunohistochemical stains were applied according to B. Romeis "Mikroskopische Technik"[70] and T. Boenisch's "Handbuch Immunchemische Färbemethoden"[72]. The staining protocols were followed according to the primary antibody manufacturer's specification.

2.5.1 Histological stains

Masson-Goldner stain

The Masson-Goldner dye is an established method used for imaging connective tissue and musculature in specimens. After successful staining, cell nuclei stain brown to black, cytoplasm and muscle fibres orange to red, connective tissue and mucosa green.

Chemicals required for this stain are:

Chemical	**Manufacturer**
Haematoxylin cryst.	*Merck KGaA, Darmstadt*
Ferric chloride	*VWR International GmbH, Darmstadt*
Hydrochloric acid 25%	*Merck KGaA, Darmstadt*
Azophloxine Chroma®	*Waldeck GmbH & Co. KG, Münster*
Fuchsine acid Certistain®	*Merck KGaA, Darmstadt*
Ponceau de Xylidine, Chroma®	*Waldeck GmbH & Co. KG, Münster*
Orange G Certistain®	*Merck KGaA, Darmstadt*
Light green SF yellowish Certistain®	*Merck KGaA, Darmstadt*
Glacial acetic acid	*Merck KGaA, Darmstadt*
Phosphotungstic acid hydrate	*Acros Organics, Geel*

Table 8: **Chemicals needed for Masson-Goldner stain and manufacturers**

With these chemicals, following reagents are prepared:

Reagents needed for Masson-Goldner stain	
Weigert's iron haematoxylin staining solution	**Solution A**: dissolve 1g of haematoxylin in 100ml 96% ethanol. Let it sit for one week. **Solution B**: mix 4ml 29% ferric chloride with 1ml 25% hydrochloric acid and 95ml distilled water Before using, mix both solutions to equal parts, mixed the solution only lasts one week.
Masson solution	boil 0.2g Ponceau de Xylidine with 0.1g Fuchsine acid in 300ml distilled water, add 0.6ml glacial acetic acid and filter the solution
Azophloxin solution	add 0.2ml glacial acetic acid to 100ml distilled water, dissolve 0.5g of azophloxin in it
Ponceau-Fuchsine acid-Azophloxin	mix 7ml Masson solution (see above) and 2ml Azophloxin solution (see above) with 88ml 0.2% acetic acid.
Phosphotungstic acid orange G solution	dissolve 3-5g of phosphotungstic acid and 2g Orange G in 100ml of distilled water.
Light Green SF solution	add 0.2ml glacial acetic acid to 100ml distilled water and dissolve 0.1-0.2g light green SF in it.

Table 9: **Reagents needed for Masson-Goldner stain**
Listing of preparation of reagents needed for the Masson-Goldner stain. g = gram, ml= millilitre

The staining procedure is as following[71]:

Firstly, the slides were deparaffinated and hydrated (see figure 6). Then, the slides were introduced into the Weigert's iron haematoxylin staining solution for 2 min. Subsequently, they

were rinsed under running tap water for 10min. Thereafter, they were stained in the Ponceau-Fuchsine acid-Azophloxin solution for 7 min and were then rinsed with 1% acetic acid. For 2 min, they were put into the Phosphotungstic acid orange G solution and were then rinsed again with 1% acetic acid. Thereafter, for 5min, the slides were stained with the light green SF solution and next were washed out with 1% acetic acid for 5 min. Afterwards, they were quickly dehydrated with absolute isopropanol twice for 2min each and were cleared with xylol 3 times for 5min each. Finally, the microscopic slides were coverslipped with Depex and coverglasses (Menzel™ Microscope Coverslips (Thermo Scientific Menzel)).

Elastica Haematoxylin van Gieson stain

The Elastica haematoxylin van Gieson stain (El HvG) is an established method to visualize collagen and elastic fibres and allows a differentiation between these two connective tissue components. After successful staining, elastic components are stained black to purple, collagen fibres are reddish, nuclei blue to black and muscle fibres yellow.

Chemicals required for this stain are:

Chemical	**Manufacturer**
Resorcin Fuchsine	*Carl Roth GmBH + CoKG, Karlsruhe*
Ethanol	*VWR International GmbH, Darmstadt*
Hydrochloric acid	*VWR International GmbH, Darmstadt*
Haematoxylin	*Carl Roth GmBH + CoKG, Karlsruhe*
Ferric Chloride	*VWR International GmbH, Darmstadt*
Picric acid	*VWR International GmbH, Darmstadt*
Fuchsine acid	*VWR International GmbH, Darmstadt*

Table 10: **Chemicals needed for Elastica Haematoxylin van Gieson stain and manufacturers**

With these chemicals, following reagents are prepared:

Reagents needed for Elastica Haematoxylin van Gieson stain	
Elastica solution	Dissolve 10g resorcin fuchsine in 1000ml of warm (not boiling!) 80% ethanol. Let cool, then add 20ml concentrated hydrochloric acid, filter the solution.
Weigert's iron haematoxylin staining solution	**Solution A**: dissolve 1g of haematoxylin in 100ml 96% ethanol. Let it sit for one week. **Solution B**: mix 4ml 29% ferric chloride with 1ml 25% hydrochloric acid and 95ml distilled water Before using, mix both solutions to equal parts, mixed the solution only lasts one week.

Van Gieson solution	add 7.5ml 1% Fuchsine acid to 100ml saturated aqueous picric acid.

Table 11: **Reagents needed for Elastica Haematoxylin van Gieson stain**
Listing of preparation of reagents needed for the Elastica Haematoxylin van Gieson stain. g = gram, ml = millilitre

The staining procedure is as following:

Firstly, the slides were deparaffinated and prepared in 70% ethanol (see Figure C). They were then placed into the Elastica solution for 15min. Subsequently, they were rinsed in tap water until the water was clear. Thereafter, the slides were stained for 5 min in the Weigert's iron haematoxylin staining solution and were then first rinsed with tap water for 5 min and secondly with distilled water for another 5min. For exactly 1min, the slides were placed into the Van Gieson solution and were then shortly rinsed twice with distilled water. Then, they were quickly dehydrated with 96% ethanol twice and with 100% ethanol twice. Afterwards, they were cleared in xylol and coverslipped with Depex and coverglasses.

Azan according to Heidenhain stain

The Azan according to Heidenhain stain is composed of the two staining components Azocarmine G and Aniline, hence its name. It is an established method to visualize and differentiate connective tissue and musculature. After successful staining, collagen and reticular connective tissue are stained deep blue, muscle fibres orange to red, neurons and glia cells red to purple.

Chemicals required for this dye are:

Chemical	**Manufacturer**
Azocarmine G	*Merck KGaA, Darmstadt*
Aniline blue	*Merck KGaA, Darmstadt*
Orange G Certistain®	*Merck KGaA, Darmstadt*
Glacial Acetic acid	*Merck KGaA, Darmstadt*
Aniline	*Merck KGaA, Darmstadt*
Phosphotungstic acid hydrate	*Acros Organics, Geel*

Table 12: **Chemicals needed for Azan according to Heidenhain stain and manufacturers**

With these chemicals, following reagents are prepared:

Reagents needed for Azan according to Heidenhain stain	
Azocarmine solution	boil 0.1g Azocarmine G in 100ml distilled water, let cool and filter the solution and then dilute each 100ml filtrate with 1ml glacial acetic acid

Aniline blue – Orange G mixture	dissolve 0.5g Aniline blue and 2g Orange G with 100ml distilled water, add 8ml glacial acetic acid, boil, let cool and filter the mixture.
Aniline-alcohol solution	Add 0.1ml aniline to 100ml 90% ethanol
Acetic alcohol	Add 1ml of glacial acetic acid to 100ml 96% ethanol
Phosphotungstic acid solution	Add 5g of phosphotungstic acid in 100ml distilled water

Table 13: **Reagents needed for Azan according to Heidenhain stain**
Listing of preparation of reagents needed for the Azan according to Heidenhain stain. g = gram, ml = millilitre.

The staining procedure is as following:

Firstly, the slides were deparaffinated and hydrated (see Figure C). Then, the sections were introduced for 5min into aniline-alcohol solution. Thereafter, the slides were stained in preheated Azocarmine solution for 15min at 56°C in the oven. For further 10min, the slides were stained in cool Azocarmine solution. Then, the slides were placed for 1min into aniline-alcohol solution. The sections were washed out for 1min in acetic alcohol. Hereafter, the slides were 40min in phosphotungstic acid solution. After draining, they were placed in one-part Aniline blue – Orange G mixture and two-parts distilled water for 15 min. Then, they were put int 96% ethanol for 2 minutes for differentiation. Thereafter, the slides were dehydrated in absolute ethanol for 2 minutes twice and cleared with xylol three times for 5 minutes each turn. Finally, the microscopic slides were coverslipped with Depex and cover glasses.

2.5.2 Immunohistochemical stains

All immunohistochemical stains used in this study are based on the labelled Streptavidin-Biotin (LSAB) method. This method is based on enzyme-marked staining, which is achieved by a biotinylated secondary antibody, streptavidin which binds with high affinity to biotin (and thus, the secondary antibody), an enzyme marker (horseradish peroxidase) and a substrate (H_2O_2)-chromogene (AEC) solution.

For each immunohistochemical stain, a positive control (stomach mucosa) and an isotype (negative) control of each specimen block were run through the same staining process. The isotype control was not treated with the primary antibody but an isotype control antibody, which should not bind to any cells in the specimens. However, the isotype control antibody has similar properties as the primary antibody in terms of immunoglobulin type and heavy and light chains. Thus, the isotype control sections demonstrate the non-specific binding of mouse or goat antibodies to the here investigated sections in general. The positive control was processed in the same way as the study specimens. It stains lightly with the immunohistochemical stains and serves the purpose of establishing the ideal moment to finish the staining with AEC without

under- or overstaining the tissues. Further, it is a control to prove that the staining procedure was successful even if the investigated tissue shows no staining.

General immunohistochemical staining procedure

As all immunohistochemical stains used are based on the same method, they were all stained similarly. The following table summarises the chemicals used in most or all immunohistochemical stains and their purpose.

Chemical *(Manufacturer)*	Purpose
Antigen Unmasking Solution, Citrate-Based, pH 6, H-3300 *(Vector Laboratories, Inc., Burlingame)*	Heat-induced epitope retrieval: to improve the immune reactivity of the specimens which might have been reduced by the fixation in formaldehyde
Phosphate buffered saline (PBS) self-mixed: Contains NaCl, Na_2HPO_4 x $2H_2O$, KCl, KH_2PO_4 (all from *Carl Roth®, Karlsruhe)* diluted in demineralised water	Isotonic buffer solution, used to rinse specimens in between the staining steps
Triton X-100 *(Santa Cruz Biotechnology, Inc., Santa Cruz)*	Reduces the surface tension of the PBS, improves tissue infiltration
Serum, donor horse *(MP Biomedicals, Irvine)*	Reduces cross-reactivity of the secondary antibody with endogenous (from the specimen itself) immunoglobulins
Hydrogen peroxide, 35 %, pure, stabilised *(Carl Roth®, Karlsruhe)*	Substrate to horseradish peroxidase, blocks endogenous peroxidases
Streptavidin-Horseradish Peroxidase, 405210 *(BioLegend®, San Diego)*	Streptavidin binds to biotinylated antibody, horseradish peroxidase functions as enzyme marker
AEC Substrate Kit, Peroxidase (HRP), (3-amino-9-ethylcarbazole) SK-4200 *(Vector Laboratories, Inc., Burlingame)*	Chromogen, gets oxidated by peroxidase and forms a red, alcohol soluble final product at antibody location
Hematoxylin solution acc. to Gill II *(Carl Roth®, Karlsruhe)*	General counterstain
Lithium carbonate ACS reagent, ≥99.0% *(Sigma-Aldrich, Merck KGaA, Darmstadt)*	Fades the general dark blue counterstain by the Haematoxylin solution, creates thereby a greater colour gradient between the background and antibody stain
ROTI®Mount Aqua, 2848.2 *(Carl Roth®, Karlsruhe)**	Aqueous solution for coverslipping the

	sections after staining
Roti®Mount ready-to-use *(Carl Roth GmBH + CoKG, Karlsruhe)**	Anhydrous solution for coverslipping the sections after staining

Table 14: **Chemicals needed for immunohistochemical stains, *manufacturers,* and their function**
*Listing of chemicals required for immunohistochemical stains plus the function they have for the staining process. NaCl = sodium chloride, Na2HPO4 x 2H2O = di-Sodium hydrogen phosphate dihydrate, KCl = potassium chloride, KH2PO4 = Potassium dihydrogen phosphate, *for the MBP stain* Roti®Mount ready-to-use *(Carl Roth GmBH + CoKG, Karlsruhe) was used, in the other stains the aqueous solution* ROTI®Mount Aqua, 2848.2 *(Carl Roth®, Karlsruhe) was used.*

All stains were prepared similarly, only some timings were varying.

The slides were fixed in the oven for 2-3 hours at 70°C, then deparaffinated and hydrated (see Figure 6). To optimise epitope retrieval, the slides were heated for 4-5 minutes in Antigen Unmasking Solution, Citrate-Based, pH 6, H-3300 (Vector Laboratories, Inc., Burlingame) in a commercial pressure cooker. After gently cooling down to room temperature, the slides were washed in phosphate buffered solution (PBS).

For 10 minutes, the slides were bathed in 0.6% H_2O_2, diluted in PBS at room temperature. Next, there were cleaned with PBS and the tissues were encircled with Super Pap Pen Liquid Blocker (COSMO BIO co., LTD., Tokyo). Thereby, a barrier was created around the specimen to ensure that the following antibodies do not flow off the specimen.

The next steps diverged depending on the immunohistochemical stain (see below).

Pan Neurofilament stain

Neurofilaments form part of the neuronal cytoskeleton and provide structural support to the axon. Staining with a neurofilament antibody allows the recognition of neuronal structures in specimens.

We decided to stain the specimens for neurofilament to explore the presence and number of proprioceptive structures in the tissues. This immunohistochemical stain was first applied to all 36 specimens. After investigating the inconsistent staining results, we stained specimens of donor 4 and of the new donor 7 according to the modified staining protocol.

The following antibodies were used:

Antibody *(Manufacturer)*	Purpose
Purified anti-Neurofilament Marker (pan axonal, cocktail) Antibody, 837904, *(BioLegend®, San Diego)*	Primary monoclonal antibody
Purified Mouse IgG1, κ Isotype Ctrl Antibody,	Isotype control antibody for negative

401402, *(BioLegend®, San Diego)*	controls
Purified Mouse IgM, λ Isotype Ctrl Antibody, 401102, *(BioLegend®, San Diego)*	Isotype control antibody for negative controls
Horse Anti-Mouse IgG Antibody (H+L), Biotinylated, BA-2000 *(Vector Laboratories, Inc., Burlingame)*	Secondary monoclonal biotinylated link antibody
Biotin anti-mouse IgM Antibody, 406504, *(BioLegend®, San Diego)*	Secondary monoclonal biotinylated link antibody (for negative controls)

Table 15: **Antibodies needed for pan Neurofilament stain, *manufacturers,* and their function**
Listing of antibodies required for the pan Neurofilament stain plus the function they have for the staining process.

The staining protocol continues as following:

Next, the primary monoclonal antibodies purified anti-Neurofilament Marker (pan axonal, cocktail) Antibody, 837904, (BioLegend®, San Diego), purified Mouse IgG1, κ Isotype Ctrl Antibody, 401402 (BioLegend®, San Diego) and Purified Mouse IgM, λ Isotype Ctrl Antibody, 401102, (BioLegend®, San Diego) for the isotope controls were applied to the sections. All three antibodies were diluted to 2 micrograms per millilitre. During the staining of donor 4 and donor 7 specimens, the antibody concentration was increased by 10% as the antibody staining strength fades with time.

The microscopic slides were stored in horse serum over night at room temperature. The next day, the slides were washed three times in PBS for 5 minutes each. Then, the Horse Anti-Mouse IgG Antibody (H+L), Biotinylated, BA-2000 (Vector Laboratories, Inc., Burlingame) and Biotin anti-mouse IgM Antibody, 406504, (BioLegend®, San Diego) diluted to 12 micrograms per millilitre in PBS were applied to all sections. After 75 minutes, the slides were bathed in PBS twice for 5 minutes each. Hereafter, the Streptavidin-Horseradish Peroxidase, 405210 (BioLegend®, San Diego), diluted to 1:750, was administered onto the sections at room temperature. After 60 minutes, the enzyme was washed off with PBS twice for 5 minutes each.

The AEC Substrate Kit, Peroxidase (HRP), (3-amino-9-ethylcarbazole) SK-4200 (Vector Laboratories, Inc., Burlingame) was mixed, filled into a syringe, pressed through a commercial filter, and dropped onto the sections. The positive control (stomach mucosa) was observed under the microscope until the tissue was lightly stained, this took one minute. All sections were then shortly washed with water. The Haematoxylin solution after Gill II was filtered and then the sections were shortly bathed in it for 15 seconds. They were washed for 5 minutes in water and bathed in saturated lithium carbonate solution for 90 seconds under microscopic control to lighten the general Haematoxylin staining, thereby increasing the colour gradient between

antibody-marked structures and the structures around. Finally, the slides were shortly washed in water and coverslipped with ROTI®Mount Aqua, 2848.2 (Carl Roth®, Karlsruhe).

Tyrosine Hydroxylase stain

Tyrosine Hydroxylase is the first and rate-limiting enzyme in the catecholamine synthesis pathway. It converts L-tyrosine to L-DOPA and was firstly described in 1964 by Nagatsu et al.[73] This enzyme is found in sympathetically innervated tissue, the brain and the adrenal medulla. Therefore, we decided to stain our specimens with anti-tyrosine hydroxylase antibodies to explore if they are sympathetically innervated.

This stain was applied to the 6 specimens of one donor (donor 6, see table 7). This donor was chosen because his tissues were infiltrated the shortest with formaldehyde before the start of this study. Therefore, better epitope retrieval was expected. Unfortunately, results showed only inconsistent and small signals. Therefore, we decided to repeat this stain in the new donor 7 (see table 7), who was only very shortly infiltrated in formaldehyde. Here, better epitope retrieval was observed.

The following antibodies were used:

Antibody *(Manufacturer)*	Function
Anti-Tyrosine Hydroxylase Antibody, clone LNC1, MAB318 *(Sigma-Aldrich, Merck KGaA, Darmstadt)*	Primary monoclonal antibody
Purified Mouse IgG1, κ Isotype Ctrl Antibody, 401402 *(BioLegend®, San Diego)*	Isotype control antibody for negative controls
Horse Anti-Mouse IgG Antibody (H+L), Biotinylated, BA-2000 *(Vector Laboratories, Inc., Burlingame)*	Secondary monoclonal biotinylated link antibody

Table 16: **Antibodies needed for Tyrosine Hydroxylase stain, *manufacturers,* and their function**
Listing of antibodies required for the Tyrosine Hydroxylase stain plus the function they have for the staining process.

The staining protocol continues as following:

Following this, the primary monoclonal antibodies Anti-Tyrosine Hydroxylase Antibody, clone LNC1, MAB318 (Sigma-Aldrich, Merck KGaA, Darmstadt) and Purified Mouse IgG1, κ Isotype Ctrl Antibody, 401402 (BioLegend®, San Diego) for the isotope controls were applied to the sections. Both antibodies were diluted to 12 micrograms per millilitre. The microscopic slides were stored in horse serum over night at 4°C.

The next day, the slides were washed three times in PBS for 5 minutes each. Then, the Horse Anti-Mouse IgG Antibody (H+L), Biotinylated, BA-2000 *(Vector Laboratories, Inc., Burlingame)*, diluted to 12 microgram per millilitre was applied to all sections. After 45 minutes, the slides were bathed in PBS three times for 5 minutes each. Hereafter, the Streptavidin-Horseradish Peroxidase, 405210 (BioLegend®, San Diego), diluted to 1:800, was administered onto the sections at room temperature. After 40 minutes, the enzyme was washed off with PBS three times for 5 minutes each.

The AEC Substrate Kit, Peroxidase (HRP), (3-amino-9-ethylcarbazole) SK-4200 *(Vector Laboratories, Inc., Burlingame)* was mixed, filled into a syringe, pressed through a filter, and dropped onto the sections. The positive control (stomach mucosa) was observed under the microscope until the tissue was lightly stained. All sections were then shortly washed with water. The Haematoxylin solution after Gill II was filtered and then the sections were shortly bathed in it for 10 seconds. They were washed for 5 minutes in water and then bathed in saturated lithium carbonate solution for 120 seconds. Finally, the slides were shortly washed in water and coverslipped with ROTI®Mount Aqua, 2848.2 (Carl Roth®, Karlsruhe).

S100 stain

S100 proteins are found in a series of tissues but especially in Schwann cells. This family of proteins was first identified by B.W. Moore in 1965[74]. This stain is often used in pathology to stain for tumour cells. We decided to use this stain to visualize the myelinated afferent nerve fibres and as supplement to the pan Neurofilament stain.

The following antibodies were used:

Antibody *(Manufacturer)*	Function
S-100 Mouse Monoclonal Antibody, Isotype Ig2a *(Dianova GmbH, Hamburg)*	Primary monoclonal antibody
Purified Mouse IgG2a, κ Isotype Ctrl, 401502 *(BioLegend®, San Diego)*	Isotype control antibody for negative controls
Horse Anti-Mouse IgG Antibody (H+L), Biotinylated, BA-2000 *(Vector Laboratories, Inc., Burlingame)*	Secondary monoclonal biotinylated link antibody

Table 17: **Antibodies needed for S100 stain, *manufacturers,* and their function**
Listing of antibodies required for the S100 stain plus the function they have for the staining process.

The staining protocol continues as the following:

Then, the primary S-100 Mouse Monoclonal Antibody, Isotype Ig2a *(Dianova GmbH, Hamburg)*, diluted to 1:200 was applied to the sections. Purified Mouse IgG2a, κ Isotype Ctrl, 401502 *(BioLegend®, San Diego)*, diluted to 1:500, was applied to the isotope controls. The sections were stored in horse serum for 75 minutes at room temperature.

Similar to the other stains, the slides were then washed three times in PBS for 5 minutes each. The Horse Anti-Mouse IgG Antibody (H+L), Biotinylated, BA-2000 *(Vector Laboratories, Inc., Burlingame)* was applied. After 45 minutes at room temperature, the slides were washed again with PBS twice for a total of 10 minutes.

After that, the AEC Substrate Kit, Peroxidase (HRP), (3-amino-9-ethylcarbazole) SK-4200 *(Vector Laboratories, Inc., Burlingame)* was prepared and applied as in the previous stains. The positive control was observed under the microscope until a light stain was seen, then all slides were quickly washed water. The Haematoxylin solution after Gill II was filtered and then the sections were shortly bathed in it for 5 seconds. They were washed twice for a total of 6 minutes in water and then bathed in saturated lithium carbonate solution for 120 seconds. Finally, the slides were shortly washed in water and coverslipped with ROTI®Mount Aqua, 2848.2 (Carl Roth®, Karlsruhe).

Myelin Basic Protein stain

Myelin Basic Proteins (MBP) are abundant in the myelin sheaths of the central nervous system. They play a great role in the diagnosis of multiple sclerosis, as it seems that the demyelination of nerves in this disease is created by autoimmune attacks against MBP[75]. We decided to use this stain complimentary to pan Neurofilament, S100, and TRCP4 to visualise proprioceptive structures.

The following antibodies were used:

Antibody *(Manufacturer)*	Function
Purified Mouse anti-Myelin Basic Protein Antibody, IgG1, 836504 *(BioLegend®, San Diego)*	Primary monoclonal antibody
Purified Mouse IgG1, κ Isotype Ctrl Antibody, 401402 *(BioLegend®, San Diego)*	Isotype control antibody for negative controls
Horse Anti-Mouse IgG Antibody (H+L), Biotinylated, BA-2000 *(Vector Laboratories, Inc., Burlingame)*	Secondary monoclonal biotinylated link antibody

Table 18: **Antibodies needed for MBP stain, *manufacturers,* and their function**
Listing of antibodies required for the MBP stain plus the function they have for the staining process.

The staining protocols follows on with:

The sections were covered with Purified Mouse anti-Myelin Basic Protein Antibody, IgG1, 836504 *(BioLegend®, San Diego)*, the negative control sections were covered with Purified Mouse IgG1, κ Isotype Ctrl Antibody, 401402 *(BioLegend®, San Diego)*. Then, all sections were bathed in horse serum over night at 4°C.

The next morning, the sections were washed three times in PBS for a total of 15 minutes and then covered with Horse Anti-Mouse IgG Antibody (H+L), Biotinylated, BA-2000 *(Vector Laboratories, Inc., Burlingame)* for 45 minutes at room temperature. Then, the sections were washed again with PBS for a total of 10 minutes and incubated in Streptavidin-Horseradish Peroxidase, 405210 *(BioLegend®, San Diego)* for 40 minutes. After washing the sections again in PBS, they were placed in AEC Substrate Kit, Peroxidase (HRP), (3-amino-9-ethylcarbazole) SK-4200 *(Vector Laboratories, Inc., Burlingame)* for approximately one minute during which the positive control was observed under the microscope. After getting a light red stain, the sections were washed in water and counterstained with freshly filtered Hematoxylin solution acc. to Gill II *(Carl Roth®, Karlsruhe).* Next, the sections were washed with water and placed in Lithium carbonate ACS reagent, ≥99.0% *(Sigma-Aldrich, Merck KGaA, Darmstadt)* for 120 seconds. They were then washed with water and in reverse order to Figure C dehydrated and cleared. Finally, the sections were coverslipped with Roti®Mount ready-to-use *(Carl Roth GmBH + CoKG, Karlsruhe.*

Transient receptor potential canonical channel 4 stain

Transient receptor potential canonical channel 4 (TRPC4) is a variably calcium-permeable cation channel which is involved in many different processes such as neurotransmitter release or cell proliferation[76,77]. The TRCP 4 antibody stains nerval fibres and we decided to use it as a complimentary stain to pan Neurofilament, S100 and MBP.

The following antibodies were used:

Antibody *(Manufacturer)*	Function
TRPC4 Polyclonal Goat Antibody, IgG # PA5-18987 *(ThermoFisher Scientific Inc, Waltham)*	Primary polyclonal antibody
Goat IgG Isotype Control, 31245 *(ThermoFisher Scientific Inc, Waltham)*	Isotype control antibody for negative controls
Horse Anti-Goat IgG Antibody (H+L),	Secondary biotinylated link antibody

Biotinylated, BA-9500 *(Vector Laboratories, Inc., Burlingame)*	

Table 19: **Antibodies needed for TRPC4 stain, *manufacturers,* and their function**
Listing of antibodies required for the TRPC4 stain plus the function they have for the staining process. NaCl = sodium chloride, Na2HPO4 x 2H2O = di-Sodium hydrogen phosphate dihydrate, KCl = potassium chloride, KH2PO4 = Potassium dihydrogen phosphate

The staining protocol continues with:

The sections were covered with TRPC4 Polyclonal Goat Antibody, IgG # PA5-18987 *(ThermoFisher Scientific Inc, Waltham).* The negative control was covered with Goat IgG Isotype Control, 31245 *(ThermoFisher Scientific Inc, Waltham)*. Following, the sections were all stored in horse serum for 90 minutes at 35°C. Then, they were washed in PBS three times for a total of 15 minutes and stored in Horse Anti-Goat IgG Antibody (H+L), Biotinylated, BA-9500 *(Vector Laboratories, Inc., Burlingame)* one hour at room temperature. After being washed again with PBS for 15 minutes, the sections were incubated in Streptavidin-Horseradish Peroxidase, 405210 *(BioLegend®, San Diego)* for 40 minutes at room temperature. Then, they were washed again with PBS for 15 minutes and stained with AEC Substrate Kit, Peroxidase (HRP), (3-amino-9-ethylcarbazole) SK-4200 *(Vector Laboratories, Inc., Burlingame)* until the positive control showed a light red stain under the microscope. After that, the sections were washed with water and counterstained with freshly filtered Haematoxylin solution acc. to Gill II *(Carl Roth®, Karlsruhe)* for approximately 5 seconds. Next, the sections were washed with clear water for 6 minutes in total and bathed for 2 minutes in Lithium carbonate ACS reagent, ≥99.0% *(Sigma-Aldrich, Merck KGaA, Darmstadt)*. Last, the sections were washed again with water and coverslipped with ROTI®Mount Aqua, 2848.2 (Carl Roth®, Karlsruhe).

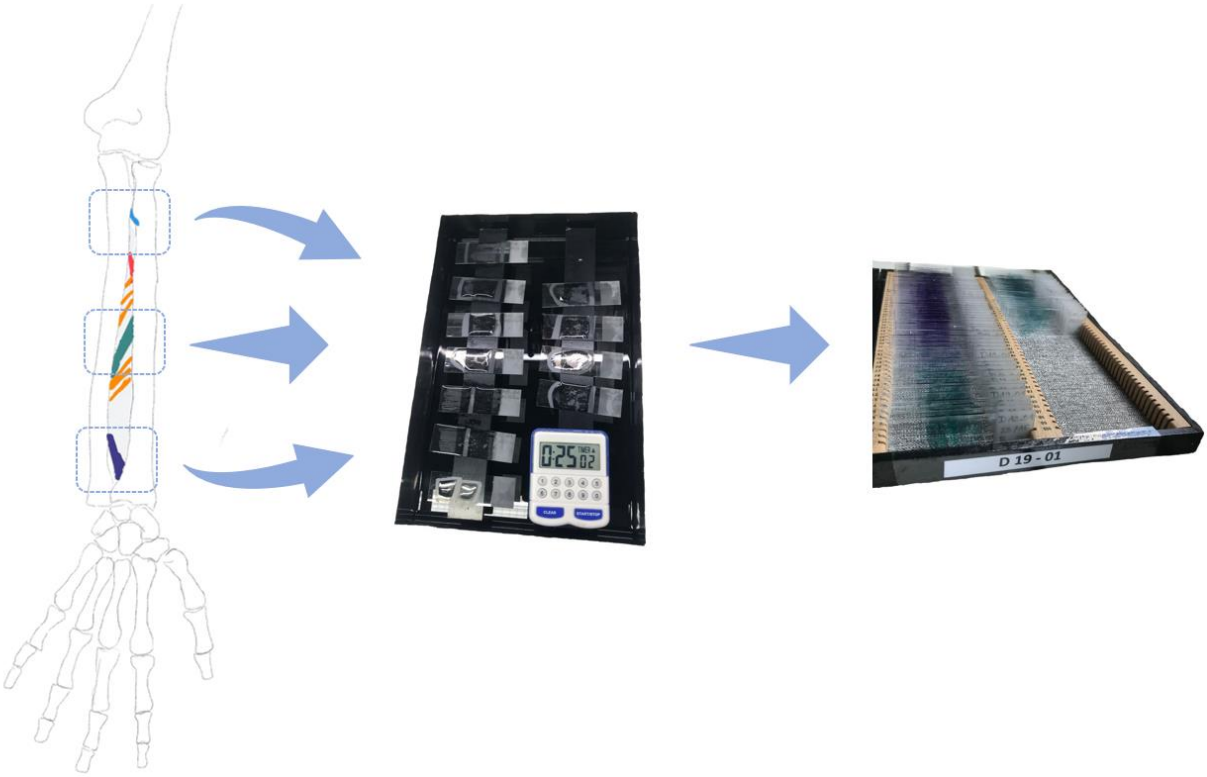

Figure 7: Graphical Summary of Methodology – From Sample Extraction over Staining to Final Result

The three marked areas of the IOM were excised, for presentation purposes the overlying muscle tissue was not displayed. The ligaments of the IOM are shown corresponding to Noda et al.[10]. In the middle for presentation purposes some sections stained with one antibody of an immunohistochemical stain are displayed. On the right some Masson-Goldner and Azan-stained sections are shown in their storage box.

2.6 Analysis of Samples

2.6.1 Scanning of slides

After staining, the sections were scanned with the Motic EasyScanner, Infinity 100 (VWR International GmbH, Darmstadt) and saved on a laboratory computer and an Extreme Portable SSD 1TB by SanDisk.

2.6.2 Collection of data

The scans were analysed with the computer software MoticAssistant DS. Thereby, possible oxidation-related, time-depending fading of the stains did not impact the analysis of sections. The histological scans were examined thoroughly, structures were marked and categorized, and their locations (in the IOM, at the border of the IOM, or in the adjacent muscle fibres) were noted.

Then, the immunohistochemical scans were analysed. The structures found in the histological stains were reviewed for positive signals in the immunohistochemical stains pan Neurofilament, S100, MBP, and TRPC4. Further, the TRPC4 scans were checked for Golgi tendon organ signals within the IOM. The Tyrosine Hydroxylase scans were checked for signals indicating a sympathetic efferent supply of the IOM. Through the complementary stains, possible artefacts in one stain did not impair the analysis.

The software Word (Microsoft Office Word 365) was used to collect the relevant information first. The information was then coded and transferred to Excel (Microsoft Office Excel 2008). The data was saved in a table with the following variables: donor number, sex, the specimens location, the structure location, the stain, the name of the structure: Vater-Pacini bodies, Golgi-Mazzoni corpuscles, Ruffini bodies, Golgi-Tendon organs, muscle spindles and sympathetic efferent nerve endings.

2.6.3 Statistical Analysis

The statistical software SPPS (IBM® SPSS™ Version 28) was used to analyse the collected information. Therefore, the data was transferred from Excel to SPPS and Kruskal–Wallis Non Parametric Hypothesis test and Mann-Whitney-U test were performed.

3 Results

3.1 General Findings

Mechanoreceptors were identified according to the original descriptions as described above[51,59]. It was specifically distinguished between Vater-Pacini and Golgi-Mazzoni corpuscles after Ruffinis description[51]. This means if a single capsule was seen or a truncated capsule was identified at the border of a specimen, we classified the structure as Vater-Pacini corpuscle. If a lamellated structure composed of more than one capsule or of multiple swirls in very close proximity was found, it was classified as Golgi-Mazzoni corpuscle. In donor 7, we investigated serial sections and if in the proceedings of the sections we discovered that there was more than a single capsule, the structure was classified as Golgi-Mazzoni corpuscle.

The specimens were analysed correspondingly to their anatomical locations i.e. proximal, medial and distal as well as left and right. Further, mechanoreceptors were categorized according to the tissue they were lying in i.e. within the IOM, directly at the border of the IOM, in the tissue surrounding the IOM. Where possible, a further division into muscle tissue and connective tissue was performed. In addition, mechanoreceptors which were found in the longitudinal sections of the most recently deceased donor are listed separately to avoid bias. As we were specifically interested in the sympathetic innervation of the IOM, the analysis of sympathetic nerves was restricted upon the IOM. Further, the analysis of Golgi-Tendon organs was limited upon the IOM. Limited staining results as described in the methods section as well as their physiological restriction to tendon-muscle transition or presence within ligaments or tendons led to this decision[60].

We can confirm the presence of mechanoreceptors in the IOM as well as in the bordering and surrounding tissues.

We found Ruffini bodies, muscle spindles and Vater-Pacini corpuscles within the IOM. Further, we discovered few Golgi-Tendon organs as well as little sympathetic efferent supply. At the border towards the IOM, we found Ruffini bodies, muscle spindles, Vater-Pacini corpuscles as well as Golgi-Mazzoni corpuscles. In the surrounding structures, we discovered multiple Ruffini bodies, muscle spindles and Vater-Pacini corpuscles. Further, few Golgi-Mazzoni corpuscles were discovered in females.

In the following, we will describe in detail our findings according to the tissue the mechanoreceptors were found in and their anatomical locations.

Golgi-Mazzoni corpuscles are only scarcely researched in comparison to the other mechanoreceptors we found. Therefore, we will portray these structures specifically.

The results of the statistical tests, detailed above in the methods section, will also be outlined.

3.2 Neural structures in the IOM

3.2.1 Vater-Pacini corpuscles

Proximally

Within the proximal part of the IOM, no Vater-Pacini corpuscles were found, neither in the left nor in the right samples.

Medially

Medially, one Vater-Pacini corpuscle was found in the right IOM of a female. This Vater-Pacini corpuscle was located centrally within the IOM. In the remaining specimens, no Vater-Pacini corpuscles were seen.

Distally

Distally, one Vater-Pacini corpuscle was found in the left IOM of a male (see Figure 8). This Vater-Pacini corpuscle was similarly located centrally within the IOM. No Vater-Pacini corpuscles were found in the other specimens.

Longitudinally

No Vater-Pacini corpuscles were found in the longitudinal section of the proximal, medial, and distal part of the IOM.

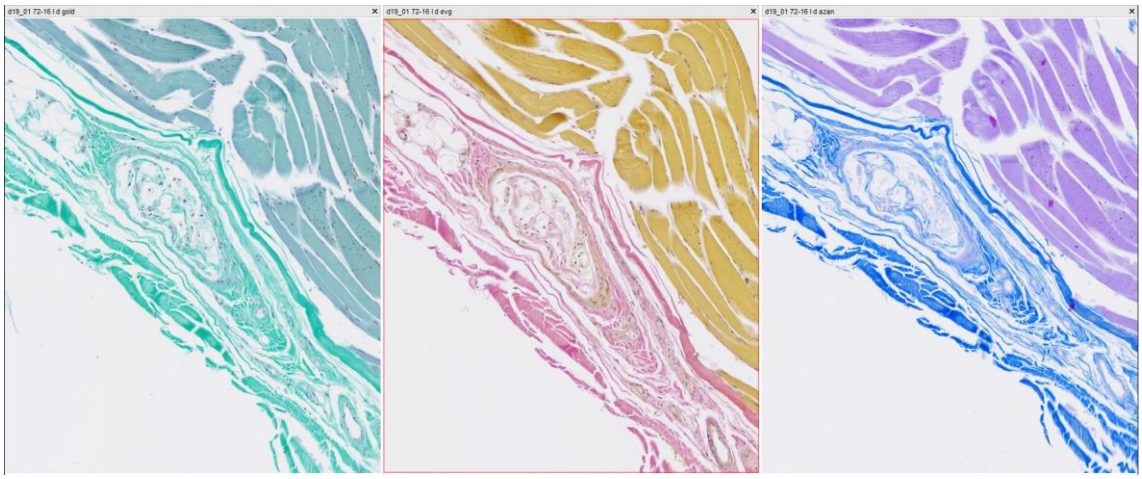

Figure 8: **Intramembranous Vater-Pacini corpuscle in the left, distal IOM of donor 5 (male)**
Original magnification: 7x, from left to right stained with Goldner stain, Elastica van Gieson stain, Azan stain

3.2.2 Golgi-Mazzoni corpuscles

Proximally

Proximally, no Golgi-Mazzoni corpuscles were found.

Medially

Medially, no Golgi-Mazzoni corpuscles were found.

Distally

Distally, no Golgi-Mazzoni corpuscles were found.

Longitudinally

Longitudinally, no Golgi-Mazzoni corpuscles were found.

3.2.3 Ruffini bodies

Proximally

Proximally, in one male donor 14 Ruffini bodies were found on the right side. These 14 Ruffini bodies were all located centrally within the IOM. In one female donor, one Ruffini body was found on the right side, which was located within the IOM but at the border towards muscle tissue. In the left specimens of one female and one male donor, one Ruffini body was found each centrally within the IOM.

Medially

Medially, one Ruffini body was found centrally within the IOM in a male, right specimen. In another male, right specimen, one Ruffini body was found within the IOM but at the border towards connective tissue. Further, one Ruffini body was found centrally within the IOM in two female, left specimens each.

Distally

In one female, right specimen two Ruffini bodies were located centrally within the IOM. In one male, right specimen and in one female, right specimen one centrally lying Ruffini body each was found. In the left specimens, no Ruffini bodies were seen.

Longitudinally

Longitudinally, in the left proximal specimen one Ruffini body was found centrally within the IOM. Further, in the left distal specimen two Ruffini bodies were found centrally within the IOM. In the right proximal and distal specimens as well as in both medial slices, no Ruffini bodies were detected.

3.2.4 Muscle spindles

Proximally

Proximally, one muscle spindle was found in the right IOM of a male donor.

Medially

Medially, no muscle spindles were found within the IOM.

Distally

Distally, in the same male donor as proximally, two muscle spindles were found in the right IOM. No muscle spindles were found in the left IOMs.

Longitudinally

Longitudinally, no muscle spindles were found within the IOM.

3.2.5 Golgi-Tendon organs

The innervation of Golgi-Tendon organs was only investigated within the IOM of the most recently deceased donor because prior staining results in the other donors yielded inconsistent results.

Proximally

Proximally, no Golgi-Tendon organs were identified.

Medially

Medially, one Golgi-Tendon organ was observed in the right, transverse specimen. Two Golgi-Tendon organs were seen in the left, transverse specimen (see Figure 9). All Golgi-Tendon organs were situated within the IOM at the border towards muscle tissue.

Distally

Distally, one Golgi-Tendon organ was identified centrally in the right, longitudinal specimen.

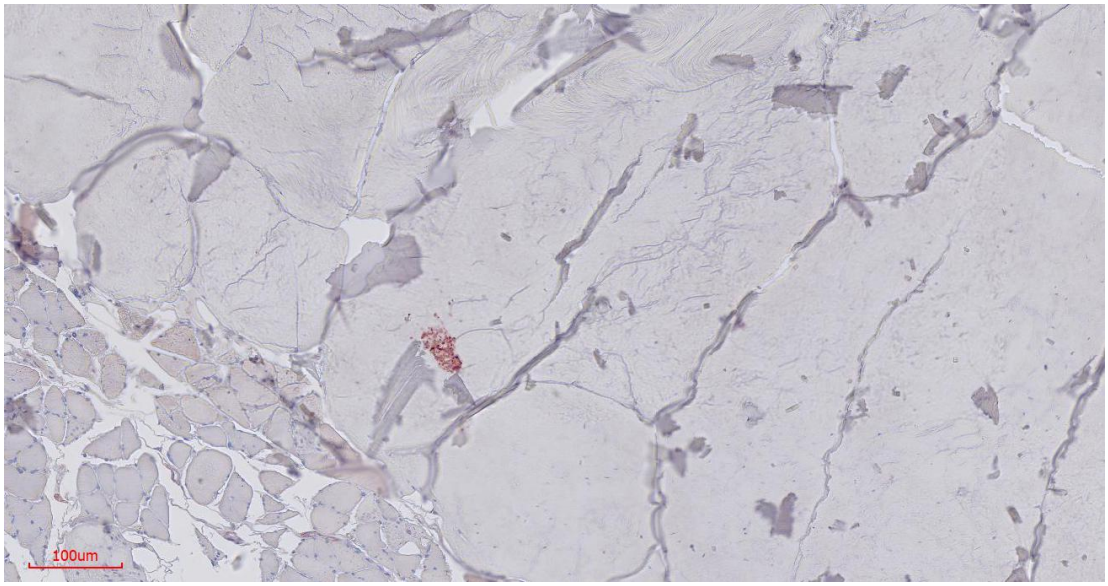

Figure 9: **Golgi-Tendon organ in a left, middle, transverse specimen**
Original magnification: 7x, scale bar size: 100µm, stained with TRCP4 stain

3.2.6 Sympathetic innervation

The sympathetic innervation was only investigated within the IOM of the most recently deceased donor because prior staining results in the other donors yielded inconsistent results.

Proximally

Proximally, only few signals were seen within the membrane on both sides. There were no differences between the longitudinal and transverse sections.

Medially

Medially, similarly to proximally, only few signals were identified on the right and left side. There were no differences between the longitudinal and transverse sections.

Distally

Distally, similarly to proximally and medially, only few signals were identified on the right and left side (Figure 10). In the transverse sections, highly innervated vessels were seen.

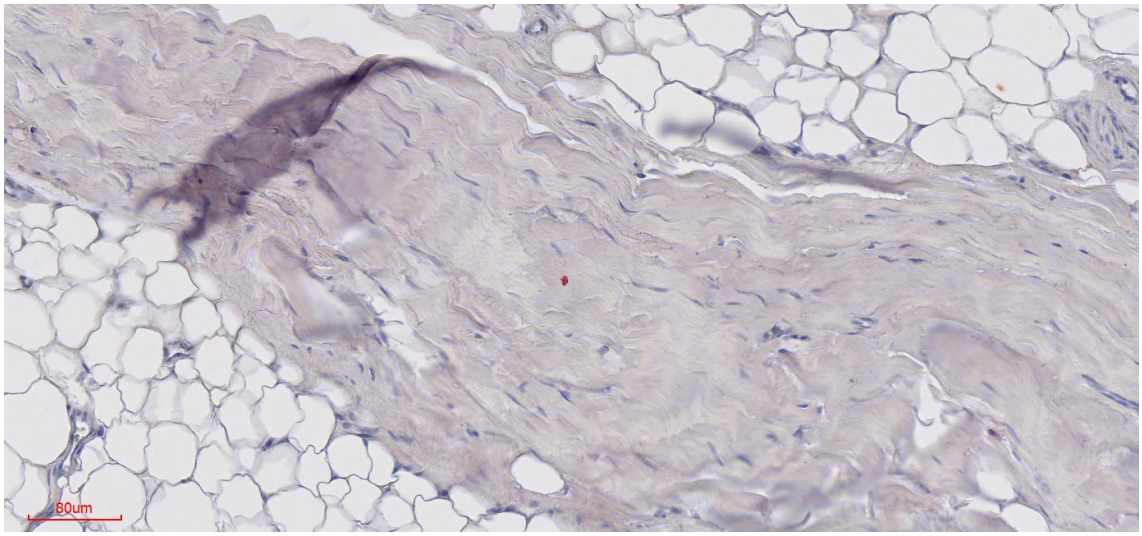

Figure 10: **Sympathetic nerve signal in a left, distal, female specimen**
Original magnification: 15x, scale bar size: 80µm, stained with Tyrosine hydroxylase stain

3.3 Mechanoreceptors at the border of the IOM

3.3.1 Vater-Pacini corpuscles

Proximally

Proximally, one Vater-Pacini corpuscle was found in a female, right specimen within connective tissue directly bordering the IOM. Two Vater-Pacini corpuscles were found in a male, right specimen also within connective tissue directly adjacent to the IOM. Further, one Vater-Pacini corpuscle was found in a male, left specimen, also in connective tissue at the border of the IOM.

Medially

Medially, one Vater-Pacini corpuscle each were found in two female, left specimens within connective tissue bordering the IOM. No Vater-Pacini corpuscle were found in the right specimens.

Distally

Distally, one Vater-Pacini corpuscle was found in the connective tissue of a female, right specimen. In the left specimens, one Vater-Pacini corpuscle was found in the connective tissue of a female donor and three Vater-Pacini corpuscles were seen in the connective tissue of a male donor. All Vater-Pacini corpuscles were directly at the border of the IOM.

Longitudinally

Proximally, one Vater-Pacini corpuscle was found on the right. Medially, one Vater-Pacini corpuscle was found on the left. Distally, there was one Vater-Pacini corpuscle on the right and two on the left. All Vater-Pacini corpuscles were situated in connective tissue adjacent to the IOM.

3.3.2 Golgi-Mazzoni corpuscles

Proximally

Proximally, one Golgi-Mazzoni corpuscle was seen in one female donor on the right, two Golgi-Mazzoni corpuscles were seen in another female donor on the right. In the specimens of the left side, one Golgi-Mazzoni corpuscle was found in a male donor. All Golgi-Mazzoni corpuscles were situated in connective tissue adjacent to the IOM.

Medially

Medially, no Golgi-Mazzoni corpuscles were found, neither on the right side nor on the left side.

Distally

Distally, one Golgi-Mazzoni corpuscle was identified in two female, right specimens each. In the specimens from the left side, three Golgi-Mazzoni corpuscles were found in a female specimen (Figure 11, 14) and one Golgi-Mazzoni corpuscle was found in another female specimen. All Golgi-Mazzoni corpuscles were found in connective tissue at the border towards the IOM. In male specimens no Golgi-Mazzoni corpuscles were found.

Longitudinally

Proximally, one Golgi-Mazzoni corpuscle was identified in the left specimen within connective tissue. In the remaining specimens, no Golgi-Mazzoni corpuscles were found.

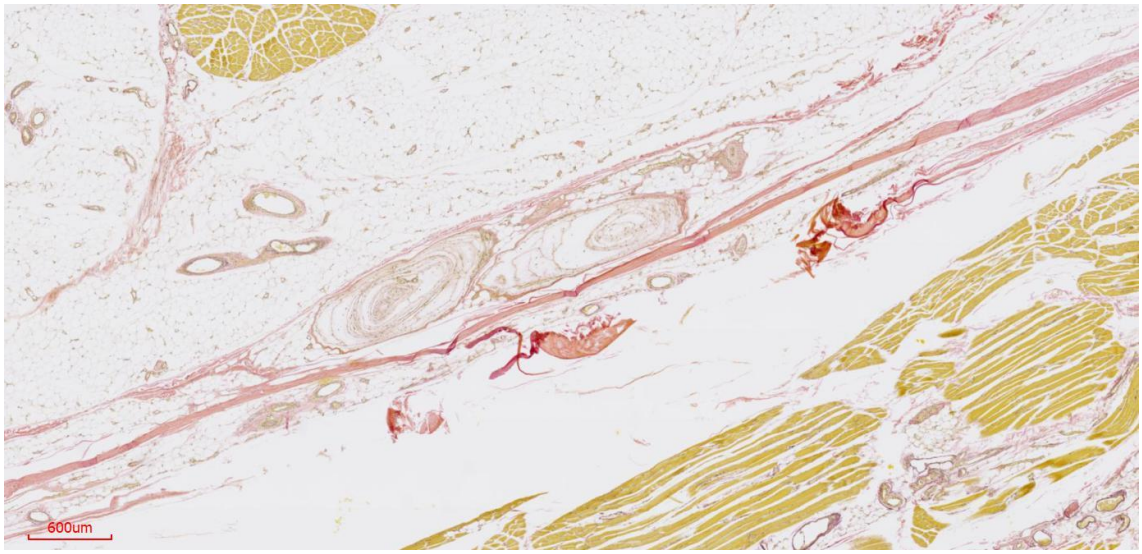

Figure 11: **Golgi-Mazzoni corpuscle consisting of two capsules close adjacent to the IOM**
Original magnification: 2x, scale bar size: 600µm, stained with Elastica van Gieson stain

3.3.3 Ruffini bodies

Proximally

Proximally, two Ruffini bodies were found in a female, right specimen, one in connective tissue, the other in muscle tissue. Four Ruffini bodies were found in the right specimen of a male donor. These four Ruffini bodies were all situated in connective tissue. Two Ruffini bodies were identified in a female specimen within muscle tissue on the left side. Further, one Ruffini body was found in the connective tissue of a male left specimen.

Medially

Medially, in the specimens from the right side, in two female donors, one Ruffini body was found, each within muscle tissue. In another female, on the right side as well, one Ruffini body was found within connective tissue. In specimens of the left side, one Ruffini body was found in

two females, each within connective tissue. In a further female donor, two Ruffini bodies were found on the left side within connective tissue.

Distally

Distally, in the specimens from the right side, two Ruffini bodies were found, one in a female, and the other in a male specimen. On the left side, one Ruffini body was identified in a female sample. All Ruffini bodies found were located within connective tissue adjacent to the IOM.

Longitudinally

Longitudinally, no Ruffini bodies were identified.

3.3.4 Muscle spindles

Proximally

Proximally, no muscle spindles were identified, neither on the right nor on the left side.

Medially

Medially, one muscle spindle was found in the right-sided specimen of a female donor within muscle tissue. No muscle spindles were identified in specimens from the left side.

Distally

Distally, one muscle spindle was identified within the connective tissue of a female right specimen. Further, one muscle spindle was found in the muscle tissue of a male right specimen and another one in the muscle tissue of a male left specimen. No muscle spindles were detected in the specimens from the left side.

Longitudinally

Longitudinally, two muscle spindles were found proximally within connective tissue. Proximally, on the right side as well as medially and distally, no muscle spindles were identified.

3.4 Mechanoreceptors around the IOM

3.4.1 Vater-Pacini corpuscles

Proximally

Proximally, in one male, right and in one female, right specimen one Vater-Pacini corpuscle was found each within connective tissue. In the specimens from the left side, two Vater-Pacini corpuscles were found within connective tissue in two female specimens each. In one female, left specimen one Vater-Pacini corpuscle was identified within muscle tissue. In one male, left specimen one Vater-Pacini corpuscle was found within connective tissue.

Medially

Medially, one Vater-Pacini corpuscle was identified in a female, left specimen within connective tissue. In the specimens from the right side, no Vater-Pacini corpuscles were found.

Distally

Distally, one Vater-Pacini corpuscle was found within the connective tissue of a female, left specimen. In the specimens from the right side, no Vater-Pacini corpuscles were found.

Longitudinally

Longitudinally, no Vater-Pacini corpuscles were identified.

3.4.2 Golgi-Mazzoni corpuscles

Proximally

Proximally, one Golgi-Mazzoni corpuscle was identified in the muscle tissue of a female, right specimen. One Golgi-Mazzoni corpuscle was identified in the specimens from the left arms in two female specimens each. Both Golgi-Mazzoni corpuscles were found in connective tissue.

Medially

Medially, no Golgi-Mazzoni corpuscles were found, neither on the right nor on the left side.

Distally

Distally, no Golgi-Mazzoni corpuscles were found, neither on the right nor on the left side.

Longitudinally

Proximally, no Golgi-Mazzoni corpuscles were identified. In the medial specimens, three Golgi-Mazzoni corpuscles were identified on the left side. Distally, two Golgi-Mazzoni corpuscles were found on the left within connective tissue.

3.4.3 Ruffini bodies

Proximally

Proximally, multiple Ruffini bodies were found. In the specimens from the right side within muscle tissue, two Ruffini bodies were found in a female specimen, in another female specimen 24 Ruffini bodies were found, in a third female specimen three were identified. In one male, 20 Ruffini bodies were found, in another male seven. Within connective tissue, two Ruffini bodies were found in a female, one Ruffini body was found in two females and one male each.

In specimens from the left side within muscle tissue, six Ruffini bodies were found in a female donor, eight in another female donor. In one male donor one Ruffini body was found, in another 26 and in a third one two Ruffini bodies were identified. Within connective tissue, one Ruffini body each was found in two female and two male donors.

Medially

Medially, a similar number of Ruffini bodies were found. In specimens from the right side within muscle tissue, five Ruffini bodies were found in three females each, in another female four Ruffini bodies were identified. In one male donor 22 Ruffini bodies were found, nine in another and two in a third male donor. Within connective tissue, in two female specimens one Ruffini body each was identified.

In specimens from the left side within muscle tissue, six Ruffini bodies were found in one female, seven in another, eleven in a third and three in the fourth female donor. In the male specimens, three Ruffini bodies were found in one male, seven in another and five in the third. Within connective tissue, two Ruffini bodies were found in a female, one Ruffini body in another, and three in a third female.

Distally

Distally, an even higher number of Ruffini bodies were identified. In specimens from the right side within muscle tissue, 19 Ruffini bodies were found in one female, in another 21, in a third 22 and in the fourth two. In the male specimens, 18 Ruffini bodies were found in one donor, six in another, five in the third. Within connective tissue, one Ruffini body was found in a female donor and one in a male donor.

In specimens from the left side within muscle tissue, twelve Ruffini bodies were identified in one female, nine in another, in the third 33, in the fourth five Ruffini bodies were found. In the male specimens, 17 Ruffini bodies were seen in one male donor, ten in another, and six in the third (see Figure 12). Within connective tissue, three Ruffini bodies were detected in one female, two in another, one Ruffini body in two males each, and three in the third male.

Longitudinally

Longitudinally, there were only two Ruffini bodies found in the distal specimen from the right side: one in muscle tissue, one in connective tissue. Proximally, medially, and distally in the left specimens, no Ruffini bodies were identified.

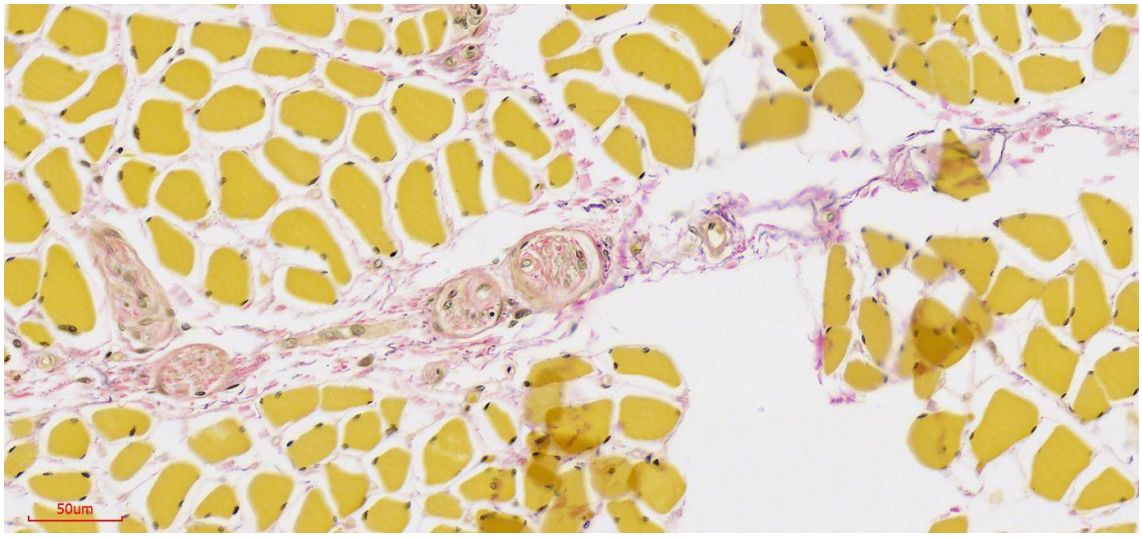

Figure 12: **Ruffini body in muscle tissue surrounding the IOM in a left, distal, male specimen**
Original magnification: 23x, scale bar size: 50µm, stained with Elastica van Gieson stain

3.4.4 Muscle spindles

Proximally

Proximally and in the specimens from the right side, two muscle spindles were identified in two female donors each. In one male donor two muscle spindles were identified as well and in another male donor one muscle spindle was found. In specimens from the left side, two muscle spindles were found in one female donor, in another female donor 13 muscle spindles were identified in muscle tissue and one within connective tissue. Further on the left side, one muscle spindle was found in two male donors each, in another male four muscle spindles were identified.

Medially

Medially and in specimens from the right side, one muscle spindle was found in a female donor, five in another. In one male donor, two muscle spindles were found and in another male donor four muscle spindles were identified. These were all situated within muscle tissue.

In specimens from the left side, four muscle spindles were found in one female donor, two muscle spindles in another, and seven muscle spindles were found in a third female donor. One muscle spindle each was found in two males. These were all situated within muscle tissue.

Distally

Distally and in specimens from the right side, two muscle spindles were found in one female, nine muscle spindles were identified in another and in a third female three muscle spindles were found. In the male donors, six muscle spindles were identified in one, four in another, and 14 in the third. These were all situated within muscle tissue. Within connective tissue, one muscle spindle was found in two female and one male donor each, in a further male two muscle spindles were identified.

In specimens from the left side, ten muscle spindles were found in one female, two muscle spindles in another, 13 in a third (see Figure 13) and four in a fourth female. In the male donors, five muscle spindles were found in one male and five in another. These were all situated within muscle tissue. Within connective tissue, one muscle spindle was found in two female donor each. In a third female donor two muscle spindles were found within connective tissue. In one male donor, seven muscle spindles were found within connective tissue.

Longitudinally

Proximally, one muscle spindle was identified in muscle tissue on the right side, and two muscle spindles on the left side within muscle tissue. Medially and distally no muscle spindles were identified.

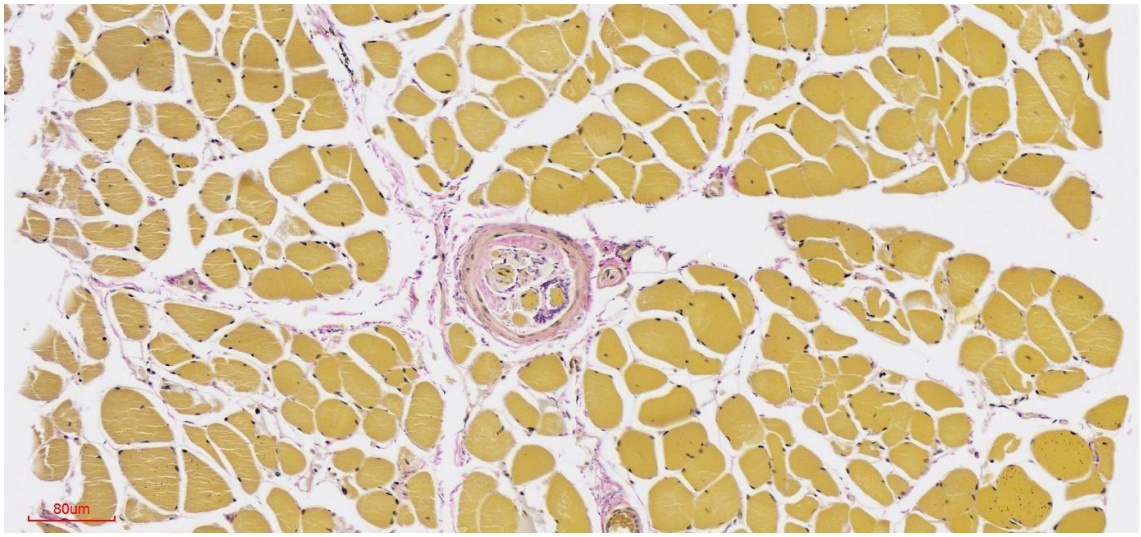

Figure 13: **Muscle spindle in muscle tissue surrounding the IOM in a left, distal, female specimen**
Original magnification: 15x, scale bar size: 80µm, stained with Elastica van Gieson stain

3.5 New findings in morphology of Golgi-Mazzoni corpuscles

During the histological analysis, we found structures which we identified as Golgi-Mazzoni corpuscles based on the clear description by Ruffini in 1905[51].

They were onion-bulb like structures, grouped in clusters of two to six. Some of these clusters were composed of multiple "swirls" of layers within one big capsule, some others consisted of multiple capsules sticking together or laying in very close proximity. With the Elastica-van-Gieson stain, the layers stained light pink, some were lying very closely together, other were more spaced out. The layers often got denser towards the middle of the structures. The most outward layer was stained in a darker pink. Dark violet nuclei were visible, which increased towards the middle. Most structures found were round to oval shaped. In three structures, a nerve running directly adjacent to the capsules was seen (see Figure 14). A distinct connective tissue layer surrounding all capsules of one corpuscle was found in two structures (see Figure 14, 15). Most of the Golgi-Mazzoni corpuscles found were close to either arteries and/ or the IOM.

3.6 Distribution of Golgi-Mazzoni corpuscles

In total, 19 Golgi-Mazzoni corpuscles, 13 in the cross-sectional specimens, 6 in the longitudinal specimens were found. 18 of the 19 Golgi-Mazzoni corpuscles were found in women. In the cross-sectional specimens, seven Golgi-Mazzoni corpuscles were found proximally, six were found distally. In the longitudinal sections, one Golgi-Mazzoni corpuscle was found proximally, three medially, and two distally.

The Golgi-Mazzoni corpuscles found in the cross-sectional sections varied in total length of the cluster from 739µm to 2886µm (mean length (ML): 1696µm; standard deviation (SD): 754,24) and in total width from 323µm to 2472µm (mean width (MW): 925µm; SD: 603,69). In the longitudinal sections, the total length varied from 501µm to 2885µm (ML: 1468,17µm; SD: 838,44) and the total width from 288µm to 1155µm (MW: 716µm, SD: 304,97). Most of the Golgi-Mazzoni corpuscles were composed of 2 capsules or 2 swirls (13/19). One corpuscle in the longitudinal sections was composed of three swirls. In the cross-sectional sections, two Golgi-Mazzoni corpuscles were composed of two capsules and one further swirl, one Golgi-Mazzoni corpuscle consisted of three capsules and four swirls within one capsule, and two other Golgi-Mazzoni corpuscles consisted of three and the other of four capsules.

In most Golgi-Mazzoni corpuscles, one capsule was bigger than the other(s). The length and width of the biggest capsules in the cross-sectional sections varied from 437µm to 2499µm (ML: 1183µm; SD: 641,57) and 323µm to 1323µm (MW: 678,46µm, SD: 292,06), respectively. In the longitudinal sections, the biggest capsules measured in length from 351µm to 1791µm (ML: 1185,33µm; SD: 639,64) and in width from 299µm to 901µm (MW: 562,17µm, SD: 233,91). The number of layers of the biggest capsules in the cross-sectional slices varied between 6 to 24 (mean: 12,85; SD: 5,93) and 7 to 16 (mean: 11,33, SD: 3,67) in the longitudinal sections.

In the second biggest or smallest capsule, depending on the number of capsules one corpuscle was composed of, the length and width varied from 224µm to 1330µm (ML: 662,69µm, SD: 401,33) and 200µm to 807µm (MW: 445,46µm, SD: 152,15), in the cross-sectional sections and 122µm to 1438µm (ML: 555,67µm, SD: 513,15) and 103µm to 676µm (MW: 303µm, SD: 238,59) in the longitudinal sections, respectively. The layers of the capsules varied from 4 to 21 (mean: 11,3, SD: 6,38) in the cross-sectional sections and 5 to 11 (mean: 7,5; SD: 2,29) in the longitudinal sections.

The following third capsules varied in length from 251µm to 457µm (ML: 361,2, SD: 73,35) and in width from 157µm to 718µm (MW: 381,4µm, SD: 213,83) in the cross-sectional slices. The capsules had between seven to fifteen layers. The only third capsule in the longitudinal section measured 147µm in length, 88µm in width and had 12 layers. The remaining capsules in

the two Golgi-Mazzoni corpuscles with four to six capsules/ swirls, the length varied from 184µm to 338µm (ML: 258µm, SD: 64,31) and 125µm to 295µm (MW: 183,5µm, SD: 75,85) in width. The layers varied between 6 to 14 (mean: 9, SD: 3,83).

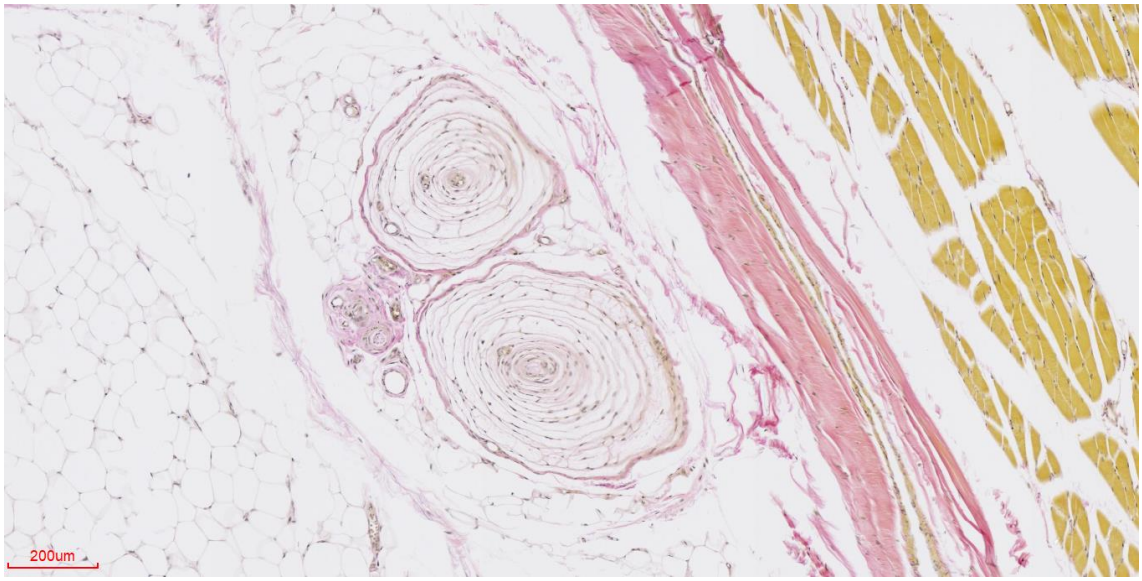

Figure 14: **Golgi-Mazzoni corpuscle consisting of two capsules and one adhering axon in donor 1 (female)**
Original magnification: 5x, scale bar size: 200µm, stained with Elastica van Gieson stain

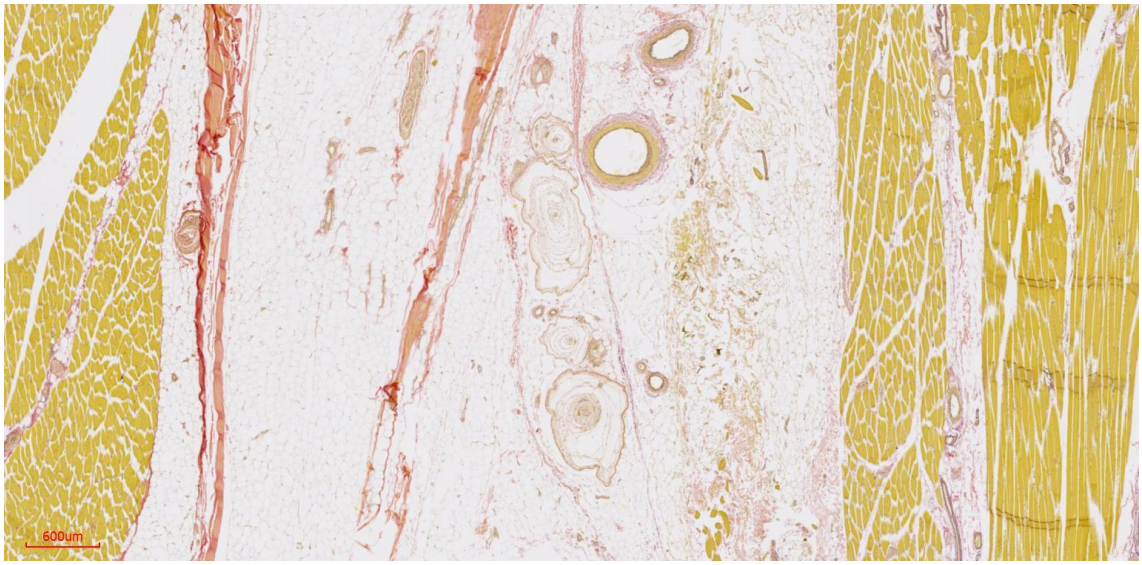

Figure 15: **Golgi-Mazzoni corpuscle consisting of four capsules in donor 2 (female)**
Original magnification: 2x, scale bar size: 600µm, stained with Elastica van Gieson stain

3.7 Statistical Results

Description of analysed data

We statistically analysed both IOMs of seven donors (three male, and four female donors). This statistical analysis is limited to the cross-sectional specimens and excludes the longitudinal sections from donor 7.

Therefore, a total of 294 areas composed of three areas of each IOM categorized into seven different tissue regions were investigated for four parameters. The seven tissue regions were within the IOM, at the border towards muscle tissue but still within the IOM, at the border towards connective tissue but still within the IOM, at the border to the IOM within muscle tissue, at the border to the IOM within connective tissue, in muscle tissue surrounding the IOM, in connective tissue surrounding the IOM. The four parameters investigated were Ruffini bodies, muscle spindles, Golgi-Mazzoni corpuscles and Vater-Pacini corpuscles (see Table 20).

Statistics	Ruffini bodies	Muscle spindles	Golgi-Mazzoni corpuscles	Vater-Pacini corpuscles	Sum
Areas investigated	294	294	294	294	-
Sum of corpuscles found	451	156	13	23	643

Table 20: **Summary of number of areas investigated and corpuscles found**
Calculation for areas investigated: 7 donors x (3 IOM regions x 2 sides) x 7 tissue areas investigated = 294 areas investigated. In total 643 mechanoreceptors were identified in the cross-sectional sections, thereof 451 Ruffini bodies, 156 muscle spindles, 13 Golgi-Mazzoni corpuscles and 23 Vater-Pacini corpuscles.

Ruffini bodies

We found up until 33 Ruffini bodies within one section. In 72% of sections no Ruffini bodies were found. In total, 451 Ruffini bodies were discovered in all sections.

Muscle spindles

We found up until 14 muscle spindles within one section. In 15% of sections, muscle spindles were seen. In total, 156 muscle spindles were discovered.

Golgi-Mazzoni corpuscles

These rather rare structures were discovered in more than 3% of all specimens. The largest number of Golgi-Mazzoni corpuscles found within one specimen were three. In total, 13 Golgi-Mazzoni corpuscles were found in the cross-sectional specimens.

Vater-Pacini corpuscles

Vater-Pacini corpuscles were identified in 6% of all sections. We found up to three of them in one section. In total, 23 Vater-Pacini corpuscles were found.

Requirements for statistical comparison of age, gender, body side and localisation regarding the distribution of mechanoreceptors

Age, gender, body side

The group of data was neither paired nor normally distributed but right-skewed (positive skewness) and pointed (positive kurtosis). Therefore, the Kruskal–Wallis Non Parametric Hypothesis test was used. A p-value of <0,05 was set to establish statistical significance.

Statistics	Ruffini bodies	Muscle spindles	Golgi-Mazzoni corpuscles	Vater-Pacini corpuscles
Variable Age				
Kruskal-Wallis-H	3.6565	1.8914	9.9226	4,946
p-value for asymptotic significance	0.723	0.9294	0.128	0.5508
Variable Gender				
Kruskal-Wallis-H	0.59051	0.26483	**4.566**	0.66849
p-value for asymptotic significance	0.4422	0.6068	**0.03261**	0.4136
Variable Body sides				
Kruskal-Wallis-H	0.0067568	0.007488	0.0000047734	2.1555
p-value for asymptotic significance	0.9345	0.931	0.9983	0.1421

Table 21: **Results of Kruskal–Wallis Non Parametric Hypothesis test for the variable age, gender and body sides.**

Age, gender, and body sides were tested for statistically significant differences. No significant differences were found regarding body side and age in all mechanoreceptors and gender in muscle spindles, Ruffini bodies and Vater-Pacini corpuscles. Therefore, for further tests regarding tissues regions, areas of the IOM and correlations regarding the presence of mechanoreceptors the data was pooled.

Gender-wise, a statistically significant difference between the presence of Golgi-Mazzoni corpuscles in female and male was found with the Kruskal–Wallis Non Parametric Hypothesis test, with more Golgi-Mazzoni corpuscles in females. In the Mann-Whitney-U test, the p-value for the different distribution between both genders was 0.05049, thus not statistically significant. Therefore, for the following tests, this data was also pooled.

IOM portions

Focussing on the comparison of the single membrane portions, there were significant differences in the Kruskal–Wallis Non Parametric Hypothesis test for muscle spindles (p-value: 0.006136). To determine the exact difference, we choose the Mann-Whitney-U test.

Significant differences for muscle spindles were found between the distal and proximal sections (p-value: 0.01152) and distal and medial sections (p-value: 0.007313), both times with a greater number of muscle spindles distally. The number of muscle spindles found in each section hinge on the muscle tissue included in each section. As the surrounding muscle tissue in each section was largely dependent on the IOM thickness as well as further connective tissue content and was not our primary research goal, these statistical values should only be seen as indicators for future research needs.

p-value for asymptotic significance	**Proximal - medial**	**Distal - proximal**	**Distal – medial**
Muscle spindles	0.8474	**0.01152**	**0.007313**

Table 22: **Results of Mann-Whitney-U test for muscle spindles regarding IOM portions**

Tissue zones

In the Kruskal–Wallis Non Parametric Hypothesis test, all mechanoreceptors showed statistically significant differences with $p < 0{,}001$ regarding the tissue zones. To determine the exact differences, Mann-Whitney-U test was performed. The following tables display the results. Only significant values are shown. The columns always display the tissue zone with significant more mechanoreceptors.

Ruffini bodies							
p-value for asymptotic significance	**Within the IOM**	**Within, at the border to muscle**	**Within, at the border to CT**	**Bordering in muscle**	**Bordering in CT**	**Muscle**	**CT**
Within the IOM						**< 0.001**	**0.012**
Within, at the border to muscle	**0.007**				**0.004**	**< 0.001**	**< 0.001**
Within, at the border to CT	**0.007**				**0.004**	**< 0.001**	**< 0.001**
Bordering in muscle						**< 0.001**	**< 0.001**
Bordering in CT						**< 0.001**	**0.021**
Muscle							
CT						**< 0.001**	

Table 23: **Results of Mann-Whitney-U test for Ruffini bodies regarding tissue zones**

Muscle spindles							
p-value for asymptotic significance	**Within the IOM**	**Within, at the border to muscle**	**Within, at the border to CT**	**Bordering in muscle**	**Bordering in CT**	**Muscle**	**CT**
Within the IOM						**< 0.001**	**0.026**
Within, at the border to muscle						**< 0.001**	**0.002**
Within, at the border						**< 0.001**	**0.002**

to CT							
Bordering in muscle						**< 0.001**	
Bordering in CT						**< 0.001**	**0.007**
Muscle							
CT						**< 0.001**	

Table 24: **Results of Mann-Whitney-U test for muscle spindles regarding tissue zones**

Golgi-Mazzoni corpuscles							
p-value for asymptotic significance	**Within the IOM**	**Within, at the border to muscle**	**Within, at the border to CT**	**Bordering in muscle**	**Bordering in CT**	**Muscle**	**CT**
Within the IOM					**0.006**		
Within, at the border to muscle					**0.006**		
Within, at the border to CT					**0.006**		
Bordering in muscle					**0.006**		
Bordering in CT							
Muscle					**0.026**		
CT							

Table 25: **Results of Mann-Whitney-U test for Golgi-Mazzoni corpuscles regarding tissue zones**

Vater-Pacini corpuscles							
p-value for asymptotic significance	**Within the IOM**	**Within, at the border to muscle**	**Within, at the border to CT**	**Bordering in muscle**	**Bordering in CT**	**Muscle**	**CT**
Within the IOM					**0.042**		
Within, at the border to muscle					**0.003**		**0.006**
Within, at the border to CT					**0.003**		**0.006**
Bordering in muscle					**0.003**		**0.006**
Bordering in CT							
Muscle					**0.014**		**0.026**
CT							

Table 26: **Results of Mann-Whitney-U test for Vater-Pacini corpuscles regarding tissue zones**

4 Discussion

4.1 Summary of Evidence

Based on prior research on the nerval innervation of the IOM, we expected to find mechanoreceptors within the IOM[25]. We assumed to find mechanoreceptors also in the surrounding tissues. We did not expect to find this quantity of Golgi-Mazzoni corpuscles. In total, we found Ruffini bodies, muscle spindles, Vater-Pacini corpuscles, and some Golgi-Tendon organs, as well as a small number of sympathetic nerves within the IOM. At the border towards the IOM and in the surrounding tissues, we found Ruffini bodies, muscle spindles, Vater-Pacini corpuscles as well as Golgi-Mazzoni corpuscles. This range of mechanoreceptors and the stimuli they detect reflect the range of demands on the IOM, the connective tissue, and muscle tissue around: from supporting micromovements in the hands to facilitating maximal movements of the entire upper limb.

To our knowledge, there is only one other study who investigated the presence of sensory free nerve endings in the IOM yet[25]. They found generally few structures within the IOM, in 13 of 62 structures they found no sensory nerve endings, however, they also checked the single ligaments for free nerve endings[25]. We found no mechanoreceptors in 29 out of 42 cross-sectional sections, however the tissues at the border to and surrounding the IOM were always highly innervated. It seems that the IOM itself may be less important for providing sensory feedback itself, but that its movement is very closely monitored by the multitude of the mechanoreceptors around it.

Rein et al.[25] found Vater-Pacini bodies, Ruffini endings and Golgi-like endings within the IOM. In our specimens, we found the same mechanoreceptors plus some muscle spindles within the IOM. In 24 specimens, Rein et al.[25] found corpuscles, they could not classify. For classification, they used the system by Freeman and Wyke[63] with the adaptation of Hagert[67]. We identified and classified the sensory nerve endings found according to the original descriptions. Although, the sensory nerve endings varied partly greatly in their morphology, there were always some unifying characteristics which matched the original descriptions. The different classification systems and the high number of unclassifiable corpuscles in the other study, complicate the comparison of findings.

Stecco et al.[78] investigated the innervation of the deep fascia of the upper extremity and focused, amongst others, on the middle third of the anterior region of the antebrachial fascia and the flexor retinaculum. As the antebrachial fascia also has septae connected to the IOM, the fact that the researchers found a rich innervation of mechanoreceptors and free nerve endings[78], supports our findings.

With our research, we want to add to the current knowledge about the innervation and role of the IOM in the forearm and will discuss our findings in the following.

Vater-Pacini corpuscles

Within the membrane

We found two Vater-Pacini corpuscles within the IOM. They were situated within a female, right, medial and a male, left, distal specimen. While we only found those two corpuscles within the IOM, Rein et al.[25] found Vater-Pacini corpuscles within 10 IOM portions. They found the corpuscles significantly more often in the distal oblique bundle than in any other ligament.

Proximally

Interestingly, we found no Vater-Pacini corpuscles within the proximal parts of the IOM, however we found four Vater-Pacini bodies proximally at the border to the IOM and eight Vater-Pacini corpuscles proximally in the surrounding tissues. Morley et al.[66] performed a similar study to ours but on the interosseous membrane cruris. They found that the Vater-Pacini corpuscles were only located on the surface of the interosseous membrane, where muscle fibres insert. Their findings correspond at least partially with ours, as dependent on the sectioning, Vater-Pacini corpuscles laying in connective tissue at the border to the IOM could be interpreted as laying on the surface of it.

Medially

Medially, next to the Vater-Pacini corpuscle found within the IOM, we found two Vater-Pacini corpuscles at the border to the IOM and one corpuscle within the surrounding tissues. Except for the Vater-Pacini corpuscle within the IOM, all other corpuscles were found in specimens from the left side.

Distally

In the distal specimens, next to the Vater-Pacini corpuscle found within the IOM, we found five further corpuscles at the border to the IOM and one in the surrounding tissue. Thus, we found more Vater-Pacini corpuscles proximally than distally. This deviates from the results of Rein et al.[25], who found more Vater-Pacini corpuscles in the distal IOM than in the middle or proximal IOM.

Longitudinally

Longitudinally, no Vater-Pacini corpuscles were found within the IOM. At the border to the IOM one Vater-Pacini corpuscle was found proximally, one medially and three distally. There were no Vater-Pacini corpuscles in the surrounding tissues. This could be either due to the limited amount of surrounding tissues in the longitudinal sections or because of the previous

stated hypothesis that the Vater-Pacini corpuscles bordering the IOM are actually laying on the surface of the IOM. The latter would match with the other findings regarding Vater-Pacini corpuscles.

Sides

There was no difference in distribution of the Vater-Pacini corpuscles between the left and right sides.

Particularities

All Vater-Pacini corpuscles except one were found in connective tissue. This trend was statistically significant. The one Vater-Pacini corpuscle found in muscle tissue laid between muscle fibres running in different directions. We offer the hypothesis that due to its special location in the middle of muscle fibres this Vater-Pacini corpuscle fulfils the purpose to detect displacements of these muscle fibres against each other.

While there has only been one further study investigating the presence of Vater-Pacini corpuscles in the IOM[25], the innervation of the crural interosseous membrane has been studied more intensively. Hunt already explored the crural interosseous membrane in cats in 1960 and noted encapsulated structures that he classified as Vater-Pacini corpuscles[79]. Zelená investigated in 1978 the development of Vater-Pacini corpuscles in the interosseous membrane cruris in rats[80]. Fleming hypothesised in 2013 that one possible function of the Vater-Pacini corpuscles, especially those lying in the interosseous membrane cruris could be to sense transmitted vibrations through the skeletal system[53]. The vibration could either be caused by movement of the animal or come from an external source, for example announce predators in the surroundings[53]. In 2019, Morley et al.[66] confirmed the presence of Vater-Pacini corpuscles in the interosseous membrane cruris in humans. Similarly to Flemings hypothesis[53], we believe that the Vater-Pacini corpuscles found within the IOM and at the border to and surrounding it, serve the purpose of detecting vibration of the hand and forearm and transmitting this sensation to the brain.

We noticed that in some individual donors there were more Vater-Pacini corpuscles than in others. Notably, in one male donor (donor 3) there were none. We will discuss this finding later in synopsis with the other mechanoreceptor results.

<u>Golgi-Mazzoni corpuscles</u>

Golgi-Mazzoni corpuscles differ amongst others from Vater-Pacini corpuscles by their composition of multiple capsules which are orientated into different directions and thus detect stimuli from a multitude of directions.

Within the IOM

We found no Golgi-Mazzoni corpuscles within the IOM. These were the only mechanoreceptors we did not find there. One hypothesis for this is that there might be no need for Golgi-Mazzoni corpuscles within the single ligaments as these only move unidirectional and therefore an innervation with Vater-Pacini corpuscles is sufficient to detect vibration.

Proximally

Proximally, at the border to the IOM, we identified four Golgi-Mazzoni corpuscles, three in females and one in the male donor 6. This is the only Golgi-Mazzoni corpuscle that we identified in a male donor. In the surrounding tissues, we identified three Golgi-Mazzoni corpuscles in three different female donors, one in each. Two of these were on the left side within connective tissue. The third Golgi-Mazzoni corpuscle laid within muscle tissue in a right sided specimen. Vater-Pacini corpuscles and Golgi-Mazzoni corpuscles were both not present in the proximal IOM portion, but in the tissues around it. As there are many muscles running along this portion of the IOM, we assume that the three-dimensional detection of vibration allowed by the Golgi-Mazzoni corpuscles is important to provide feedback about coordinated movements by different muscles.

Similarly, to the Vater-Pacini corpuscles, most of the Golgi-Mazzoni corpuscles laid in connective tissue. We only found one Golgi-Mazzoni corpuscle in muscle tissue. This corpuscle consisted of two capsules, one very big and a smaller one on top, which laid centrally within a string of muscle fibres. Next to these muscle fibres was a big artery. This Golgi-Mazzoni corpuscle was located on the left side of the section, and therefore structures at the left of it were cut. We assume that it is either located at this position to detect the filling state of the artery or for another structure which was cut.

Medially

In the cross-sectional slices, we found no Golgi-Mazzoni corpuscles. First, we assumed that these 3D-mechanoreceptors are not required in or around the middle portion of the IOM as in comparison to the proximal and distal parts of the IOM, there is only little rotational or flexion-extension movement at the middle part of the IOM. However, then we identified three Golgi-Mazzoni corpuscles within the longitudinal section in the connective tissue around the IOM, all within the left sample. Therefore, we believe that also there might be less Golgi-Mazzoni corpuscles in the medial sections, their presence is still required for ideal function of the forearm. Considering that the middle portion of the IOM serves as tendon of origin for different flexor and extensor muscles, the need for three-dimensional detection of vibration is evident.

Distally

Distally, we found Golgi-Mazzoni corpuscles only at the border to the IOM, not within it and not in the tissues surrounding it. In one female donor, distally, we found one Golgi-Mazzoni corpuscle in the specimen from the right IOM and 3 Golgi-Mazzoni corpuscles in the IOM from the left. Additionally, we found two Golgi-Mazzoni corpuscles in two further females, one in each. Referring to the argument made further above, that mechanoreceptors at the border towards the IOM are probably lying on the surface of it[66], we hypothesise that there is a great requirement for detection of small changes in movement at this level of the IOM. As dorsiflexion, palmarflexion, abduction, adduction, pronation, and supination are taking place in this area of the forearm, a multitude of stimuli have to be detected thoroughly to guarantee optimal movement[81].

Longitudinally

In the longitudinal samples, which were all from one female donor, we only found Golgi-Mazzoni corpuscles within the specimens from the left arm. Within the IOM, there were no Golgi-Mazzoni corpuscles, equally to the cross-sectional specimens. Proximally, we found one Golgi-Mazzoni corpuscle at the border to the IOM. In the surrounding tissues, we found three and two Golgi-Mazzoni corpuscles in the medial and in the distal portions, respectively. Although, we did not identify Golgi-Mazzoni corpuscles within the medial slices of the cross-sectional sections, the finding of Golgi-Mazzoni corpuscles in the medial longitudinal slice contradicts the hypothesis of many researchers that the middle portion of the IOM has a solely biomechanical role. This sensory innervation might be necessary in the middle ligamentous region of the IOM because of the attaching muscles whereas in the proximal and distal membranous regions they possibly rather detect the movement of the joints. Regardless of the underlying reason, the medial region of the IOM seems to have a great role in proprioception.

Sides

We observed an interesting difference in distribution of Golgi-Mazzoni corpuscles between the individual donors. In donor 1, we only found Golgi-Mazzoni corpuscles in the specimens from the left arm, whereas in donor 2, there were only Golgi-Mazzoni corpuscles in the right-sided specimens. In donor 4, we found these corpuscles in the right and in the left sided specimens. In donor 7, we found no Golgi-Mazzoni corpuscles in the cross-sectional slices but six in the longitudinal slices and these were all in the left-sided specimens. As the handedness of the donors is unknown, we are unfortunately unable to draw valid conclusions from this striking finding.

Further notes

We found an interesting gender difference in distribution of Golgi-Mazzoni corpuscles. This difference was statistically significant in the Kruskal-Wallis test but not in the Mann-Whitney-U test. This difference in result is probably due to the small number of corpuscles. A greater sample size might clarify this trend.

In the male donor 3 and donor 5, we found no Golgi-Mazzoni corpuscles and in the third male donor 6 only one, on the left. In all four female donors, we identified Golgi-Mazzoni corpuscles. Comparing our results to Rein et al.[25], it is remarkable that they found Pacini-like corpuscles within ten IOM structures whereas we only found Vater-Pacini corpuscles in two. Rein et al.[25] did not differentiate between Vater-Pacini or Golgi-Mazzoni corpuscles. However, in contrast to Rein et al.[25] our sample group consisted of four female and three males and 14 forearms in total while their study sample consisted of eleven forearms of six women and one male. This unbalanced gender distribution in the other study could explain the discrepancy between our results. It is known that mechanoreceptors have a great role in nociception[78] and that pain is differently perceived by women and man[82,83]. Therefore, our results indicating that women may have more Golgi-Mazzoni corpuscles may be one reason why women are more often affected by pain syndromes in the upper limb such as CRPS Type I[41,44,46].

Looking at the distribution of both Golgi-Mazzoni corpuscles and Vater-Pacini corpuscles, it is noticeably that we found neither of both mechanoreceptors in donor 3, who is a male and the youngest deceased donor with 67 years. In the other two male donors, we found some Vater-Pacini corpuscles proximally and distally. Therefore, we assume that either some people do have less or no Golgi-Mazzoni or Vater-Pacini corpuscles or that there is a sample bias as donor 7 also had no Golgi-Mazzoni corpuscles in the transsectional sections but in the longitudinal specimens. Nevertheless, we found Vater-Pacini corpuscles in the transsectional sections of donor 7, restricting this theory. The fact that we did not find these two mechanoreceptors in our youngest donor but in the older ones are in line with the findings of García-Piqueras and colleagues[84], that Vater-Pacini corpuscles do not atrophy with age.

Many of the Golgi-Mazzoni corpuscles we identified laid between the IOM and blood vessels, particularly arteries. As the IOM and the arteries were not always running completely parallelly to each other, we assume that the Golgi-Mazzoni corpuscles, with their three-dimensional detection areas through the differently directed capsules, are laying close by to detect stimuli from both structures.

The sizes of most capsules within one Golgi-Mazzoni corpuscle differed from each other. This could be due to slicing at a particular level and hence, would not reflect the reality. However,

the capsules could also differ in sizes depending on their orientation and the number and force of stimuli they should detect.

In three Golgi-Mazzoni corpuscles, a nerve was running close by. We assume that this nerve might branch the afferent axon[51], shortly before dividing into two or more axons running to the single capsules (see Figure 16). Some Golgi-Mazzoni corpuscles consisted of one big capsule with a few swirls within or of two or more capsules with one containing swirl. We believe that these swirls develop into single capsules at another level than our sectioning level like buds of a flower. The most outside layers of the single capsules stained more darkly with our EvG-stain than the layers within the capsule. This is probably due to the myelin sheath of the entering axon remaining outside and wrapping around the capsule (see Figure 16).

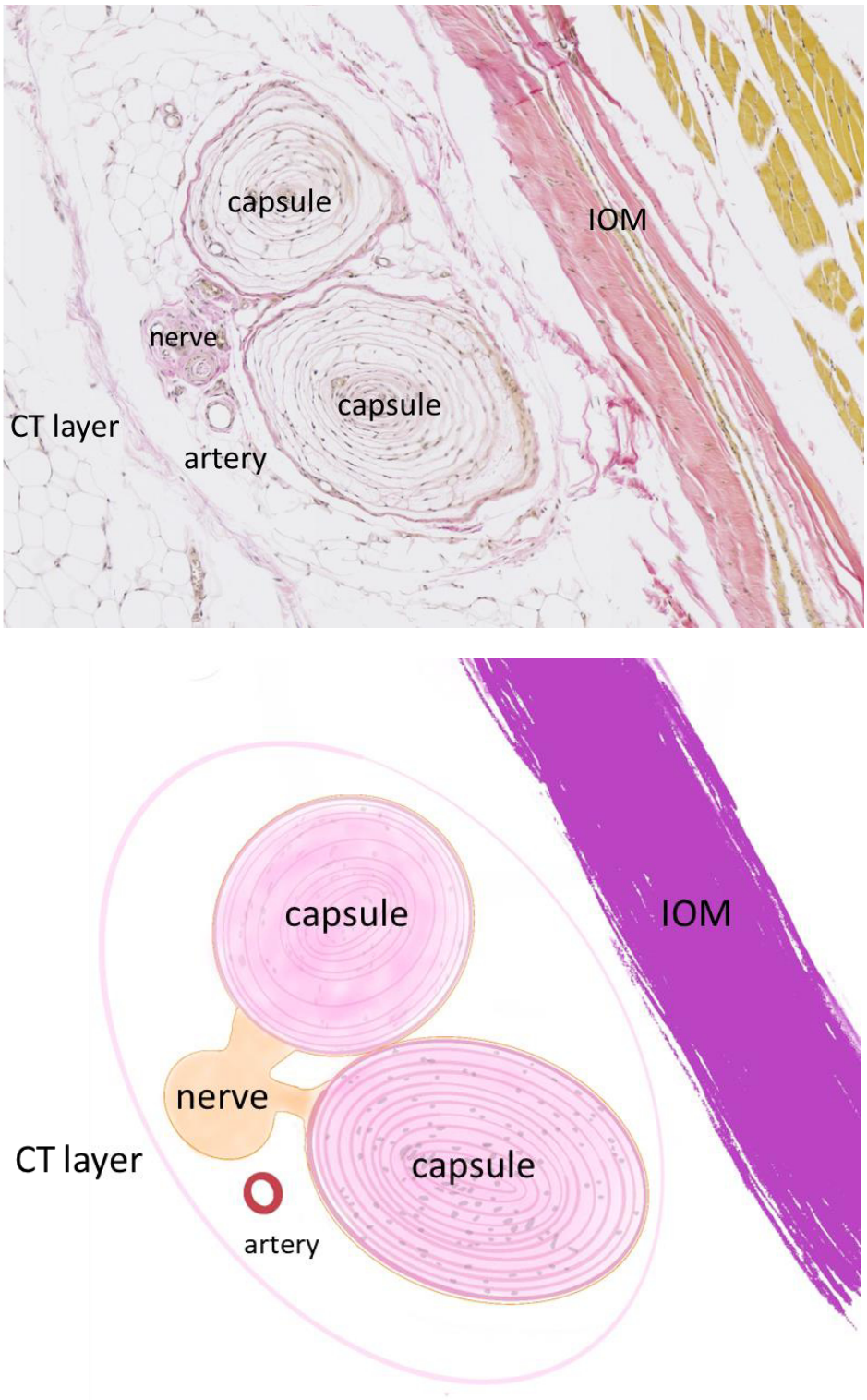

Figure 16: **Structure of a Golgi-Mazzoni corpuscle consisting of two capsules close to the IOM**
Connective tissue layer (CT layer) surrounding the corpuscle. There is a nerve, splitting into two axons to supply two capsules. The myelin sheath of the axons joins into the most outward layer of the capsule. The amount of layers differ largely between different capsules. Little, dark-stained granula are spread in the different capsules. The Golgi-Mazzoni corpuscle lies close to the IOM.

Muscle spindles

Within the IOM

Within the IOM, we found muscle spindles in the male donor 3. In his proximal right IOM, we found one and in his distal right IOM two muscle spindles. It is striking that he is the only donor we found muscle spindles within the IOM in but also the only one without Vater-Pacini corpuscles. In addition, we also found no Golgi-Mazzoni corpuscles in his specimens. We assume that these muscle spindles were remains of attached muscle fibres which were cut from the IOM.

Proximally

In the proximal specimens, there were no muscle spindles at the border to the IOM. Around the IOM, there were many more muscle spindles. Noticeably, in some donors, there was a greater number of muscle spindles, especially on the left.

Medially

In the medial specimens, we found one muscle spindle at the border to the IOM in the most recently deceased donor 7. There were many muscle spindles in the surrounding muscle tissue of the IOM.

Distally

Also distally, we only found few muscle spindles at the border to the IOM. Distally, we found the greatest number of muscle spindles in the surrounding tissues, interestingly some in connective tissue. Similarly, to the muscle spindles within the IOM, we assume that the muscle spindles in connective tissues are actually remains of attached muscle fibres which were cut.

Longitudinally

In the longitudinal specimens, we only identified muscle spindles in the proximal sections, some directly at the border to the IOM but the majority in the surrounding tissues. In the medial and distal specimens, we did not identify muscle spindles. This can be due to the fact that the IOM was thicker medially and distally, and only little muscle tissue was harvested with the specimens.

Sides

In some donors, there seems to be a predominance of muscle spindles on one side. However, there was no connecting trend between the individual donors, therefore we assume that this may be due to the unknown handedness. Statistically, no significant difference between body sites were found, although this could also be due to the small sample size.

Further notes

We identified muscle spindles in every donor which shows how vital these mechanoreceptors are. Most of the muscle spindles found lay in the tissues surrounding the IOM, the only area in our specimens with muscle fibres. Therefore, the few muscle spindles found outside of the muscle tissue i.e. within the IOM or in connective tissue around are worthwhile to discuss. We offer the hypothesis that these muscle spindles are remains of muscle fibres which were cut during histological preparation. It is interesting that these muscle spindles are located at the transition to other tissues, which indicates how important stretch-detectors are at these sites.

Regarding the different anatomical locations, we found most muscle spindles distally with no gender difference. In the medial sections we found less muscle spindles and those that we found were divided between all donors. Proximally, there was one donor with many muscle spindles whereas in others we found none or only few. Although, the distribution of muscle spindles was different, the number of muscle spindles found in total is similar proximally and medially. This trend was confirmed by the statistical tests. There were significantly more muscle spindles distally than medially and proximally. We hypothesise that distally, minimal differences in muscle length are more important to register to control hand movement efficiently and therefore more muscle spindles are present.

Ruffini bodies

Within the IOM

Within the IOM, we only found few Ruffini bodies. The male donor 3 stood out because especially proximally he had more intramembranous Ruffini bodies than the other donors. Interestingly, this donor also had more muscle spindles within the proximal membrane than the others. In total, we found Ruffini bodies within 11 IOMs. Rein et al.[25] found these mechanoreceptors in nine IOM structures: in the distal oblique bundle, the distal accessory band, the proximal accessory band and the proximal oblique cord. They found no statistical differences regarding the distribution of Ruffini bodies between the different ligaments. In comparison to Rein et al.[25], we also found some Ruffini bodies in the medial portion within a thicker portion of the IOM. We assume that this portion might rather correspond to the central band than to accessory bands. This would mean that contrary to the previous beliefs[25], the middle section of the IOM plays a role in pressure detection or detection of deformation of tissues. As many muscles are attaching to the middle portion of the IOM, tensioning of these muscles might lead to a deformity of the IOM. To prevent injury and protect the tissues, this sensory innervation is crucial.

Proximally

Proximally, we only found few Ruffini bodies at the border to the IOM. There were more Ruffini bodies in the surrounding tissues, most in muscle tissue, but we also identified some in connective tissue.

Medially

Medially, similar to proximally, we only found few Ruffini bodies at the border to the IOM. There were more Ruffini bodies in the surrounding tissues, most in muscle tissue, but we also identified some in connective tissue.

Distally

Distally, we only identified four Ruffini bodies at the border to the IOM. We identified many more in the surrounding tissues, much more than proximally and medially. We assume that there are more Ruffini bodies distally for the same reason as there are more muscle spindles – because of the proximity to the hand already tiny differences in length and in pression need to be registered to guarantee optimal movement and prevent injury.

Longitudinally

Longitudinally, we found three Ruffini bodies within the IOM, interestingly only in the left-sided specimens. This stands in congruence with our findings of Golgi-Mazzoni and Vater-Pacini corpuscles in the longitudinal sections and we assume that it might be due to the handedness of the donor. In the surrounding tissues, we identified two Ruffini bodies distally in the right-sided specimen.

Sides

We see great individual differences in side distribution of the Ruffini bodies. Similar to the Vater-Pacini and Golgi-Mazzoni corpuscles, we assume that this might have to do with the handedness of the donors.

Further notes

We found most Ruffini bodies in the muscle tissue around the membrane and some within connective tissue around the membrane. There were only few within the membrane. As the IOM consists of different layers of connective tissue, we hypothesise that the intramembranous Ruffini bodies serve the purpose to monitor shear forces created by the movement of the layers against each other[10,18].

Golgi-Tendon organs

We only identified three Golgi-Tendon organs. Rein et al.[25] similarly only found few of these mechanoreceptors in the IOM. Different to the other mechanoreceptors, we only looked for

Golgi-Tendon organs within the IOM, making our findings even more comparable to those of Rein et al. One reason for the limited number found might be that there was a loss of Golgi-Tendon organs during the sample collection and histological preparation process. Similarly, it could be due to a limited staining success. Other researcher investigating the IOM cruris[66] or the deep fascia of the upper extremity[78] did not report on Golgi-Tendon organs. Golgi-Tendon organs measure muscle tension[55] and as the IOM serves as muscle attachment, we assumed that we would find more of them. An explanation for the low number of Golgi-Tendon organs might be that muscle tension only has a limited impact on the total tension within the IOM which is mostly created by the movement of the ulna and radius against each other. Another possible explanation might be that Ruffini bodies and muscle spindles already sense tension changes of the IOM, rendering Golgi-Tendon organs redundant. Therefore, Golgi-Tendon organs might be less important in the IOM.

Sympathetic innervation and Pain synthesis

Ongoing vibration may cause discomfort and tissue damage, therefore Vater-Pacini corpuscles and Golgi-Mazzoni corpuscles have an important safe-guarding purpose[48]. Likewise, Ruffini bodies feedback about the stretching of tissues and have especially the purpose to communicate about harmful lengthening of tissues[48].

Similarly, to the function of these three mechanoreceptors, pain as sensation is primarily intended to prevent injury to the body. It has a guarding function. To achieve this, pain creates a local defence reaction such as pulling away or interrupting a movement. Unfortunately, sometimes, pain is felt although the movement is not threatening to the tissues. This phenomenon is called allodynia and happens in pain syndromes such as CRPS Type I. We hope to add to the current knowledge about the pathophysiology of this pain syndrome with our findings.

Free nerve endings were the sensory nerve endings that Rein et al.[25] identified most in their study. They found them particularly in the distal oblique cord. We did not investigate all types of free nerve endings but specialised on nerves with sympathetic supply. Rein et al.[25] hypothesised that the free nerve endings found indicate a great nociceptive function of the IOM as monitor for physiological movement and loading. As the sympathetic system plays an enormous role in pain synthesis and maintenance, we were surprised to only find this limited sympathetic innervation. Reasons therefore could be an atrophic innervation because of the old age of our donors, the long post-mortem time or that the forearms were uninjured and healthy at time of death, so nociception was not required.

Stecco et al.[78] stated that if mechanoreceptors are overstretched, they may become nociceptors. This may be a reason why although we found only little sympathetic innervation of the IOM

pain syndromes in the forearm exist. A healthy person might only have little sympathetic supply of the deep structures in the forearm, but after a sudden trauma in which these structures and the associated mechanoreceptors are overstretched, these mechanoreceptors might develop into nociceptors and previous non-painful movements may be experienced as painful. This reduced pain threshold might lead to an increased sympathetic innervation and consequentially sympathetically maintained pain in form of pain syndromes such as CRPS Type I.

In addition, we found many Vater-Pacini and Golgi-Mazzoni corpuscles close to arteries, probably measuring the pulsation and filling state of the vessels. In case of injury and resultant inflammation, hyperaemia is created by filling of the blood vessels and thus greater pulsation. This triggers the corpuscles, reducing their perception threshold. Thereby, also small stimuli may already trigger the Vater-Pacini and Golgi-Mazzoni corpuscles, forming them into nociceptors and creating allodynia. This theory could explain the pathogenesis of CRPS Type I, where the first state is often called the "warm" phase because of hyperaemia[85].

To investigate this hypothesis, it would be interesting to analyse the IOM and surrounding structures in patients with CRPS Type I. This could be performed on amputated forearms of CRPS Type I patients[86] as well as in donor patients with a CRPS Type I history. These two different sampling strategies would allow for a comparison of a rather acute stage versus a potentially already chronified illness depending on the time of diagnosis and time of decision to amputate or death, respectively.

Consequences for function and role of the different IOM ligaments

Many researchers in the last decade investigated the structure and function of the IOM according to its ligament structure, first described by Noda et al.[10]. Only in the last years, some researchers went back to separating the IOM into a proximal, medial and distal part because of interindividual differences in presence of these ligaments[15,18]. Because of our methodological approach to also investigate the tissues surrounding the IOM, we decided to choose the latter approach. In the next section, we want to apply our findings to the different ligaments as far as possible and to compare our results to those of previous researchers.

Proximal oblique cord

Some researchers believe that the proximal oblique cord has no important function in the human[10]. Other researchers hypothesise that this cord may act as restrain from excessive pronation[11]. Rein et al.[17] found that the proximal oblique cord has more elastic fibres than most other ligaments of the IOM except for the distal oblique bundle. Therefore, they assume that this cord has a supportive role during rotation[17]. Kholinne et al. found that there is fluctuating strain on the cord during rotation[21].

Patel et al.[87] investigated the presence and function of the proximal oblique cord in non-human primates and found it consistently in anthropoid primates. This researcher team suggests that this cord fulfils a stabilising function in primates with quadruple gait and therefore assume that it is only a remnant in bipedal humans.

In our study, we investigated the proximal part of the IOM at the level of the tuberculum radii. According to Noda et al.[10], the proximal oblique cord runs from the coronoid process of the ulna to the distal end of the radial tuberosity. As we took samples from the IOM on the height of the radial tuberosity, we assume that our findings correspond most likely to the proximal oblique cord. We identified only one muscle spindle and one Ruffini body within the proximal IOM. However, in the bordering and surrounding tissues we found all four mechanoreceptors, Vater-Pacini corpuscles, Golgi-Mazzoni corpuscles, muscle spindles and Ruffini bodies, abundantly. This richness of mechanoreceptors makes it very unlikely that the proximal oblique cord has no important function in the human[10,87].

Rein et al.[25] found that the proximal oblique cord together with the distal oblique bundle has a greater innervation of sensory nerve endings than the other ligaments. They draw the conclusion that this richness of innervation is due to closeness to the PRUJ and DRUJ respectively and the purpose to monitor tension effectively and sensitively during forearm rotation.

We join Rein et al. in concluding that the proximal oblique cord has an important monitor function, probably because to the closeness to the PRUJ. We further add to this hypothesis that most of this monitoring takes place directly at the border to the IOM which corresponds probably to the surface of the IOM.

Dorsal oblique accessory cord

Other researchers hypothesise that the dorsal oblique accessory cord may work as possible restrain from excessive pronation[11] and that it probably has an important role in stabilizing the proximal forearm as it is very stiff[14]. Rein et al.[17] discovered that in seven of the eleven dorsal oblique accessory cords they investigated elastic fibres were absent. They hypothesise that it functions to resist tensile forces. In another study, Rein et al.[25] found that next to the central band, the dorsal oblique accessory cord has the least innervation by sensory nerve endings.

In our study, we did not explicitly explore the dorsal oblique accessory cord for its innervation. It runs outside of the areas we extracted our samples from. It would be interesting to investigate this cord and its surrounding tissues for the presence of mechanoreceptors to explore its role in proprioception.

Proximal accessory band

Some researchers assume that the proximal accessory band has a complimentary role to support the central band[10]. Noda et al. described this band as very delicate and it was absent in 17 out of their 30 specimens.[10] Due to our methodology, we did not explicitly check for its presence. Therefore, we cannot hypothesise whether mechanoreceptors are present within or around it.

Central band

As the central band is the biggest ligament within the IOM and lays in the medial part of the IOM, it is very likely that the IOM that we explored in our medial samples corresponds to the central band.

Researchers agree that the central band is the most important stabilizer in preventing radial head migration after trauma or radial head excision[6,9]. After radial head removal, the central band might not be able to withstand to the pressure forced on it and might get insufficient with time, therefore some people may suffer from instability problems[9]. Moritomo et al.[11] found that the central band is isometric and hypothesises that it works as a stabilizer of the forearm. Rein et al. found in 5 out of 11 specimens no elastic fibres[17]. Kholinne et al.[16] discovered that the central band is under constant strain during forearm rotation.

In their study, Rein et al.[25] found that the central band is only sparsely innervated in comparison to other ligaments. Therefore, they suggest that during surgical reconstruction of this structure, non-sensory tissue may be used.

In our study, we found two Ruffini bodies on each side as well as one Vater-Pacini corpuscle on the right side. Additionally, we found many further mechanoreceptors at the border to and around the IOM. As the surrounding and bordering tissues are richly innervated and there is some innervation within the IOM, we do not fully support the hypothesis of Rein and colleagues regarding the reconstruction of the central band with non-sensory tissue. It should be sought to cause as little damage as possible to the surrounding tissues of the central band during surgery as plenty of mechanoreceptors exist. Even if the detection of stimuli is not taking place within the IOM, but mostly at the border to it or in the tissues around it, it seems to have an important role in proprioception. We hypothesise that the purpose of the mechanoreceptors at this level is to monitor and feedback about the transition of the IOM into the deep forearm muscles.

Distal accessory band

The distal accessory band is stated to have a complimentary role for the central band[10] and to be isometric and work as a stabilizer of the forearm[11]. Noda et al.[10] found this structure in different variations in 27 out of their 30 specimens. Due to our methodology, we did not explicitly check

for its presence. Therefore, we cannot hypothesise whether mechanoreceptors exist within or around it.

Distal oblique bundle

According to current research the distal oblique bundle functions as stabilizer at the distal radio-ulnar joint in conjunction with the triangular fibrocartilage complex[10]. Further, it was found to be isometric and is thus hypothesised to work as stabilizer of the forearm[11] as well as secondary stabilizer of the distal radio-ulnar joint[11]. It has more elastic fibres than any other ligament of the IOM except for the proximal oblique cord[17] and is believed to have a supportive role during rotation[17]. During rotation, there is a fluctuating strain upon the ligament[21].

Rein et al.[25] found that the distal oblique bundle together with the proximal oblique cord had a greater innervation of sensory nerve endings than the other ligaments. They hypothesised that the closeness to the DRUJ presupposes an increased need for detection and monitoring of tension during forearm rotation. In addition, they found most Vater-Pacini corpuscles in the distal oblique bundle. Rein et al.[25] assume that the Vater-Pacini corpuscles in this structure provide neuromuscular control during pro- and supination of the forearm.

We assume that our distal sample corresponds most likely to the distal oblique bundle. In our distal samples, we found four Ruffini bodies and two muscle spindles in the IOM from the right-side and one Vater-Pacini corpuscle in a left IOM. In the bordering and surrounding tissues, we found all the four mechanoreceptors. Statistically, in the surrounding tissues, we found more muscle spindles than proximally and medially. This suggests that not only the IOM but also the surrounding tissues are very sensible in this body area. Therefore, we hypothesise that the distal IOM plays an important role in sensory feedback, imaginable as a gatekeeper in detecting and transmitting movements and sensations from the hand and wrist guaranteeing optimal physical effort to perform fine motor tasks. This allows fine-tuned everyday tasks such as writing, typing, drawing, palpating and cooking.

Generally

Birkbeck et al.[22] discovered that the IOM is important for the load transfer from the wrist joint to the elbow. Our results suggest that this load transfer is closely measured and monitored by the mechanoreceptors in and around the IOM to prevent too heavy and harmful loading.

4.2 Clinical Implications

Although this study is a biomedical basic study its findings have great implications for the clinic. In the recent years the research about proprioception and mechanoreceptors has increased vastly and many researchers hope to optimise treatment with these new findings[50]. Previous studies have shown that the thoracolumbar fascia is greatly innervated by mechanoreceptors[88,89] and current research indicates that it plays a big role in the pathogenesis of backache. The proprioceptive innervation of the forearm is much less studied than the innervation of other areas of the body[90], although the forearm plays an important role in everyday task and injuries to it are very limiting[90]. Our findings may help surgeons to better understand the IOM so that reconstructive surgeries can be optimised and may help pain specialists in finding the underlying reason for chronic pain.

All investigated parts of the IOM are innervated by mechanoreceptors. This is particularly important for the central band, because until now this structure had often been seen as a solely biomechanical structure[25]. Bin abd Razak et al.[15] and Rein et al.[17] already pointed out that the consistency in presence of the central band in comparison to the other rather variably present ligaments, underlines the functional importance of this structure. Our findings support the idea, that the central band not only has an important biomechanical role but is also very important for proprioception. The concept of LaStayo et al.[23] and Soubeyrand et al.[24] to consider the medial part of the IOM as functional joint might render this proprioceptive role easier to grasp.

Clinically, these findings should be considered after injury to the IOM, especially because the IOM only has limited healing potential[29,91]. Masouros[29] hypothesizes for this reason that the central band is not able to heal by itself after injury. This limiting healing capacity could also play an important role in the pathogenesis of pain syndromes. While other tissues such as bones and muscles are healing, the IOM remains injured with subsequent release of inflammatory markers. Thereby, sympathetically maintained pain can develop and lead to pain syndromes such as Complex Regional Pain Syndrome Type I. Before replacement surgery the proprioceptive function of all ligaments of the IOM should be considered and the replacement with sensorily innervated bands should be sought.

We also investigated the tissues surrounding the IOM which are very close to both forearm bones. These tissues were richly innervated by mechanoreceptors. Blecher et al.[92] studied mice and discovered that muscle spindles and Golgi-Tendon organs play a role in regulation of fracture repair and restoration of bone morphology. This positive influence even increased with the age of the mice. Evolutionary, the optimal function of the forearm was crucial for survival for example for hunter-gatherers. Thus, a rich innervation of the deep tissues in the forearm by mechanoreceptors, amongst others optimising bone repair after trauma, was a survival benefit.

4.3 Limitations

Due to the study design and methodology some limitations were inevitable:

Our donors were aged between 67-91 years and do therefore not reflect the mean age of society. Because of the old age, some structures may already have atrophied during life such as the sympathetic innervation. However, it was shown that Vater-Pacini corpuscles do not atrophy with age, at least in the skin[84]. García-Piqueras et al.[84] investigated the ageing of mechanoreceptors in the skin in three different age groups in patients aged 20-39 years, 40-59 years and over 60 years and found no variations regarding Vater-Pacini corpuscles. Lennartson et al.[93] explored the presence of muscle spindles in the human digastric muscles in five humans between 23 and 73 years of age and found no direct connection between the number of muscle spindles and age.

Because of our interest in the surrounding tissues of the IOM and to prevent injury to the mechanoreceptors in these tissues by removing excessive muscle fibres[66], we did not dissect all attaching muscle fibres to the IOM. Thus, the single IOM ligaments were covered by muscle and connective tissue, and it was not possible to identify each ligament for its presence and shape. Therefore, we cannot certainly assign the found mechanoreceptors to single ligaments. We were able to identify the IOM in every specimen as dark red connective tissue band in the EVG stain, although these bands differed vastly in thickness. A clear classification according to Noda et al.[10] definitions such as that the dorsal oblique cord is thicker than 0,5mm was not possible.

As the membrane was thicker in some specimens than in others, the percentages of IOM, muscle and CT varied in the same-sized specimens. The different amount of surrounding tissue might have led to a different number of identifiable mechanoreceptors.

The information we have about the donors are limited and do not contain their handedness. Consequently, we were only able to make assumptions about the intraindividual differences in side distribution of mechanoreceptors.

We explored two-dimensional slices which means that a three-dimensional analysis of the development of mechanoreceptors was not possible. This is a limitation especially regarding the differentiation of Golgi-Mazzoni and Vater-Pacini corpuscles. In donor 7, we conducted a series of histological stains which allowed an analysis of sequential sections and showed that some primarily assumed Vater-Pacini corpuscles were rather Golgi-Mazzoni corpuscles.

4.4 Outlook

Our findings reveal some research gaps, which should be investigated near-term to expand on our knowledge and help patients with pathologies of the forearm.

We recommend investigating the presence of sympathetic innervation in the IOM and surrounding tissues in patients with CRPS Type I. It would be particularly interesting to compare the results of acute and chronic CRPS Type I patients. A possibility to explore this disease in younger patients could be to analyse the forearms of young CRPS Type I patients, who got an amputation because of the excruciating pain[86].

Further, we recommend investigating the presence of mechanoreceptors in the IOM and surrounding tissues in young donors.

To our knowledge, the intraindividual differences in distribution of mechanoreceptors in relation to the handedness has never been investigated. A possible difference might have great impact on therapy planning after trauma to the forearm, especially if replacement therapy is considered.

To expand on our findings of Golgi-Mazzoni corpuscles at the border to the IOM, a study investigating the entire longitudinal IOM with bordering tissues would be intriguing.

Another aspect that could be of great relevance for forearm surgery would be to particularly compare and differentiate between the innervation of the flexor and extensor sides.

In the last decades the IOM has been the subject of many biomechanical studies regarding its function. In addition, many researchers were interested in its anatomy. In the future, we assume that the IOM will still be of great interest to the scientific world but that the focus of studies will rather shift to its sensory role in the body.

4.5 Conclusion

This study is the second study investigating the presence and distribution of sensory nerve endings within the IOM. To our best knowledge, it is the first study to also explore the tissues at the border to the IOM and surrounding it. We can validate the findings of Rein and colleagues of mechanoreceptors in the IOM[25]. Even more interesting is the rich innervation of the tissues close to the IOM, indicating that there is a great requirement of close monitoring and detection of movement of the IOM.

The forearm is unique in its richness of different movements. No other part of the body has to accommodate and adapt to the continuous challenge created by this set of movements. This fine balance between instability and restriction of movement is amongst others monitored by the mechanoreceptors we found. Particularly highlightable is the great number of Golgi-Mazzoni corpuscles we discovered. These three-dimensional vibration detecting mechanoreceptors have only been scarcely researched until now. Our study adds important knowledge about their morphology and possible specific function.

Without any doubt, the IOM plays not only a crucial role for the biomechanics of the forearm but is also of great importance for the sensory feedback of every single movement of the upper extremity.

In the future, this sensory role should be further explored to fill the gaps in our current knowledge and optimise the diagnosis and treatment of patients with forearm pathologies.

5 Literature

1. Sacks OW, Stein SM. The Disembodied Lady *The Man Who Mistook His Wife for a Hat*: British Journal of Psychiatry; 1995 p26-32.

2. Moore KL, Dalley AF, Agur AMR. *Clinically Oriented Anatomy*. 7th Edition ed: Lippincott Williams & Wilkins; 2013.

3. Postan D, Poitevin LA, Daniel F. The Development of the Interosseous Membrane of the Forearm. *Hand* 2016;11(1_suppl):20S-21S.

4. Kreutzer L. Die Faserarchitektur der neonaten Membrana interossea antebrachii *54. Kongress der Deutschen Gesellschaft für Handchirurgie, Düsseldorf*: German Medical Science GMS Publishing House; 2013.

5. Moore KL, Dalley AF, Agur AMR. Skeletal System *Clinically Oriented Anatomy*. 7th Edition ed: Wolters Kluwer; 2013.

6. Hotchkiss RN, An KN, Sowa DT, et al. An Anatomic and mechanical study of the interosseous membrane of the forearm - pathomechanics of proximal migration of the radius. *Journal of Hand Surgery-American Volume* 1989;14(2):256-61.

7. Morrey BF, An KN, Stormont TJ. Force transmission through the radial head. *JBJS* 1988;70(2):250-56.

8. Werner JA, Koebke J. The function of the antebrachial interosseous membrane. *Anatomy and Embryology* 1987;176(1):127-31.

9. Skahen JR, 3rd, Palmer AK, Werner FW, et al. The interosseous membrane of the forearm: anatomy and function. *Journal of Hand Surgery* 1997;22(6):981-5.

10. Noda K, Goto A, Murase T, et al. Interosseous Membrane of the Forearm: An Anatomical Study of Ligament Attachment Locations. *Journal of Hand Surgery-American Volume* 2009;34A(3):415-22.

11. Moritomo H, Noda K, Goto A, et al. Interosseous Membrane of the Forearm: Length Change of Ligaments During Forearm Rotation. *The Journal of Hand Surgery* 2009;34(4):685-91.

12. Hohenberger GM, Schwarz AM, Weiglein AH, et al. Prevalence of the distal oblique bundle of the interosseous membrane of the forearm: an anatomical study. *Journal of Hand Surgery (European Volume)* 2017;43(4):426-30.

13. Poitevin LA, Postan D, Valente S. Distal-Ulna Stump Stability: The Role of Distal Interosseous Membrane: Myth or Reality? Anatomical Research. *Hand (N Y)* 2021:1558944721999728.

14. Carrillo F, Suter S, Casari FA, et al. Digitalization of the IOM: A comprehensive cadaveric study for obtaining three-dimensional models and morphological properties of the forearm's interosseous membrane. *Scientific Reports* 2020;10(1):15.

15. Bin Abd Razak HRB, Yew KSA, Moideen ISB, et al. An anatomical and biomechanical assessment of the interosseous membrane of the cadaveric forearm. *Journal of Hand Surgery-European Volume* 2020;45(4):369-74.

16. Kholinne E, Kwak JM, Sun YC, et al. The forearm interosseous ligament: comparative mechanical properties of the proximal, central, and distal bands. *Journal of Hand Surgery-European Volume* 2020:4.

17. Rein S, Kremer T, Houschyar KS, et al. Structural topography of the interosseous membrane of the human forearm. *Ann Anat* 2020;231:151547.

18. Kholinne E, Kwak J-M, Sun Y, et al. Forearm Interosseous Ligaments: Anatomical and Histological Analysis of the Proximal, Central, and Distal Bands. *The Journal of Hand Surgery* 2021;46(11):1029.e1-29.e8.

19. Anderson A, Werner FW, Tucci ER, et al. Role of the interosseous membrane and annular ligament in stabilizing the proximal radial head. *Journal of Shoulder and Elbow Surgery* 2015;24(12):1926-33.

20. Werner FW, LeVasseur MR, Harley BJ, et al. Role of the Interosseous Membrane in Preventing Distal Radioulnar Gapping. *Journal of Wrist Surgery* 2017;6(2):97-101.

21. Kholinne E, Kwak JM, Sun YC, et al. The role of the interosseous ligament in forearm rotation: A bio-mechanical study. *Journal of Orthopaedic Surgery* 2020;28(3):6.

22. Birkbeck DP, Failla JM, Hoshaw SJ, et al. The interosseous membrane affects load distribution in the forearm. *Journal of Hand Surgery* 1997;22(6):975-80.

23. LaStayo PC, Lee MJ. The forearm complex: anatomy, biomechanics and clinical considerations. *Journal of hand therapy : official journal of the American Society of Hand Therapists* 2006;19(2):137-44.

24. Soubeyrand M, Wassermann V, Hirsch C, et al. The middle radioulnar joint and triarticular forearm complex. *Journal of Hand Surgery (European Volume)* 2011;36(6):447-54.

25. Rein S, Esplugas M, Garcia-Elias M, et al. Immunofluorescence analysis of sensory nerve endings in the interosseous membrane of the forearm. *Journal of Anatomy* 2020;236(5):906-15.

26. Okada K, Moritomo H, Miyake J, et al. Morphological evaluation of the distal interosseous membrane using ultrasound. *European Journal of Orthopaedic Surgery & Traumatology* 2014;24(7):1095-100.

27. Fester EW, Murray PM, Sanders TG, et al. The efficacy of magnetic resonance imaging and ultrasound in detecting disruptions of the forearm interosseous membrane: a cadaver study. *Journal of Hand Surgery* 2002;27(3):418-24.

28. Essex-Lopresti P. Fractures of the radial head with distal radio-ulnar dislocation; report of two cases. *Journal of Bone and Joint Surgery (British Volume)* 1951;33b(2):244-7.

29. Masouros PT, Apergis EP, Babis GC, et al. Essex-Lopresti injuries: an update. *Efort Open Reviews* 2019;4(4):143-50.

30. Curr JF, Coe WA. Dislocation of the inferior radio-ulnar joint. *BJS (British Journal of Surgery)* 1946;34(133):74-77.

31. Trousdale RT, Amadio PC, Cooney WP, et al. Radio-ulnar dissociation. A review of twenty cases. *JBJS* 1992;74(10).

32. Grassmann JP, Hakimi M, Gehrmann SV, et al. The treatment of the acute Essex-Lopresti injury. *Bone Joint J* 2014;96-B(10):1385-91.

33. Artiaco S, Fusini F, Colzani G, et al. Chronic Essex-Lopresti injury: a systematic review of current treatment options. *International Orthopaedics* 2019;43(6):1413-20.

34. Masouros PT, Apergis EP, Mavrogenis AF, et al. Reconstruction of the forearm interosseous membrane: a biomechanical study of three different techniques. *Journal of Hand Surgery-European Volume* 2020;45(4):360-68.

35. Monteggia G. Lussazioni delle ossa delle estremita superiori. *Instituzioni Chirurgiches* 1814;2:131-33.

36. Galeazzi R. Di una particolare sindrome traumatica dello scheletro dell' avambraccio. *Atti e memorie della Società lombarda di chirurgia* 1934;2:663-66.

37. Ozkan T, Aydin A, Ozer K, et al. A surgical technique for pediatric forearm pronation: brachioradialis rerouting with interosseous membrane release ¹. *Journal of Hand Surgery* 2004;29(1):22-27.

38. Harden RNB, Stephen. Stanton-Hicks, Michael. Wilson, Peter R. Proposed New Diagnostic Criteria for Complex Regional Pain Syndrome. *Pain Medicine* 2007;8(4):326-31.

39. Harden RN, Bruehl S, Perez RSGM, et al. Validation of proposed diagnostic criteria (the "Budapest Criteria") for Complex Regional Pain Syndrome. *Pain* 2010.

40. Birklein F, Schlereth T. Complex regional pain syndrome-significant progress in understanding. *Pain* 2015;156(4):S94-S103.

41. Sandroni P, Benrud-Larson LM, McClelland RL, et al. Complex regional pain syndrome type I: incidence and prevalence in Olmsted county, a population-based study. *Pain* 2003;103(1-2):199-207.

42. Kim H, Lee CH, Kim SH, et al. Epidemiology of complex regional pain syndrome in Korea: An electronic population health data study. *PLoS ONE* 2018;13 (6) (no pagination)(e0198147).

43. de Mos M, de Bruijn AGJ, Huygen FJPM, et al. The incidence of complex regional pain syndrome: A population-based study. *Pain* 2007;129(1).

44. Pons T, Shipton EA, Williman J, et al. Potential Risk Factors for the Onset of Complex Regional Pain Syndrome Type 1: A Systematic Review. *Anesthesiology Research and Practice* 2015;Volume 2015.

45. Beerthuizen A, Stronks DL, van't Spijker A, et al. Demographic and medical parameters in the development of complex regional pain syndrome type 1 (CRPS1): Prospective study on 596 patients with a fracture. *PAIN* 2012;153(6):1187-92.

46. de Mos M, de Bruijn AGJ, Huygen FJPM, et al. The incidence of complex regional pain syndrome: A population-based study. *Pain* 2007;129(1):12-20.

47. Tuthill JC, Azim E. Proprioception. *Current Biology* 2018;28(5):R194-R203.

48. Mueller SM, Winkelmann C, Grunwald M. *Lehrbuch Haptik - Grundlagen und Anwendung in Therapie, Pflege und Medizin*: Springer Berlin, Heidelberg; 2022.

49. Sherrington CS. On the proprio-ceptive system, especially in its reflex aspect. *Brain* 1907;29(4):467-82.

50. Cobo R, García-Piqueras J, Cobo J, et al. The Human Cutaneous Sensory Corpuscles: An Update. *J Clin Med* 2021;10(2).

51. Ruffini A. Les dispositifs anatomiques de la sensibilité cutanée sur les expansions nerveuses de la peau chez l'homme et quelques autres mammifères *Revue générale d'histologie*: Storck, A.; 1905.

52. Ciaccio GV. *Lezioni di notomia minuta generale e degli organi dei sensi dettate nella Regia Università di Bologna.*: Bologna, Gamberini e Parmeggiani, 1890-95.; 1890-1895.

53. Fleming MS, Luo W. The anatomy, function, and development of mammalian Aβ low-threshold mechanoreceptors. *Front Biol (Beijing)* 2013;8(4).

54. Palmer CI, Gardner EP. Simulation of motion on the skin. IV. Responses of Pacinian corpuscle afferents innervating the primate hand to stripe patterns on the OPTACON. *Journal of Neurophysiology* 1990;64(1):236-47.

55. Ghosh SK. Camillo Golgi (1843-1926): scientist extraordinaire and pioneer figure of modern neurology. *Anatomy & Cell Biology* 2020;53(4):385-92.

56. Mazzoni V. Osservazioni microscopiche sopra i così detti corpuscoli terminali dei tendini dell'uomo e sopra alcune particolari piastre nervose superficiali che si trovano nei medesimi tendini. *Memorie della R. Accademia delle scienze dell'Ist. di Bologna* 1890:401-08.

57. Ruffini A. Sur un nouvel Organe nerveux terminal et sur la présence des corpuscles golgi-Mazzoni dans le conjonctif sous-cutané de la pulpe des doigts de l'homme. 1893.

58. Barker D. The innervation of the muscle-spindle. *Quarterly Journal of Microscopical Science* 1948;89(Pt 2):143-86.

59. Golgi C. Intorno alla distribuzione e terminazione dei nervi nei tendini dell'uomo e di altri vertebrati: ricerche. *Reale Istituto lombardo di scienze e lettere* 1878;11.

60. Jami L. Golgi tendon organs in mammalian skeletal muscle: functional properties and central actions. *Physiological Reviews* 1992;72(3):623-66.

61. Macefield VG, Knellwolf TP. Functional properties of human muscle spindles. *Journal of Neurophysiology* 2018;120(2):452-67.

62. Davis JN. Proceedings: Discharge properties of primary and secondary endings in human intercostal muscle spindles studied in vitro. *Journal of Physiology* 1973;234(2):30p-32p.

63. Freeman MA, Wyke B. The innervation of the knee joint. An anatomical and histological study in the cat. *Journal of Anatomy* 1967;101(Pt 3):505-32.

64. Freeman MA, Wyke B. The innervation of the ankle joint. An anatomical and histological study in the cat. *Acta Anatomica* 1967;68(3):321-33.

65. Rebmann D, Mayr HO, Schmal H, et al. Immunohistochemical analysis of sensory corpuscles in human transplants of the anterior cruciate ligament. *Journal of Orthopaedic Surgery and Research* 2020;15(1):270.

66. Morley J, Fan C, McDermott K, et al. The crural interosseous membrane re-visited: a histological and microscopic study. *European Journal of Translational Myology* 2019;29(3):8340.

67. Hagert E. *Wrist Ligaments: Innervation Patterns and Ligamento-Muscular Reflexes*. Karolinska Institutet, Stockholm, Sweden, 2008.

68. Marx SC, Kumar P, Dhalapathy S, et al. Distribution of sympathetic fiber areas of radial nerve in the forearm: an immunohistochemical study in cadavers. *Surgical and Radiologic Anatomy* 2010;32(9):865-71.

69. Balogh B, Auterith A, Behrus R, et al. [The sympathetic axons of the nerves of the hand]. *Handchirurgie, Mikrochirurgie, Plastische Chirurgie* 2002;34(6):369-73.

70. Mulisch M, Welsch U. *Romeis Mikroskopische Technik*. 18 ed. Heidelberg: Spektrum Akademischer Verlag; 2010.

71. Burck H-C. Histologische Technik : Leitfaden für die Herstellung mikroskopischer Präparate in Unterricht und Praxis. 5th ed. Stuttgart: Thieme; 1982 p115.

72. Boenisch T. *Handbuch Immunchemische Färbemethoden*. 3rd ed. Carpinteria: Thomas Boenisch; 2006.

73. Nagatsu T, Levitt M, Udenfriend S. Tyrosine hydroxylase. The initial step in norepinephrine biosynthesis. *Journal of Biological Chemistry* 1964;239:2910-7.

74. Moore BW. A soluble protein characteristic of the nervous system. *Biochemical and Biophysical Research Communications* 1965;19(6):739-44.

75. Martinsen V, Kursula P. Multiple sclerosis and myelin basic protein: insights into protein disorder and disease. *Amino Acids* 2022;54(1):99-109.

76. Samanta A, Hughes TET, Moiseenkova-Bell VY. Transient Receptor Potential (TRP) Channels. *Sub-Cellular Biochemistry* 2018;87:141-65.

77. Scientific T. *Invitrogen TRPC4 Polyclonal Antibody*. https://www.thermofisher.com/antibody/product/TRPC4-Antibody-Polyclonal/PA5-77309 (accessed 06.06.2022).

78. Stecco C, Gagey O, Belloni A, et al. Anatomy of the deep fascia of the upper limb. Second part: study of innervation. *Morphologie* 2007;91(292):38-43.

79. Hunt CC. On the nature of vibration receptors in the hind limb of the cat. *Journal of Physiology* 1961;155(1):175-86.

80. Zelená J. The development of Pacinian corpuscles. *Journal of Neurocytology* 1978;7(1):71-91.

81. Hagert E, Forsgren S, Ljung BO. Differences in the presence of mechanoreceptors and nerve structures between wrist ligaments may imply differential roles in wrist stabilization. *Journal of Orthopaedic Research* 2005;23(4):757-63.

82. Riley JLI, Robinson ME, Wise EA, et al. Sex differences in the perception of noxious experimental stimuli: a meta-analysis. *Pain* 1998;74(2):181-87.

83. Mogil JS, Bailey AL. Sex and gender differences in pain and analgesia. *Progress in Brain Research* 2010;186:141-57.

84. García-Piqueras J, García-Mesa Y, Cárcaba L, et al. Ageing of the somatosensory system at the periphery: age-related changes in cutaneous mechanoreceptors. *Journal of Anatomy* 2019;234(6):839-52.

85. Misidou C, Papagoras C. Complex Regional Pain Syndrome: An update. *Mediterr J Rheumatol* 2019;30(1):16-25.

86. Bodde MI, Dijkstra PU, Schrier E, et al. Informed Decision-Making Regarding Amputation for Complex Regional Pain Syndrome Type I. *Journal of Bone and Joint Surgery (American Volume)* 2014;96(11):930-34.

87. Patel BA. Form and function of the oblique cord (chorda obliqua) in anthropoid primates. *Primates* 2005;46(1):47-57.

88. Terzis R, Filler T, Frankewitsch T, et al. Die propriozeptive Innervation der Fascia thoracolumbalis und ihre klinische Relevanz bei Patienten mit Rückenschmerzen. *Zeitschrift für Orthopädie und Unfallchirurgie* 2020;158(S 01):DKOU20-422.

89. Wilke J, Schleip R, Klingler W, et al. The Lumbodorsal Fascia as a Potential Source of Low Back Pain: A Narrative Review. *Biomed Res Int* 2017;2017:5349620.

90. Goble DJ, Coxon JP, Wenderoth N, et al. Proprioceptive sensibility in the elderly: Degeneration, functional consequences and plastic-adaptive processes. *Neuroscience and Biobehavioral Reviews* 2009;33(3):271-78.

91. Marcotte AL, Osterman AL. Longitudinal Radioulnar Dissociation: Identification and Treatment of Acute and Chronic Injuries. *Hand Clinics* 2007;23(2):195-208.

92. Blecher R, Krief S, Galili T, et al. The Proprioceptive System Regulates Morphologic Restoration of Fractured Bones. *Cell Reports* 2017;20(8):1775-83.

93. Lennartsson B. Muscle spindles in the human anterior digastric muscle. *Acta Odontologica Scandinavica* 1979;37(6):329-33.

6. List of Tables

7. List of Figures

8. Appendix

Utilised Chemicals, Material and Equipment for Staining		
Chemicals	**General chemicals**	Ethanol *(VWR International GmbH, Darmstadt)*
		Xylene (isomers), >98 % pure *(Carl Roth GmBH + CoKG, Karlsruhe)*
		Roti®Mount ready-to-use *(Carl Roth GmBH + CoKG, Karlsruhe)* [except for most immunohistochemical stains]
		ROTI®Mount Aqua, 2848.2 *(Carl Roth®, Karlsruhe)*
	Elastica-van Gieson dye	Resorcin Fuchsine *(Carl Roth GmBH + CoKG, Karlsruhe)*
		Ethanol *(VWR International GmbH, Darmstadt)*
		Hydrochloric acid *(VWR International GmbH, Darmstadt)*
		Haematoxylin *(Carl Roth GmBH + CoKG, Karlsruhe)*
		Ferric Chloride *(VWR International GmbH, Darmstadt)*
		Picric acid *(VWR International GmbH, Darmstadt)*
		Fuchsine acid *(VWR International GmbH, Darmstadt)*
	Azan after Heidenhain dye	Azocarmine G *(Merck KGaA, Darmstadt)*
		Aniline blue *(Merck KGaA, Darmstadt)*
		Orange G Certistain® *(Merck KGaA, Darmstadt)*
		Glacial Acetic acid *(Merck KGaA, Darmstadt)*
		Aniline *(Merck KGaA, Darmstadt)*
		Phosphotungstic acid hydrate *(Acros Organics, Geel)*
	Masson-Goldner dye	Haematoxylin cryst. *(Merck KGaA, Darmstadt)*
		Ferric chloride *(VWR International GmbH, Darmstadt)*
		Hydrochloric acid 25% *(Merck KGaA, Darmstadt)*
		Azophloxine Chroma® *(Waldeck GmbH & Co. KG, Münster)*
		Fuchsine acid Certistain® *(Merck KGaA, Darmstadt)*
		Ponceau de Xylidine, Chroma® *(Waldeck GmbH & Co. KG, Münster)*
		Orange G Certistain® *(Merck KGaA, Darmstadt)*
		Light green SF yellowish Certistain® *(Merck KGaA, Darmstadt)*
		Glacial acetic acid *(Merck KGaA, Darmstadt)*
		Phosphotungstic acid hydrate *(Acros Organics, Geel)*
	General	Antigen Unmasking Solution, Citrate-Based, pH 6, H-3300

	chemicals for immuno-histochemical stains	*(Vector Laboratories, Inc., Burlingame)*
		Phosphate buffered saline (PBS) self-mixed: Contains NaCl, Na_2HPO_4 x $2H_2O$, KCl, KH_2PO_4 (all from *Carl Roth®, Karlsruhe)* diluted in demineralised water
		Triton X-100 *(Santa Cruz Biotechnology, Inc., Santa Cruz)*
		Serum, donor horse *(MP Biomedicals, Irvine)*
		Hydrogen peroxide, 35 %, pure, stabilised *(Carl Roth®, Karlsruhe)*
		Streptavidin-Horseradish Peroxidase, 405210 *(BioLegend®, San Diego)*
		AEC Substrate Kit, Peroxidase (HRP), (3-amino-9-ethylcarbazole) SK-4200 *(Vector Laboratories, Inc., Burlingame)*
		Hematoxylin solution acc. to Gill II *(Carl Roth®, Karlsruhe)*
		Lithium carbonate ACS reagent, ≥99.0% *(Sigma-Aldrich, Merck KGaA, Darmstadt)*
	Pan Neurofilament stain	Purified anti-Neurofilament Marker (pan axonal, cocktail) Antibody, 837904, *(BioLegend®, San Diego)*
		Purified Mouse IgG1, κ Isotype Ctrl Antibody, 401402, *(BioLegend®, San Diego)*
		Purified Mouse IgM, λ Isotype Ctrl Antibody, 401102, *(BioLegend®, San Diego)*
		Horse Anti-Mouse IgG Antibody (H+L), Biotinylated, BA-2000 *(Vector Laboratories, Inc., Burlingame)*
		Biotin anti-mouse IgM Antibody, 406504, *(BioLegend®, San Diego)*
	Tyrosine hydroxylase stain	Anti-Tyrosine Hydroxylase Antibody, clone LNC1, MAB318 *(Sigma-Aldrich, Merck KGaA, Darmstadt)*
		Purified Mouse IgG1, κ Isotype Ctrl Antibody, 401402 *(BioLegend®, San Diego)*
		Horse Anti-Mouse IgG Antibody (H+L), Biotinylated, BA-2000 *(Vector Laboratories, Inc., Burlingame)*
	S100 stain	S-100 Mouse Monoclonal Antibody, Isotype Ig2a *(Dianova GmbH, Hamburg)*
		Purified Mouse IgG2a, κ Isotype Ctrl, 401502 *(BioLegend®, San Diego)*

		Horse Anti-Mouse IgG Antibody (H+L), Biotinylated, BA-2000 *(Vector Laboratories, Inc., Burlingame)*
	MBP stain	Purified Mouse anti-Myelin Basic Protein Antibody, IgG1, 836504 *(BioLegend®, San Diego)*
		Purified Mouse IgG1, κ Isotype Ctrl Antibody, 401402 *(BioLegend®, San Diego)*
		Horse Anti-Mouse IgG Antibody (H+L), Biotinylated, BA-2000 *(Vector Laboratories, Inc., Burlingame)*
	TRPC4 stain	TRPC4 Polyclonal Goat Antibody, IgG # PA5-18987 *(ThermoFisher Scientific Inc, Waltham)*
		Goat IgG Isotype Control, 31245 *(ThermoFisher Scientific Inc, Waltham)*
		Horse Anti-Goat IgG Antibody (H+L), Biotinylated, BA-9500 *(Vector Laboratories, Inc., Burlingame)*
Material		Human stomach mucosa or human tongue (positive control)
		Super Pap Pen Liquid Blocker *(COSMO BIO co., LTD., Tokyo)*
		Syringe (commercial)
		Filter (commercial)
		Menzel™ Microscope Coverslips *(Thermo Scientific Menzel)*
Equipment		Drying oven *(Memmert GmbH + Co. KG, Schwabach)*
		Pressure cooker (commercial)
		Laboratory pipette (commercial)
		Fridge (commercial, at 4°C)

Table 2: **Utilised Chemicals, Material and Equipment for Staining**
Listing of chemicals divided accordingly to the different stains, material and equipment which were used to stain the sections

9. Acknowledgments

First, I want to express my deep gratitude for my supervisor Prof. Dr. med Filler. He developed the idea for this thesis and supported me throughout the entire project. Your feedback always helped me to examine the topic from different perspectives.

Special thanks to Robert Kubitza for his friendly welcoming in the anatomy lab and for his ongoing help and support throughout the entire project. Further, I would like to acknowledge Andrea Paas for her help with staining the sections. Together, with Robert Kubitza, you both introduced me to histological working.

I would like to express my deepest appreciation for the donors and their families. Their selfless gift enabled this project and I hope that the new findings will help to improve medical care in a way they would have wished for.

I would especially like to thank my parents for their ongoing motivation and encouragement. Each of you motivated and supported me in different ways.

I thank my sister for her help with the statistic section and many other issues that arised through the years. I thank my brother for his regular enquiries about the study, which motivated me to stay on track.

I thank my friends Tabea, Hannah B., Anastasija, Lilly and Hannah K. for their friendship and support throughout the years.

Finally, I want to thank and acknowledge you Malte. Thank you for your patience and encouragement through all these years.